Search for exosomes in NG2-glial cells

Doctoral thesis

to obtain a doctorate (PhD)

from the Faculty of Medicine

of the University of Bonn

Dmitry Andreevich Fedorov

from Moscow, Russia

2022

Written with authorization of
the Faculty of Medicine of the University of Bonn

First reviewer: Prof. Dr. Christian Steinhäuser

Second reviewer: Dr. Etienne Audinat

Day of oral examination: 01.02.2022

For the Institute of Cellular Neurosciences
Director: Prof. Dr. Christian Steinhäuser

Dedicated to my family.

"Science doesn't know everything"... well Science knows it doesn't know everything – otherwise it would stop...

Dara Ó Briain

Table of contents

Abbreviations

A	ampere
a	atto
ACSF	artificial cerebrospinal fluid (nACSF – normal ACSF)
AMPA	α-amino-3-hydroxy-5-methyl-4-isoxazolepropionic acid
AOTF	Acousto-optic tunable filter
ATP	adenosine triphosphate
APC	adenomatous polyposis coli
ARI	adjusted Rand index
BAPTA	1,2-bis(o-aminophenoxy)ethane-N,N,N',N'-tetraacetic acid
bp	base pair
BNC	Bayonet Neill–Concelman
C	Capacitance (Membrane capacitance)
°C	degree Celsius
CA	Cornu Ammonis
CCD	Charge-coupled device
CCTV	close-circuit television
CD	cluster of differentiation
CLEM	correlated light-electron microscopy
C_m(C)	membrane capacitance
CNS	central nervous system
Cre	cyclization recombination (enzyme)
C_p	pipette capacitance
DAPI	4′,6-diamidino-2-phenylindole
DG	dentate gyrus
DHPG	3,5-Dihydroxyphenylglycine
DNA	deoxyribonucleic acid
DMEM	Dulbecco's modified medium
DMSO	Dimethylsulfoxide
EDTA	ethylenediaminetetraacetic acid
EGF	epidermal growth factor
EGTA	ethylene glycol tetraacetic acid
EGFP	enhanced green fluorescent protein
EM	electron microscopy
EPSC	excitatory postsynaptic current
ESCRT	endosomal sorting complexes required for transport
EV	extracellular vesicle
EYFP	enhanced yellow fluorescent protein
F	Farad
f	femto
FCS	fetal calf serum
FVB/N	Friend leukemia virus B
Fig	figure
FITC	Fluorescein isothiocyanate
fl/fl	floxed (loxP sites) on both allels
g	gram
G	giga

G	conductance (Siemens)
G_M	membrane conductance
GABA	γ-aminobutyric acid
GFAP	glial fibrillary acidic protein
GFP	green fluorescent protein
G_S	access conductance
h	hour
HEPES	4-(2-hydroxyethyl)-1-piperazineethanesulfonic acid
HET	Haus für experimentelle Tiertherapie
hsACSF	high-sucrose artificial cerebrospinal fluid
Hz	Hertz
I	current (Ampere)
IBA1	ionized calcium-binding adapter molecule 1
IDE	insulin degradation enzyme
IZN	Institute for Cellular Neurosciences (University Clinic Bonn)
k	kilo
Kir	inwardly-rectifying K^+ channel
ko	knock-out
LAMP	lysosome-associated membrane protein
LBPA	Lysobisphosphatidic acid
loxP	locus of crossing over P
LSM	laser scanning microscope
LTP	long-term potentiation
M	molar
MBP	myelin basic protein
mf	mossy fibers
mg	milligram
min	minute
MIP	maximum intensity projection
m	minute
ml	milliliter
mM	millimolar
mmol	millimole
MOhm	mega Ohm
mOsm	milli Osmoles
mRNA	messenger ribonucleic acid
ms	millisecond
mV	milli volt
MVB	multivesicular body
nAChRs	nicotinic acetylcholine receptors
NG2	nerve/glia antigen 2, a chondroitin sulfate proteoglycan
NGF	nerve growth factor
NGS	Normal goat serum
NMDA	N-methyl-D-aspartic acid
n	nano
n_c	number of cells
n_g	number of granules
OHT	4-hydroxytamoxifen

OPC	oligodendrocyte precursor cell
OLP	oligodendrocyte progenitor cell
OpAmp	operational amplifier
p(P)	postnatal day
PBS	Phosphate buffered saline
PCR	polymerase chain reaction
PDGFRα	platelet-derived growth factor receptor α
PenStrep	penicillin-streptomycin
pF	picofarad
PFA	paraformaldehyde
PLP	proteolipid protein
PM	plasma membrane
pmol	picomol
pp(PP)	perforant pathway
psi	pound-force per square inch
px	pixel
Q	charge (Coulombs)
R	resistance (Ohm)
R_m	membrane resistance
r.m.s.	root mean square
RNA	ribonucleic acid
ROI	region of interest
RPMI	Roswell Park Memorial Institute medium
R_a (R_s)	Access resistance (series resistance)
RT	room temperature
SC	Schaffer’s collaterals
SD	standard deviation
s	second
SEM	scanning electron microscope
SLM	stratum lacunosum moleculare
SM	stratum moleculare of the dentate gyrus
SR	stratum radiatum
TRITC	Tetramethylrhodamine
TEM	transmission electron microscopy
TTL	time to live
µ	micro
V	volt
Vhold	holding potential
YFP	yellow fluorescent protein

1. Introduction

1.1.1 Central nervous system and cell types

The central nervous system consists of the brain and the spinal cord. The brain is divided into multiple regions according to the morphology and functions of the substructures. The tissues of the brain are classically divided into white and grey matter. The distinction comes from the content of myelin – a fatty substance that is used to insulate the conducting axons of nerve cells and increase the speed of action potential propagation. Tissues with more myelin appear white, while the tissues where there is less myelin appear grey. White matter is specialized around signal transduction and consists mainly of axonal fiber tracts, while grey matter houses bodies of neurons and allows for close interactions between many neurons, which results in multiple neuronal functions such as computation, memory formation and cognition. Processes of neurons in white matter do not contain myelin themselves – instead, they are wrapped into extensions of other kind of cell – the oligodendrocyte, which contains the myelin. There are multiple types of cells found in the brain, and, besides the tissues which belong to the vascular system, all cells of the brain are typically classified into neurons and glia. Neurons themselves are represented by multiple subtypes distinct in function, morphology, role in the network, genetic and proteomic profiles, and so on. The glial cells are typically divided into astrocytes, oligodendrocytes and microglia, with 4th type of glia – the NG2-glia – being grouped out of astrocytes relatively recently. Only neurons are known to produce action potentials – the kind of excitation which supports the transfer of signal across one neuron towards a synaptic connection with the next neuron. The neurons connect to each other using synapses – chemical junctions that can be modulated - and form networks. Neurons are believed to be largely sedentary in a mature brain, because of the importance of stability of networks that they create.

The astrocytes, the most abundant type of glia, were previously thought of as predominantly the structural support element of the brain – therefore the term glia, “glue” – but their functions are far more numerous and diverse. Astrocytes form their own network by connecting to each other using gap junctions – special channels that permit the flow of materials across many astrocytes. They enable the transfer of nutrients from the blood to the neurons, and removal of metabolic waste in the opposite direction, and

control the oxygen pressure in the tissues. Astrocytes also modulate the network of neurons by increasing or decreasing the uptake of extracellular neuromediators that they collect in the vicinity of synapses. Tight interaction of at least three cells – presynaptic neuron, postsynaptic neuron, and an astrocyte – around a synapse is known as tripartite synapse (Araque et al., 1999).

Microglia is a class of resident immune cells of the brain. Since brain is immune privileged organ, it is shielded from the immune cells of the rest of the body, which are not allowed to travel to the brain and act there under normal circumstances. This is due to critical importance of the brain cells for survival of whole organism. There are two general phenotypes of microglia, ramified and amoeboid, with some forms in between (Karperien et al., 2013). The ramified microglia is considered the default, “resting” state of cell, and amoeboid form is the result of cell’s activation. Ramified microglia resembles other types of brain cells by being stellate in shape. Both forms are highly motile. Microglia travels through the brain tissue and surveys the immunological profile of surrounding cells. It also consumes atypical substances, viruses, dead cells, parts of living cells, breaking them down into soluble components (Bachiller et al., 2018). Other notable function of microglia is synaptic pruning (Paolicelli et al., 2011).

Oligodendrocytes are the kind of cell that is specifically tasked to maintaining long-distance connectivity of neurons (Simons and Nave, 2016). The longest axon of a neuron can extend up to a meter in length in human. This is a lot compared to size of neuron’s body, which is usually below 30 μm. Moving all materials and nutrients along the whole length of an axon to and from the neuron’s body is very time- and energy-consuming. Oligodendrocytes provide protection for the delicate axons along the whole length of each of the processes, they also maintain the favorable conditions inside myelin sheath (Frühbeis et al., 2013). Myelin insulation dramatically speeds up the passage of action potentials along the axon without increasing the axon’s diameter. Loss of myelin is a symptom of a group of neurological disorders that typically lead to neurodegeneration.

The NG2-glia is a peculiar kind of glial cell that was first thought of as an unusual glia that has both neuronal and glial properties (Stallcup, 1981; Wilson et al., 1981). It bears features which link it to all the other kinds of cells: its membrane channels resemble that of a neuron and it is able to form synapses as a receiving cell (Bergles et al., 2000), yet

it itself is not able to fire an action potential like a neuron. It can even differentiate into an astrocyte in some conditions (Raff et al., 1983) – but the NG2-glial cell doesn't have gap junctions and does not form a coupled network. It moves through the tissue (Fok-Seang et al., 1995; Hughes et al., 2013), like a microglial cell, surveying the surroundings with motile processes (Haberlandt et al., 2011), although its movement is slower and the cell is not known to have phagocytic activity. NG2-glial cell is known to be a lineage predecessor to oligodendrocytes (Hill and Nishiyama, 2014), however it is as common in the grey matter, where oligodendrocytes are few, as it is in white matter, where the oligodendrocytes are many. The NG2-glia is discussed further in more detail.

1.1.2 Hippocampus

The hippocampus is a popular structure to study in neuroscience thanks to its features. It is exhaustively studied in terms of morphology across many species. The edges of the hippocampus are easy to define thanks to its location in the brain. The internal connectivity of hippocampus was likewise described to high detail, thanks in large to Dr. S. Ramon Y Cajal (1893). Importantly, compared to other regions of the brain, the hippocampus is relatively well-understood in terms of function and information flows that come in and out of it. It was early recognized as a hub for afferent information from multiple sensory systems (Papez, 1937). Since the mid-20th century hippocampus is known to be critical for formation of new declarative memories, since the subject who had both sides of this hippocampus damaged developed anterograde amnesia, but also did not lose the memories that were already formed before the loss of structure (Scoville and Milner, 1957). The hippocampus is also critical for recalling of the consolidated memory which is believed to be stored in the cortex. More recently, with the discovery of place cells it was found to be involved in spatial navigation, maintaining what can be described as a cognitive map of a known area (O'Keefe and Nadel, 1978).

The hippocampus in mouse has a complex three-dimensional shape which resembles curved horns or two banana fruits joined together at one end (medially and forward – the septal part) and spreading out into temporal lobes at the free ends (temporal part). The shape on each side is actually a bundle of similarly-shaped longitudinal structures all curving together. The structures are: the dentate gyrus (DG), which connects through the mossy fibers to CA3. CA3 is connected to CA1 through Schaffer collaterals. One cell

in DG can project to multiple cells in the target area. The projections between the areas are unidirectional. The information enters the hippocampus from entorhinal cortex, different layers of which project into DG, CA3 and CA1 parts of hippocampus. Each of parts mentioned (DG, CAs) has few distinct layers, one of which is densely packed with neuron bodies. The thicker neuronal layer in the DG is called the granular layer, forming a triangular cord tightly packed with neuron bodies (also known as granule cells) that curves along each hippocampus length, while the thinner neuronal layers in CA1-CA3 are called pyramidal layers, and form somewhat thinner bands of tightly packed pyramidal neurons that also follow the shape of hippocampus. These neurons receive and send out information from and to the entorhinal cortex (and, ultimately, to and from all the other areas of the brain), they provide the hippocampus function. The hippocampus is considered to be grey matter, since the number of myelinating oligodendrocytes there is relatively low. Different cuts through brain (along the transverse, frontal/coronal or sagittal planes) would create different anatomical pictures of the hippocampus, with internal structure being most visible in coronal or transverse cuts (Fig. 1).

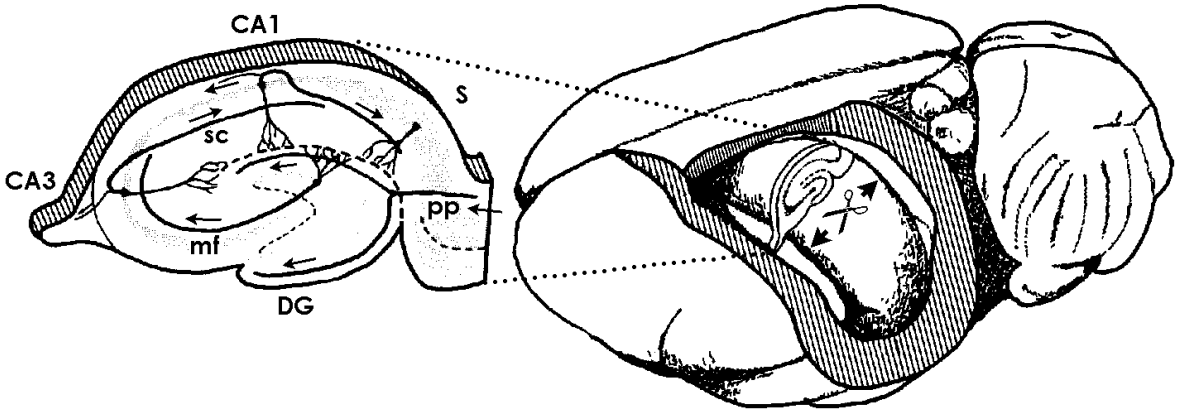

Fig. 1 Hippocampus anatomy and basic connectivity. Adapted from Amaral and Witter (Amaral and Witter, 1989). Rat brain, with olfactory cortex and part of the cortex above left hippocampus removed. S – septal part, CA – cornu ammonis, DG – dentate gyrus, mf - mossy fibers, pp – perforant pathway, sc – Schaffer's collaterals.

1.1.3 NG2-glial cells

Historically, among different authors NG2-glial cells were (and still are) referred to by many names, each reflecting the developing understanding of their function and the dominating idea about the potential overall purpose of those cells. To this day, there is

no universal consensus, largely because it is not known just how heterogeneous NG2-glia really is.

Initially, NG2-glia was regarded as a population of glial cells with some neuronal features. The characteristic electrophysiological whole cell current pattern of NG2-glia led to its classification as “complex” astrocytes. In contrast, astrocytes with voltage independent, linear whole cell current patterns and very low input resistance were termed “passive” astrocytes. The latter expressed glial fibrillary acidic (GFAP) protein, had endfeet at blood vessels and formed huge functional syncytia via extensive gap junction coupling. “Complex” astrocytes showed higher membrane resistance, no gap junction coupling (Steinhaüser et al., 1992; Steinhäuser et al., 1994; Wallraff et al., 2004) and comparatively little GFAP mRNA with lack of fully assembled GFAP protein (Jabs et al., 2005).

Parallel research into newly discovered neuron-glial-2 (NG2) membrane chondroitin sulfate, first found on non-neuronal rat brain tumor cells, linked NG2 to the population of oligodendrocyte precursor cells (OPCs) (Stallcup and Beasley), which were found to differentiate into oligodendrocytes *in vitro* and *in vivo*. OPCs and “complex” astrocytes shared similar electrophysiological properties, antigen profiles and lack of gap junction coupling (Nishiyama et al., 2009).

Today, “passive” astrocytes are generally regarded as *bona fide* astrocytes, while the clear distinction between “OPC”s and “complex astrocytes” was never defined. The term “complex astrocyte” fell into disuse, hinting at the general agreement that the “OPCs” and “complex astrocyte” are two overlapping cell categories (Bergles et al., 2010). The terms OPC/OLP (with precursor/progenitor used interchangeably), polydendrocytes (Nishiyama et al., 2005, 2009), synantocytes became colloquially associated, with differential usage emphasizing what different authors see as more important – morphology, function, cellular fate, or, in case of “NG2-glia”, the membrane markers of a particular glial cell. It should be noted that NG2 is expressed on other types of cells within body – in kidneys, for example – and in the brain itself, besides glial cells, it is also expressed on morphologically distinct pericytes, which belong to vascular system. Considering this and the fact that the oligodendrocyte differentiation may not be the only fate for NG2-cells, this cell population should be more precisely referred to as “NG2-glia”. It is still important to state that the multitude of existing terms to describe what may

conveniently appear as a single cell population, in reality may reflect an unknown degree of heterogeneity of this cell type.

The evidence for heterogeneity of NG2-glia comes from spatially and temporally distinct locations of origin of NG2 marker in the mouse brain and spinal cord, as well as from several studies suggesting that different NG2-glia populations can differentiate not only to oligodendrocytes, but also to astrocytes (Zhu et al., 2008) and even neurons (Kondo and Raff, 2000). Evidence against heterogeneity includes morphological and immunological similarity of NG2-glia at different locations and the observation that NG2-glia from either proliferating source, given enough time, will likely repopulate all of the brain tissues, even if one of the sources is ablated (Kessaris et al., 2006). Transplantation of NG2-glia taken from grey and white matter, into white or grey matter, with comparative study of tendency to differentiate into oligodendrocytes and form myelin sheaths, again, suggests intrinsic dissimilarity. Cells derived from grey matter exhibit slower and/or less efficient myelination in white or grey matter environment, compared to cells derived from white matter, which are more efficient in both (Viganò et al., 2013). Relative contribution of particular lineage and local environment factors to those differences is a matter of discussion.

NG2-glia exhibit impressive motility. Multiple radial processes contact other glial and non-glial cells, and reorient constantly (Haberlandt et al., 2011). In the adult cortex, some NG2-glial cells demonstrate continuous migratory behavior with a speed of about 2 μm per day. This perhaps illustrates the described capacity for repopulation of large volumes of tissue. Other cells are stable for several days, weeks or maybe even longer. The movements are likely guided by local cellular interactions rather than some global cues, however, it results in a complete change of the microscopic picture on a scale of weeks to months (Hughes et al., 2013). Proliferation, differentiation and death of cells provide a continuous reshaping of NG2-glial in a grid-like pattern that is formed by repulsion between individual NG2-glia and migration towards areas recently deprived of NG2-glia “coverage”. Overall, it appears that NG2-glia actively maintains a certain slightly varying but diffuse density in different brain regions, with most, if not all, cells possessing the ability to proliferate and migrate.

The mobility and capacity for proliferation of NG2-glia is further increased under pathological conditions. Adult and postnatal NG2-glia shows increased proliferation, hypertrophy and migration in acute cortical injury. The extent of reaction, assessed by the amount of demyelination or trauma, is described in the range from “stereotypic” (Boda and Buffo, 2014) to “different” (Dimou and Gallo, 2015). Overall, early postnatal NG2-glia appears to have more plasticity than adult NG2-glia, but the question of heterogeneity still persists. More studies are required to determine if different subpopulations of NG2-glia respond differently to acute injury, hypoxia, etc. It is especially important in the context of current interest to NG2-glia as potential renewable source of autologous cells to regenerate white matter injury, or, perhaps, even neuronal damage (Egawa et al., 2020).

NG2-glia also features one of the most curious aspects of this cell type – synapses with presynaptic neurons (Bergles et al., 2000; Jabs et al., 2005; Lin and Bergles, 2004).
In a spatial sense, neurotransmitter can affect NG2-glia either via ambient level, caused by spillover from neighboring synapses, or by direct synaptic innervation. NG2-glia cells were found to be sensitive to neurotransmitters. Prolonged exposure to high ambient levels of glutamate led to excitotoxic degeneration of cells. Lower levels of glutamate, in a reversible manner, prevented NG2 cells from differentiating into oligodendrocytes (Bergles et al., 2000).
The transmitters were also found to act directly at postsynaptic receptors expressed on surface of NG2-glia (Bergles et al., 2000; Jabs et al., 2005). Electron micrographs demonstrated synaptic structures on processes of NG2-glia, complete with presynaptic vesicles and postsynaptic densities. Symmetric and asymmetric types of synapses were also described (Bergles et al., 2000; Haberlandt et al., 2011; Lin and Bergles, 2004). Functional parameters of neuron-NG2-glia synapses resemble those of neuronal synapses. Subsequent studies confirmed that recorded events originate from true synapses. Evoked and spontaneous excitatory postsynaptic currents (EPSCs) from glutamatergic and GABAergic presynaptic terminals were observed in NG2-glia. The delay between presynaptic action potentials and post-synaptic responses mimic the time course of neuronal synaptic communication. A single action potential is enough to reliably evoke EPSCs in NG2-glia. Repetitive stimulation facilitates responses and is

reliable on larger timescale, which indicates the presence of stable synaptic machinery. EPSCs with fast dynamics were observed in both young and mature animals. Synaptic innervation has been observed throughout all developmental stages and in all brain structures tested so far, including the hippocampus, cerebellum, brainstem nuclei, and white matter of *corpus callosum*. In the latter contacts are formed predominantly with sparse unmyelinated axons of cortical neurons. It is not known what initiates synapse formation, and whether they are formed by NG2-glia seeking neurons or vice versa. The former appears more likely, given high motility of NG2-glia, and the observations that NG2-glia is usually innervated by axon collaterals. In this respect NG2-glia is rather a “bystander” in an axo-dendritic junction, receiving input near the synaptic bouton or further up the axon length at a synapse-like axonal varicosity (Bergles et al., 2010; Kukley et al., 2007). It is unknown if a type of neuron and/or particular transmitter acting upon an NG2-glia leads to some kind of feedback, especially in case when a single NG2-glial cell synapses with several neurons of different types.

The impact of synaptic innervation of NG2-glia is unclear yet. The mostly non-overlapping grid-like coverage of different brain areas may serve to survey cellular environment. It may also, together with chemical cues, help to evaluate the requirements of local axons in terms of oligodendrocyte differentiation and myelination. In this case, for example, a functional synapse may provide spatial information for differentiating NG2-glia. It could indicate the location of an axon awaiting myelination. Alternatively, axons that specifically should not be myelinated can signal a certain pattern or level of activity (Barres and Raff, 1993). Such information may be important, together with other cues, for a mechanism that defines the limits of grey and white matter in the brain.

It should be noted that functional synapses are rapidly lost by NG2-glia once it commits to oligodendrocyte differentiation pathway. Therefore, if some pattern of synaptic signals conveys axons request for myelination, it should trigger a reaction that can proceed without additional electric cues for at least few days after NG2-glia downregulates the NG2 protein and before it begins myelination (Kukley et al., 2010). It also appears that the degradation of synaptic machinery first begins on the presynaptic neuronal side. It is unlikely that this event represents the trigger for differentiation of NG2-glia into

myelinating oligodendrocytes. Instead, the dismantling of synapses by a neuron is more likely a response to feedback from an NG2-glia, informing the connected neuron about an upcoming differentiation (Kukley et al., 2010).

Sakry et al. (Sakry et al., 2014) suggested an activity-dependent feedback mechanism between NG2-glia and neurons. Central role was ascribed to an enzymatically cleaved, soluble fragment of the NG2 proteoglycan ectodomain. Lack of this NG2-fragment reduced NMDA receptor-mediated LTP and altered AMPA-, but not NMDA receptor structure. This has been shown by pharmacological downregulation of an enzyme capable of cleaving NG2 protein, and in NG2(-/-) animals.

Another possible function of neuron-NG2-glia synapses is the regulation of extracellular vesicular transport. It is believed that virtually all cells in nervous system can release vesicles in one form or another. Vesicles may contain different cargo, such as mRNA, proteins in various assembly stages, neurotransmitters and nutrients – as well as toxins or viral particles (Colombo et al., 2014; Zappulli et al., 2016). Extracellular vesicles are thought to be involved in different mechanisms – ranging from waste disposal to nutritional support of neighboring cells, to intercellular messaging and immune response. It was reported that, in particular, oligodendrocytes employ exosomes to deliver substances acting in benefit of associated axons (Frühbeis et al., 2013). Particles of around 100 nm in diameter were released both inside and outside of periaxonal space in response to glutamate or glutamate receptor agonist. The vesicles were internalized by microglia and neurons, and only rarely – again by oligodendrocytes. While microglia apparently degraded the vesicles, neurons responded with increase in resistance to oxidative stress and starvation, suggesting a general neuroprotective role of vesicle cargo.

1.1.4 Extracellular vesicles and exocytosis

The topic of extracellular vesicles and exosomes in particular is inseparably associated with the exosome biogenesis, which is currently believed to be accommodated by the cell's endocytic pathway. Of several possible types of extracellular vesicles that may originate from cell, such as ectosomes/microvesciles, apoptotic bodies, viral particles, the exosomes are defined in large part by the mechanism of generation. Currently, the term extracellular vesicle (EV) is commonly used to refer to a bubble of cytosol that is

delimited by a lipid bilayer, with the size of few tens of nanometers to over a thousand. The content of the vesicle is believed to reflect the parameters and/or the state of the cell of origin (Akers et al., 2013; Colombo et al., 2014). The lipid bilayer is what distinguishes EVs from micelles, which are lipid monolayer vesicles. The list of different names that were given to different EVs by the researchers is too long to recount; the naming may follow the size of the vesicle, the bodily fluid of origin, the purported function. Currently, the nomenclature based around the mechanism of generation of vesicle is widely accepted. The definition of exosome as a vesicle of endosomal origin released by fusion of multivesicular endosome or multivesicular body (MVB) with plasma membrane (PM) was coined by Johnstone et al. (Johnstone et al., 1987) in 1987. The definition stands today, with associated implied size of resulting exosomes in range of 30-100 nm. It is, however, non-trivial to distinguish different types of EVs in experiments, as there is no single feature that would precisely distinguish one type from another.

The function of exosomes was initially thought to be a mean for cell to dispose of unwanted components. With time, however, other functions were ascribed to exosomes, for example a role in immunopresentation (Raposo et al., 1996), immune response to tumors (Théry et al., 2001), and other components of immune system, but also to cell-cell communication. A body of knowledge regards exosomes as critical for normal development of the brain in embryogenesis and in tissue regeneration (Zappulli et al., 2016). The replication of exosome-transported mRNA in target cells is another important function of exosomes (Valadi et al., 2007) that was recently described.

The endocytic pathway is one of the basic systems at the origins of cellular life. The operation and staging of pathway is controlled by multiple highly-conserved proteins and requires energy at every step. The pathway initiates with the inward budding of plasma membrane, which can be mediated by several different systems, such as caveolae, clathrin family of proteins, due to phagocytosis or pinocytosis. The resulting sack of membrane with its content then detaches from plasma membrane and becomes an early endosome. The endosome then undergoes maturation, during which its membrane is modified with receptors and proteins, and the content may be altered. Fate of the vesicle can vary, depending on the endosome content or cell's metabolic requirements. Simplified, there are three possible outcomes for the endosome's membrane. The segment of plasma membrane which constitutes the endosome wall can be either broken down to soluble components in enzymatic hydrolysis in a lysosome, it can be

reincorporated back into cell's plasma membrane, with or without modification, or it can undergo further internal budding and form intraluminal vesicles inside a late endosome. The endosome with such content would be called a multi-vesicular endosome, or multi-vesicular body (MVB). The fusion of MVB with PM would then cause the intraluminal vesicles to be released from cell to extracellular space, becoming exosomes, however the formation of MVB does not imply the necessary subsequent release of exosomes – the MVB might also fuse with a lysosome, another organelle of the endocytic pathway, and its' content to undergo hydrolysis. What governs the sorting of materials within endocytic pathway in and out of endosomes, and towards extracellular space or to lysosomes is not completely understood at the moment. It is, however, known, that the exosomal release – that is, fusion of a MVB with PM leading to release of MVB content is a controlled process mediated by Ca^{2+} ions (Colombo et al., 2014). Activity of Ca^{2+} ionophores, therefore, can trigger the fusion of MVBs. The activity can also be launched by direct depolarization, external substances or G-coupled receptor activation, due to ion influx through PM or due to release of Ca^{2+} ions from internal storage, or a combination of both.

1.1.5 Preliminary data

Unpublished data from our laboratory suggests that release of exosomes may be involved in a feedback mechanism between NG2-glia and surrounding neuronal network. There is supporting evidence for this hypothesis.

- *In-vivo* experiments with virus-based labeling of individual NG2-glia have shown the presence of a reporter protein in close vicinity of axons of neighboring neurons, but not in the soma (see chapter 5.0 for more details). NG2-glia-derived exosomes may constitute a pathway of activity-dependent feedback from NG2-glia to neurons, with associated exosome content possibly involved in trophic support or organization of extracellular matrix in target axons.
- The NG2-protein itself may be involved in the targeted structures, as it was detected in the exosomal fractions derived from Oli-neu cells (see section 5.2.2. for Oli-neu-related evidence of exosomal function).
- Haberlandt et al. (Haberlandt et al., 2011) observed in a previous study intracellular vesicles in time-lapsed micrographs of NG2-glia located in acute hippocampal slices. Individual NG2-glia cells were loaded with Alexa-594 during whole-cell recording, and imaged 30 min later. Movement of intracellular vesicles,

and elongation and retraction of processes on a time scale of around 200 s were observed in these experiments. The authors described that an intracellular vesicle disappeared between two stack recordings i.e. within 43 s. Such an observation may indicate a fusion event. The diameter of the moving intracellular vesicles was estimated to be around 500 nm – that is, within the expected range of an MVB.

The mechanism(s), the cargo, and the possible neuromodulatory effect of NG2-glia derived exosomes may provide clues for the physiological function of NG2-glia in grey matter.

2. Aims of the study

NG2-glial cells is an abundant and widely distributed subtype of glia, featuring properties not typically associated with mature glial cells, such as the ability to receive synaptic input from neurons, or an often discussed degree of multipotency (Nishiyama et al., 2009). Fast information flow from neurons to NG2-glia through synaptic structures was confirmed in several studies (Bergles et al., 2000; Jabs et al., 2005; Passlick et al., 2016). The purpose of such a fast communication, where, apparently no computation is occurring, is unclear. One of the potential functions of the innervation is the initiation of feedback from NG2-glia to neurons. The mode of such feedback is not known yet. It was suggested that neuronal activity through innervation of NG2-glia regulates its differentiation into myelinating oligodendrocytes according to the requirements of the neural circuit (Sakry et al., 2014; Sun et al., 2016). However in grey matter – which features persisting populations of NG2-glial cells together with sparse myelination – function of NG2-glia remains largely unknown. Our preliminary results demonstrate exosome release from Oli-neu cells *in vitro*. The so far identified exosomal cargo includes non-polymerized GFAP monomers and NG2-protein.

The objective of this project is to prove the existence and determine functions of NG2-glial cell-derived exosomes. For this purpose, we combine electrophysiology and imaging techniques to detect exosome-related events and to characterize exosome morphology. Initially, the project was carried out on cultured model cells. Later it was supplemented by analysis of NG2-glia in acute brain slices. This work may provide a better understanding of the enigmatic functional relationship between NG2-glia and neurons, and give clues about their role in grey matter signaling.

Specific aims of the project include

1. Search for functional evidence of exosomal release from NG2-glial cells using high resolution membrane capacitance recording techniques:
    a. Implementation of membrane capacitance recording techniques and their application to NG2-glial cells in different preparations
    b. Determine whether the resolution is sufficient to detect MVB-PM fusion events in NG2-glia
    c. Find evidence for membrane fusion events in NG2-glia
2. Search for morphological evidence of exosomal function of NG2-glial cells using combined immunofluorescent and electron microscopy approaches
    a. Using an immunofluorescence approach, with a set of immunological markers to determine the candidate structures for MVB
    b. Verify the candidate structures using electron microscopy
    c. Attempt to influence the candidate structures using pharmacological or genetic approaches

3. Materials and Methods

3.1 Devices, chemicals and software

3.1.1 Devices and materials

Osmometer (Vescor Vapor Pressure Osmometer 5520)

pH meter (Knick pH-meter 766 Calimatic)

Vibratome (Leica VT1200S)

Microscope and illumination system (Nikon FN1 Eclipse, Sumita LS-DWL)

Electronic amplifier with headstage (HEKA EPC-10 USB)

Manipulators (Narishige MHW-3, Luigs & Neumann SM-6)

Thermal control unit (Luigs & Neumann Temperaturcontroller VII)

Pump (Ismatec ISM930C)

Pipette pullers (Sutter Instruments P-97, Zeitz Instruments DMZ Zeitz-Puller)

Glass pipettes – Borosilicate glass GB150F-10 or GB150-10 (Science Products, Hofheim, Germany)

Leica TCS SP8 confocal microscope (Leica)

ASTEC MICROFLOW Biosafety cabinet, Class II, S/N: 97(1?)/03/2/002

HERAcell® 240 CO2 Incubator

Centrifuge (Heraeus Labofuge 400)

Sylgard 184 (Dow Corning)

3.1.2 Chemicals

D(+)-Glucose anhydrous (A1422,1000) (ITW Reagents)

D(+)-Sucrose for cell culture (A2188,1000) (ITW Reagents)

Potassium chloride (A1039, 1000) (ITW Reagents)

Sodium chloride for molecular biology (A2942,1000) (ITW Reagents)

Sodium hydrogen carbonate (A1940,1000) (ITW Reagents)

Magnesium sulfate heptahydrate (A6414,1000) (AppliChem)

Magnesium chloride hexahydrate (A1036,0500) (ITW Reagents)

Sodium di-hydrogen phosphate anhydrous (122018.1211) (Carl Roth)

Disodium hydrogen phosphate anhydrous (Carl Roth)

Sodium azide (Carl Roth)

Gramicidin (50845, q5002) (Sigma-Aldrich)

Gramicidin-A (Sigma Aldritch)

Carbogen (Linde CarbogenLab)
Isoflurane (Piramal Healthcare Isofluran-Piramal 250 ml)
PFA (ITW Reagents)
Ketamine (WDT, 10 %) + Xylazine (Bayer Rompun 2 %)
Poly-L-lysine (Sigma P9155-5MG)
RPMI Medium 1640(1X) (21875-034) (Gibco)
DMEM High Glucose (Gibco)
N-2 supplement (100x) (Invitrogen)
Antibodies (see below)
Acetone (Merck KgaA, Darmstadt, Germany)
Methanol (Carl Roth, Karlsruhe, Germany)
L.A.B. Solution (Liberate Antibody Solution) (24310-500) (Polysciences, Inc.)
Triton X-100 (T9284-500ML) (Sigma-Aldrich)
Hoechst 33342 (1 mg/ml frozen stock, Thermo Fischer Scientific)
Aqua-Poly/Mount (18606-20) (Polysciences, Inc.)
Normal horse serum (Thermo Fischer Scientific)
Normal goat serum (S26) (Merck KGaA)

3.1.3 Specialized software

Patchmaster v2x90.5 (HEKA Elektronik)
Tida 5 (HEKA Elektronik)
Igor Pro 7 (WaveMetrics, Lakes Oswego, USA)
Imaris 7.6.5 (Bitplane)
Fiji/ImageJ v1.53i (Wayne Rasband and contributors, NIH USA)
LAS X suite (Leica)
RStudio v.1.4.1106 (RStudio, PBC)
Zotero v.4.0.29.17
GPower 3.1.9.7

3.1.4 Antibodies used

First antibodies:

rat	anti- NG2	Invitrogen	MA524247
rabbit	anti- Flot1	Abcam	ab133497
rat	anti- CD63	BioLegend	143902
rabbit	anti- Alix	Abcam	a88388
goat	anti- Iba1	Abcam	ab5076
chicken	anti- GFP	Abcam	ab13970
rat	anti- CD68	Serotec	MCA 1957
mouse	anti- APC(CC1)	Calbiochem	OP80

Second (dye-conjugated) antibodies:

Alexa 405	donkey anti rabbit	Abcam	ab175651
Alexa 405	donkey anti rat	Abcam	ab175670
Alexa 488	goat anti chicken	Invitrogen	A11039
Alexa 488	goat anti rat	Invitrogen	A11006
Alexa 488	donkey anti rabbit	Invitrogen	A21206
Alexa 555	goat anti rat IgG	Molecular Probes	A-21434
Alexa 555	goat anti rabbit IgG	Molecular Probes	A-21429
Alexa 594	donkey anti goat	Molecular Probes	A-11058
Alexa 594	goat anti chicken	Invitrogen	A11042
Alexa 594	goat anti rat	Invitrogen	A-21213
Alexa 594	goat anti rat	Invitrogen	A11007
Alexa 647	goat anti mouse	Molecular Probes	A-21235
Alexa 647	goat anti rabbit	Invitrogen	A-21244
Alexa 647	donkey anti goat	Invitrogen	A21447
Alexa 647	goat anti rat IgG	Molecular Probes	A-21247
Cy 5	donkey anti rat	Jackson	712-175-150

3.2. Solutions

Solutions involved in patch-clamp experiments are usually different between different laboratories, even when tasked towards similar applications. In general, the extracellular solution is designed to mimic the extracellular fluid with relatively high concentration of NaCl between 125 and 160 mmol/L, and relatively low concentration of KCl, usually between 2 and 5 mmol/L, but sometimes up to 10 mmol/L. $CaCl_2$ concentration is between 1 and 2 mmol/L, glucose between 5 and 25 mmol/L, Mg^2+ ions are usually present between 0.5 and 1 mmol/L. Sucrose is used to adjust the osmolarity of solutions to 290-310 mOsm/L. Carbogen aeration of the solutions based on carbo-phosphate buffer is considered the best option. In other cases, e.g. when analyzing freshly isolated cells, HEPES-based ACSF is an alternative.

Carbogen is a gas mixture of 95 % O_2 and 5 % CO_2 that is often used in neuroscience laboratories. In cell culture, pure CO_2 is typically injected into cell culture incubators. Maintaining 5-10 % CO_2 atmosphere, as is the case with aerated ACSF, is intended to set the pH of solutions or cell culture media to physiological value of 7.38-7.4. In patch-clamp experiments, solutions are continuously delivered to the recording chamber at a rate of 0.5-1.5 ml/min, where the tissue or cell culture is immersed in the flowing ACSF.

3.2.1 Normal Artificial Cerebrospinal Fluid (nACSF):

Substance	Molecular weight [g/mol]	Concentration [mM]	1L [g]
NaH_2PO_4	120.00	1.25	0.15
NaCl	58.44	126	7.37
KCl	74.56	3	0.22
$MgSO_4$*7H2O	246.50	2	0.49
$CaCl_2$*6H2O	219.09	2	0.44
Glucose	180.20	10	1.8
$NaHCO_3$	84.01	26	2.18

Osmolarity is adjusted to 305-315 mOsm with sucrose, pH to 7.38-7.4 with 1 M HCl and carbogen aeration.

3.2.2 High Sucrose Artificial Cerebrospinal Fluid (preparation solution, hsACSF):

Substance	Molecular weight [g/mol]	Concentration [mM]	1L [g]
NaH_2PO_4	120.00	1.25	0.15
NaCl	58.44	126	7.37
KCl	74.56	3	0.22
$MgCl_2$*6H2O	246.50	2	0.49
$CaCl_2$*6H2O	219.09	2	0.44
Glucose	180.20	10	1.8
$NaHCO_3$	84.01	26	2.18
Sucrose	342.30	50	17-20

Osmolarity is adjusted to 330-340 mOsm with sucrose, pH to 7.38-7.4 with 1 M HCl and carbogen aeration.

3.2.3 10x Phosphate buffer (10xPBS):

Substance	Molecular weight [g/mol]	Concentration [mM]	1L [g]
NaH_2PO_4	120.00	17	2.04
NaCl	58.44	1500	87.6
NaH_2PO_4*2H2O	74.56	83	14.77

pH is adjusted to 7.38-7.4 with 1 M HCl and 1 M NaOH. The working concentration of 1xPBS is achieved by adding 900 ml of distilled water to 100 ml of 10xPBS. Solution forms crystals when stored at 4 ºC. The phosphate buffer was used in labeling experiments; for cell culture a commercial sterile 1xPBS was used.

3.2.4 Internal solution (artificial intracellular solution):

Substance	Molecular weight [g/mol]	Concentration [mM]	In 100 ml [g]	1 mM [g/l]
KCl	74.55	130	0.9692	0.0746
$MgCl_2$	203.31	2	0.0407	0.2033
$CaCl_2$	219.09	0.5	0.0110	0.2191
BAPTA	476.44	5	0.2382	0.4764
HEPES	238.30	10	0.2383	0.2383

Intracellular (internal) solution usually has relatively high concentration of K^+ ions, but other components vary according to the research goal. Internal solutions often contain ATP and a buffer system which does not require maintaining pH with carbogen aeration. Internal solutions are thoroughly filtered and are kept frozen prior to use; during the day internal solutions are kept on ice in small aliquots. Typical loading volume is 10-15 µl. The osmolarity of internal solution is expected around the value of 260-270 mOsm/L; pH is expected to be slightly more acidic than that of the external solution.

3.2.5 Gramicidin solution for perforated patch

Gramicidin (shipped dry, 5 mg) was diluted in DMSO (100 µl), aliquoted to 10 µl and frozen (26.563 mM). For adding to 500ul of internal solution, 1 or 0.5ul of DMSO stock was used, making a 1:500 or 1:1000 dilution (to keep DMSO content relatively low). Internal solution was then sonicated and centrifuged, since gramicidin does not dissolve well in aqueous solutions. Working concentration at the pipette tip was expected to be between 50 to 100ug/ml.

3.2.6 4 % Paraformaldehyde (PFA) solution:

1. Warm 800 ml of distilled water to under 60ºC
2. add 40 g of dry paraformaldehyde; solution becomes opaque
3. add one pellet of dry NaOH; wait for solution to become clear
4. add 100 ml of 10xPBS
5. adjust pH with 1 M HCL and 1 M NaOH
6. add distilled water to 1000 ml mark

Solution is stored at -20ºC and is used at 4ºC. Since the solution is toxic, it is to be stored, handled and disposed of separately from other solutions (using fume hood, designated vessels, scales, spoons and pH-meters) while using personal protection. In the electron microscopy experiments, 4 % PFA solution was supplemented with 0.5 % glutaraldehyde.

3.2.7 Borate buffer:

0.1 M Borate buffer was prepared by adding 1.24 g boric acid and 1.9 g sodium tetraborate in 400 ml water, pH 8.5 (adjusted with NaOH for no less than 30 minutes).

3.2.8 Poly-L-lysine solution:

Working concentration is 0.1 mg/ml in borate buffer. Usually stored as x10-40 stock in 4ºC. Poly-L-lysine is usually lyophilized on shipping – to get to the working concentration it was resuspended with borate buffer to x10 with 5 ml (1 mg/ml), and then 1.5 ml of 10x stock was added to 13.5 ml of buffer to get to working concentration. The solution is used to pre-treat the container for improved cell adhesion, in volume that covers the flat surface inside (e.g. 2 ml for 35 mm Petri dish, 8-12 ml for T75, 12-15 ml for T175.). The solution may be reused if aseptic conditions are maintained.

3.2.9 SATO medium:

SATO medium was used to culture Oli-neu cells. The composition includes the following substances and uses DMEM F/12 as base:

N-2 supplement (100x)	5	ml
Insulin (5 mg/ml)	0.5	ml
Tri-iodotyronine stock (0.5 mM)	0.5	ml
L-Thyroxine stock (4 mM)	65	µl
L-Glutamine (200 mM)	5	ml
Pen/Strep (100x)	5	ml
HEPES (1 M, pH 7.3-7.4)	5	ml
	=21	ml aliquot (good for 1x500 ml of DMEM F/12)

The medium is filtered into 50 ml aliquotes and stored at -20ºC until use. After unfreezing the medium was supplemented to 1 % normal horse serum. Aliquots were not re-frozen.

3.2.10 PC12 medium:

Base medium is 1x RPMI1640. The medium was supplemented to 10 % FCS and 1 % penicillin-streptomycin.

3.2.11 Long-term storage medium (liquid nitrogen):

The storage medium includes 45 % base medium (depending on cell type), 45 % inactivated serum (FCS or horse serum), and 10 % DMSO.

3.3. Cell cultures and animal models

3.3.1 BV-2 cell line

To begin establishing the technique of cell membrane capacitance recording, initially a BV-2 cell line was used, kindly provided by Prof. Dr. Walter's research group (Clinic of Neurology, Medical Faculty, University of Bonn). This cell line was derived by infecting a primary culture of mouse microglia with retrovirus, carrying an oncogene (Blasi et al., 1990). The line was selected for initial experiments because microglia was implicated in the observed improvement found in Alzheimer patients who received treatment with statin drugs (Glebov et al., 2015); the benefit incurred may be due to an insulin-degrading enzyme (IDE) being released from microglial cells via an unconventional exosome release pathway.

The cells were incubated in Dulbecco's Modified Eagle Medium (DMEM), supplemented with 10 % Fetal Calf Serum (FCS) and 5 % penicillin-streptomycin (PenStrep) in T75 cell culture containers, in 5 % CO_2 atmosphere, at 38°C and 100 % humidity. The BV-2 cell line was briefly involved in establishing of capacitance recording technique, however, proved difficult to work with in patch-clamp environment, especially for long-term experiments. Being highly motile, the cells exhibited acute aversive/contractile behavior towards a patch pipette in close proximity. Later, a more conventional cell line (PC12) was chosen for establishing the capacitance recording method. Additionally, a transition from an EPC800 electronic amplifier to an EPC9 amplifier was made, since the latter would allow full digital control of amplifier functions, which was necessary for capacitance recordings.

3.3.2 PC12 cell line

PC12 cells are a cell line of adrenal pheochromocytoma, derived in 1976 from adrenal medulla of a rat by Greene & Tischler (Greene and Tischler, 1976) (for review - (Westerink and Ewing, 2008)). It's an easy to incubate cancer cell line which is used extensively as a model for neurosecretion. PC12 cell line is a popular alternative to bovine chromaffin cells (usually obtained from slaughterhouse sources) and rat chromaffin cells obtained from rat/mouse. Being a cancer-derived cell, it is not equal to chromaffin cells in parameters of exocytosis. For instance, the content of catecholamines appears to be lower in PC12 compared to wild type chromaffin cells. The exact ratio varies from culture to culture. Vesicle size was found to be smaller in PC12 cells compared to wild type chromaffin cells (Schubert, 1980). The main cargo of vesicles is dopamine. Mathematical modeling on amperometry data suggests that the content of catecholamines is stable across different vesicles but their radius varies (Wightman et al., 1991). It is believed that PC12 cells produce at least two different classes of vesicles that differ by cargo content at least twofold (Westerink, 2000).

PC12 can be differentiated by NGF to resemble neurons a bit more. PC12 cells grow longer processes and appear rather polygonal than round, compared to undifferentiated cells with roundish bodies and small processes. This seemingly affects the localization of release sites, moving them towards the processes rather than soma. Upon differentiation, reduction in variation of vesicle size and cargo load was reported, as well as increase in vesicle size.

PC12 cells can also be differentiated using dexamethasone to make cells appear more chromaffin-like. The culture becomes more responsive to Ca^{2+}-related events. Cell responsiveness and event frequency per cell increase, catecholamine content also is believed to increase. The amount of potentially releasable vesicles increases as well, and vesicle sizes become more uniform (Westerink, 2000)

Chemical-induced exocytosis is also possible. Upon application of nicotine, the nicotinic acetylcholine receptors (nAChRs) create inflow of Na^{+} which causes depolarization, which in turn affects voltage-sensitive Ca^{2+} channels and allows influx of Ca^{2+} (Stallcup, 1979). Application of muscarine enables exocytosis by intracellular second messengers that release Ca^{2+} from intracellular storage (Berridge and Irvine, 1984). Rapid depolarization is also possible with KCl application. Catecholamine content is unaltered

by the mode of exocytosis trigger. The latency between application and vesicle release differs between 6 s for KCl, 37+/-5 s for nicotine and 103+/-11 s for muscarine. PC12 cells were incubated in 1x RPMI 1640 medium, supplemented with 10 % FCS and 1 % PenStrep in T75 cell culture containers, in 5 % CO2 atmosphere, at 38°C and 100 % humidity, with medium exchanged every two or three days, depending on confluence. For patch-clamp experiments, the cells were re-settled on individual 15 mm glass coverslips and cultured under same conditions in 35 mm Petri dishes. Poly-L-Lysine pre-treatment for coverslips was not used at all times, since adhesion was found sufficient on clean glass coverslips. The PC12 cells were not additionally differentiated with dexamethasone. During patch clamp experiments, to elicit responses, the cells were directly depolarized with an amplifier voltage step.

3.3.3 Oli-neu cell line

The Oli-neu cell line was conceived in 1995 (Jung et al., 1995) as a tool to study interactions of myelinating oligodendrocytes and their precursors with surrounding tissue. At the time, devising such cell lines promised an alternative for the use of primary cultures of oligodendrocyte precursors. The fine balance between malignant features of underdifferentiated cells and their usefulness in animal models had to be observed. In contrast to an analogous cell line, CG4, which was generated by continuous culturing of rat neuroblastoma cells, the Oli-neu line was created by introducing a hybrid neu oncogene linked with receptor for human epidermal growth factor (egfr-neu) to a primary NG2-glia cell culture of a mouse, using a retrovirus (Jung et al., 1995). The presence of epidermal growth factor (EGF) would control the activation of t-neu tyrosine kinase, thus providing a degree of positive control over oncogenic properties. This feature however requires strict control of culturing conditions. An imbalance in the medium will push the cell line away from oncogen-induced proliferating state towards one of the few potential terminally-differentiated states. These cells resemble astrocytes or oligodendrocytes and decrease the rate of clone proliferation. The Oli-neu cell line is considered as the best *in vitro* model of NG2-glia currently available. It potentially expresses relevant NG2-glia markers such as NG2 proteoglycan, PDGFRα, and Olig2. It interacts with surrounding neurons upon implantation and expands if co-cultured with neurons. The morphology and electrophysiological pattern is also reminiscent of NG2-glial cells located in acute

brain slices. It should be noted that the Oli-neu cell line does not fully recapitulate NG2-glial cell phenotype – which is reflected in incomplete, flawed or absent myelinization that transplanted Oli-neu cells provide in demyelination animal models (Jung et al., 1995).

We previously tested the suitability of Oli-neu cells as a model for NG2-glia. Initially, Oli-neu cells were compared to NG2-glia of acute brain slices preparations from NG2-EYFP or hGFAP-EGFP mice, aged p9-p19. All tested Oli-neu cells expressed the cell type marker NG2 and did not express polymerized GFAP fibers. However, lysate of Oli-neu cells contained monomers of GFAP except the α-isoform, NG2, and miscellaneous proteins involved in exosome release. This includes IDE, Alix, CD63, and Flotillin-1. These proteins were associated with microglia-derived exosomes (Glebov et al., 2015). Confocal microscopy of Oli-Neu cells, optimized for maximal resolution, together with fluorescent immuno-labels demonstrated strong colocalization of Flotillin-1 and IDE both in processes and in soma of Oli-Neu cells, in close vicinity of membrane.

Conditioning media of Oli-neu cells was analyzed for exosomes using differential centrifugation and subsequent western blotting. This revealed co-migration of the exosome-associated proteins in the exosome fraction. Interestingly, we found also a strong signal of NG2 protein and pan-GFAP in the same fraction. We concluded that these proteins are part of the exosome cargo. Immunoblotting analysis of exosomal fraction from Oli-Neu cells also revealed the presence of non-α-isoforms of GFAP in exosomes.

Single-cell RT-PCR of *in situ* NG2-glial cells from hGFAP-EGFP mice were compared to RT-PCR of exosome preparation, pooled from Oli-Neu cell culture. Compared to mRNA content of single astrocyte, no mRNA of α-isoform of GFAP was found in Oli-Neu *in vitro* or NG2-glial cells *in situ*. However, NG2-glia and Oli-Neu cells contained different forms of the non-α-isoform mRNA.

Taken together these preliminary results illustrate that Oli-Neu cells express miscellaneous proteins that are involved in exosome release in microglia. NG2 protein and GFAP monomers were identified as exosome cargo. The Oli-neu cell line was maintained at 10 % CO2 and 37°C and 100 % humidity. The medium used was DMEM (high glucose), supplemented with SATO medium and 5 % PenStrep, which was kept frozen for long-term storage. Before use the medium was also supplemented with 1 %

normal horse serum and sterile-filtered, then stored at +4°C until depletion. The cells were grown in Poly-L-lysine-coated containers and handled on coated coverslips as described above.

To maintain the cells in a proliferative state a careful observation of medium quality is required. If the cells are stressed (pH shifts, starvation, thermal stress) or experience imbalance in the medium composition, the culture may begin shifting towards more differentiated state. Upon electrophysiological observation, a differentiated cell will more resemble an astrocyte or an oligodendrocyte than an NG2-glial cell. Only cells which conformed to electrophysiological criteria of Oli-neu cell were included in the analysis (see Discussion section 5.1.3). With cell culture expansion and after multiple culture passages the proportion of differentiated cells in culture would increase. Careful handling and changing medium on time helps to slow down this progression.

3.3.4 Cell culture maintenance

Cell cultures were maintained in an incubator at 37ºC in a CO_2-rich atmosphere, 5 % for PC12 cells or 10 % for Oli-neu cells. All work on the open containers has been performed inside a biosafety cabinet class II under a laminar air flow. Culture medium was exchanged every 24-72 h for PC12 cells, or every 24-48 h for Oli-neu cells, depending on confluence. After passage, the cells were split onto coverslips and kept in 35 mm Petri dishes inside an incubator until needed.

On the day of experiment, the Petri dish could be safely transported to the electrophysiological recording setup within a reasonable time (several minutes), cover slips were taken out of the Petri dish and placed in the recording chamber. The cover slip was always immobilized with a flattened piece of platinum wire, made in C-shape, weighing down the cover slip from the top.

For long-term storage the cells were lifted from the culturing vessel surface using Trypsin solution, pelleted, washed, and transferred to storage aliquot containing 1:1 of normal serum and culturing medium, with addition of 10 % DMSO. The cells are then exposed to -80 °C in a freezer in a styrofoam container for gradual freezing. Later, cells were transferred into liquid nitrogen for long-term storage.

3.3.5 Glass coverslip preparation for cell culture

For patch-clamp experiments, the cells must be placed in the microscope sample chamber. This was done using 0.13-0.18 mm thick, 12-18 mm (diameter) round microscopy coverslips. The coverslips were prepared by first washing in pure HNO_3 for 24 h, then rinsed in no less than 3L of distilled water, then rinsed in pure ethanol, before being baked at 170ºC for at least 8 hours. After this the coverslips were kept in sterile conditions until needed. For improved cell adhesion, depending on culture requirements, the coverslips were treated with poly-l-lysine solution for at least 30 minutes, and then washed with distilled water.

All animals involved in the project were kept in the “Haus für experimentelle Tiertherapie” (HET) at the University Clinic Bonn under standard housing conditions with a 12/12 hours dark-light cycle. Employed keepers ensured the availability of food and drinking water at all times. Animals used in this project were handled according to the directive 2010/63/EU on the protection of animals used for scientific purposes and national and local government regulations.

3.3.6 NG2-EYFP mouse

This knock-in mouse line was generated in 2008 by Karram et. al (Karram et al., 2008) to address the issue of ambiguous labeling of NG2-glia using anti-NG2 antibodies. Since extracellular domain of NG2 is sometimes cleaved off of the cells and/or potentially deposited elsewhere in the tissue (Nishiyama et al., 1995), the resulting antibody labeling is not always ideal. Additionally, NG2 is expressed not only by NG2-glial cells, but also on the surface of pericytes that surround blood vessels in the brain. This complicates cell identification in thin slices if only NG2 labeling is available (Stallcup, 2002). Pericytes are also highlighted in NG2-EYFP mice, however they are more easily identified.

The mouse line features enhanced yellow fluorescent protein (EYFP) which is synthesized under control of native NG2 promoter. NG2-null mutant animals that each have two copies of EYFP and zero copies of NG2 are viable. The mouse line is maintained by breeding NG2-null mice with wildtype animals of C57BL6J line, or by inbreeding NG2 heterozygous mice. Simultaneous presence of NG2 and EYFP is verified by routine PCR and indicates a heterozygous NG2-EYFP animal, with bands at 900 and 750 bp for NG2 and EYFP respectively. Less than 1 % of cells in heterozygous animals were found to be NG2-positive but EYFP-negative; no cells were found to be NG2-negative while being EYFP-positive (Karram et al., 2008). Another type of NG2-positive cell in the brain – pericytes – also express EYFP in this mouse line. Their distinct shape, size and volume are accentuated by EYFP, making identification easier in comparison to anti-NG2-labeling.

The EYFP does not form intracellular aggregates over the animal lifetime (Karram et al., 2008). The absence of EYFP in the cell populations which express mature oligodendrocyte markers indicates that EYFP is also recycled after its expression is

endogenously suppressed. However some EYFP labeling remains in cells undergoing transition from NG2-glia to an oligodendrocyte, which would also be reflected in cell's electrophysiological profile. It should be noted that NG2-EYFP heterozygous animals possess only one copy of NG2 protein. Any NG2-protein dose-dependent biological process might be potentially affected.

In the present work, heterozygous NG2-EYFP mice were used in electrophysiological experiments with acute brain slices, as EYFP emission allowed for quick and precise identification of NG2-glial cells under a microscope during patch-clamp.

This mouse line was also used in the majority of immunofluorescent labeling experiments since yellow fluorescent protein is cytosolic. This provided best signal-to-noise ratio for identifying NG2-glial cells among the labeling procedures available, especially when it comes to defining shape of NG2-glial cells.

3.3.7 GFAP-tg-EGFP mice

The transgenic hGFAP-EGFP line was derived in 2001 by Nolte et. al (Nolte et al., 2001) to facilitate in-vivo and in-situ physiological experiments in astrocytes. It was generated from FVB/N mice by introducing an EGFP-encoding fragment under the control of the human GFAP promoter. GFAP is a well-characterized marker for astrocytes, where several isoforms are expressed and polymerized to create structural filaments. NG2-glial cells also express some isoforms of GFAP, which are not polymerized. This is the consequence of the lack of the α- subunit that is necessary for polymerization. As the result, there is comparatively limited expression of EGFP in NG2-glial cells of the hGFAP-EGFP mouse line. This is still sufficient to identify NG2-glial cells under a fluorescence microscope when working with an acute slice. The relatively low intensity of NG2-glia fluorescence together with visibly different morphology allows, in most cases, unambiguous identification. The benefit of the hGFAP-EGFP mouse line is that NG2-glia cells express the NG2 protein on the level of wildtype animals. In this project, the hGFAP-EGFP mouse line presented an alternative to NG2-EYFP mouse line as a tool to identify NG2-glial cells.

3.3.8 C57BL6J mice

This is a widely available standard mouse line that represents the unchanged “wildtype” phenotype of mice. This mouse line was used mostly in the immunofluorescent imaging

experiments, where cell identification could be carried out using dye-conjugated antibodies.

3.3.9 NG2-CreERT2 x Rosa26-EYFP mice

An NG2-CreERT2 mouse line was developed by Huang et al. (Huang et al., 2014) to provide more control over the expression of NG2-glia and study its effects at different developmental phases of mouse brain. This mouse line is referred to as “NGCE” in the text. The mouse line is based on Cre-LoxP site-specific recombination technology. In these animals the expression of CreERT2 enzyme is driven by NG2 promoter. The recombinase itself is a fusion of Cre enzyme and human estrogen receptor T2. This provides positive control over Cre activity in the presence of estrogen-like substances, such as tamoxifen. To control the activation of Cre the EYFP reporter was introduced by breeding the CreERT parent animal with Rosa26-EYFP “reporter” mouse, where an EYFP sequence under control of housekeeping Rosa26 promoter is sandwiched between loxP sites (“floxed”). The EYFP is therefore inactive until the loxP sequences are recognized by an active Cre recombinase which removes the stop codons, enabling the expression of EYFP (Srinivas et al., 2001). The NGCE mice begin to express EYFP in NG2-glial cells several days after tamoxifen injection. In a recent work by Dr. A.Timmerman (Timmermann et al., 2021), the expression of Kir4.1 channels was negatively controlled in mice generated from NG2CreERT x Kir4.1 fl/fl pairings. In these Kir4.1 fl/fl homozygous animals, the Kir4.1 channel in the NG2-glial cells is knocked out after tamoxifen injection. The result is the change in passive electrical properties of NG2-glial cells, which can be shortly summarized as the increased excitability in these cells. This change is also coupled with the expression of EYFP. In the text, these Kir4.1 knockout mice are referred to as “Kir4.1 ko” mice.

In this project, these animals were used to try and observe if an increased excitability of NG2-glial cells in Kir4.1ko animals changed the Flotillin-1 immunofluorescent pattern, compared to NGCE animals which should feature normal NG2-glial cell excitability, while expressing EYFP with comparable efficiency. The Kir4.1ko mice in this case can be considered a treatment group, while NGCE animals can act as a control group. Animals in both groups have received a tamoxifen injection prior to experiment (25 or 30 days before perfusion).

3.4. Methods

3.4.1 Electrophysiology

3.4.1.1 Acute brain slices preparation.

Acute brain slices were prepared from previously removed brain for the experiments involving patch-clamp, cell dye-loading, or drug application with subsequent immunofluorescent labeling and imaging. The animals were collected from the animal facility. Artificial cerebrospinal fluid (ACSF) was chilled to ice-cold temperature, and then bubbled with carbogen gas mixture. Two kinds of ACSF were used: normal ACSF (nACSF) and high-sucrose ACSF (hsACSF) with osmolarity increased above nACSF value of 310-315 by 30-40 mOsm/l, by adding sucrose. The carbogen application is necessary to set the pH of ACSF to physiological range of 7.38-7.4, and to supply oxygen to the tissue. Prior to anesthesia application, the mouse is transferred to an enclosed container. Then a tissue dabbed in isoflurane is placed alongside the animal. The evaporating isoflurane is inhaled, leading to quick high-dose anesthesia. The reflexes are checked until no twitching reaction in response to paw pinching occurs, usually few tens of seconds later. The animal is then decapitated with scissors, and brain is extracted into a shallow dish with cold hsACSF, on ice. The brain is then quickly dissected with blade, while submerged in hsACSF. For coronal slices which were used in most experiments, the back side of brain with cerebellum is cut off, then the front 1/3 of cerebrum is cut off and discarded. The remaining tissue is then glued front-side down on the magnetic mounting plate of the vibratome using general-purpose acrylic superglue. The mounting plate is then attached inside a vibratome chamber, and the chamber is filled with ice-cold hsACSF, covering the tissue. The hsACSF is bubbled for duration of slicing. The vibratome accepts a general purpose shaving razor fixated in the vibrating arm. During operation the vibrating razor advances through the tissue. In case of coronal slice the razor cuts from cupola towards base of the brain producing thin slices. For patch-clamp experiments, the thickness of 250-300 μm is preferred, while for experiments that involve subsequent fixation and immunofluorescent labeling a smaller thickness of 100-200 μm was used. As the slicing continues, slices containing coronal section of hippocampus are collected using a glass pipette. Slices are transferred into a glass beaker containing 250-300 ml of hsACSF, heated to 37°C. The slices are incubated at 37°C in hsACSF for 30 minutes. The purpose of incubation is to kill the

cells that were damaged badly enough by the slicing with temperature shock, while the cells that sustained little to no damage are able to endure through it and subsequently recover from chilling and decreased gas supply that occurred during preparation. After 30 minutes, the slices are transferred into 37°C nACSF, and the beaker is taken off water bath to slowly cool down to room temperature. The slices are then maintained for the rest of the work day under room temperature and continued bubbling with carbogen, in low-light conditions to avoid phototoxicity and bleaching of fluorescent cells. During incubation and storage slices are kept on a special raised nylon grid, which is placed inside a glass beaker, to allow ACSF to wash over the back side as well as the top side of each slice. The slices are transferred to microscope chamber using glass pipette, and immobilized with a bracket-shaped platinum wire, crossed with thin wires of nylon, all while submerged in nACSF.

In case of subsequent immunofluorescent labeling of the acute brain slices, after dye-loading of cells or after application of drugs, the slices were placed inside the wells of 24-well plate container and fixated with 4 % PFA for at least 4 hours.

3.4.1.2 Electrophysiological setup

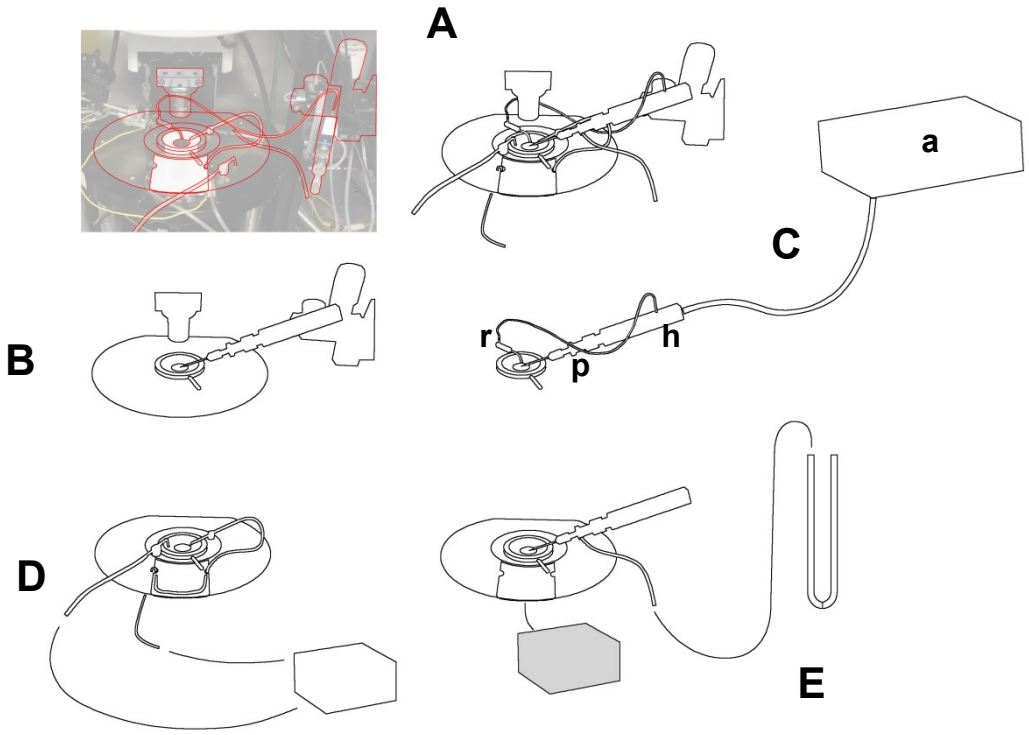

Fig. 2 Electrophysiological setup (**A**) Minimal configuration. (**B**) Shifting table, micromanipulator, recording chamber and microscope objective. (**C**) Electrical circuit with pipette (p), headstage (h), reference electrode (r) and amplifier (a). (**D**) Solution delivery and evacuation system with pump. (**E**) Air pressure control system and flow-through thermal control unit.

The electrophysiological setup which was used in the present study was mounted on a pneumatic vibration-isolated table, and surrounded by a Faraday cage. Inside the cage is the microscope equipped with DIC-optics, an x4 air objective, an x63 water-immersion objective, a CCD camera connected to a CCTV monitor and to computer through a USB signal converter, and a set of filter cubes adjusted to imaging in TRITC, FITC and YFP excitation/emission wavelengths. The removable recording chamber was installed beneath the objective in a manual driven X\Y plane-shifting table. The removable chamber is held on a table in a metallic cradle connected to a thermal control system, to enable active heating and cooling of the chamber and of the inflowing solution. Outside of the removable chamber, nozzles of inflow and outflow pump lines and the reference electrode were secured with magnets. The thermal-control unit was supplied by a constant flow-through of cooling water, to enable thermal buffering of the system at

higher ambient temperatures. The solution nozzles were pulled from glass capillary stock, their tips shaped into flat funnels. This enables constant rate of delivery and evacuation of ACSF to the sample chamber without much fluctuation of the level of liquid. Two micromanipulators were installed besides the shifting table. One accommodates the headstage with a patch pipette. Another accommodates the pneumatic substance application system nozzle/pipette holder (“Puff” system). Both manual-driven manipulators are for coarse adjustment, and hydraulic-driven at micrometer-scale. The illumination for bright-field microscopy was provided through a light guide from external halogen lamp. The excitation light for epifluorescent microscopy was supplied by a microscope-mounted high-pressure mercury lamp illuminating through a filter cube. The objective focus was motor-actuated with an external control unit. All components within the Faraday cage, as well as the electronic amplifier, were grounded to a single point of the metallic surface. The headstage was connected to an EPC-10 electronic amplifier, with additional grounding between the headstage and amplifier chassis. The headstage work end was connected to a pipette holder assembly, consisting of the BNC connector, screw-on jacket, electrode wire and the air pressure line access. The electrode wire is a Teflon-coated silver wire, with front part stripped of Teflon and coated with silver chloride. The rear part of the wire was soldered to a BNC-jack. Assembled, the pipette holder would have a filled pipette slide over the electrode so that the chlorinated tip would immerse in the intracellular solution, and jacket tightened around the pipette to seal the internal space of the pipette holder. This provides pressure control through a pressure line and mouthpiece. The pressure line leads from the headstage to a three-way valve, behind which the mouthpiece, water column and amplifier-controlled pressure pulse could be accessed. By switching the valve, at the working end of pipette low, high, or pulse pressure could be applied, to manipulate the cell membrane.

The electronic amplifier was connected to a computer with a USB cable and was digitally-controlled by either the Patchmaster 9 or TIDA 5 software. The Patchmaster software provides the extended functionality including scripting and on-line data analysis, and TIDA software, while not fully supported by an EPC-10 amplifier, could be used to provide data in an analysis-friendly legacy format. Both software systems could control the basic amplifier functionality equally well, with Patchmaster offering specialized modes and functions, such as software sine wave lock-in recording.

3.4.1.3 Experimental procedure for patch-clamp experiment

All patch-clamp experiments involve guiding a glass-made patch pipette to the surface of a cell. The tip of the pipette forms with the plasma membrane of the cell a tight, irreversible connection. This connection is an electrically-insulating connection with recorded resistance between the patch pipette solution and the reference electrode of over 1 GOhm. This connection is called “giga-seal” or simply “a seal”. The seal is created by tight adherence of fatty cell membrane to clean inner wall of a glass capillary. It is believed that atomic-scale forces create the seal. Seals are strong enough to prevent the passage of charge-carrying ions between cell membrane and glass of the pipette.

The procedure for all experiments was carried out as follows: The glass pipette was back-filled with a micro-loading pipette with 6-12 µl of artificial intracellular solution. The solution resembles the intracellular cytosol in terms of ion concentrations. It also has buffering agents and ATP as energy source. The pipette is then controlled for presence of air bubbles, and slid over the chlorinated silver electrode until its back end is secured inside the pipette holder jacket. By using a U-shaped water column, pressure is applied to the back of the pipette through the air pressure line of the holder.

The pipette is then immersed in the recording chamber where the biological specimen is already present. The amplifier is in the voltage-clamp mode at this time, repeatedly sending a command to step the voltage from 0 to +10 mV at the pipette electrode. The resulting small currents are necessary to observe the capacitance artifacts and to record the resistance at the pipette. As the pipette touches the surface of the conductive solution in the bath chamber, the circuit is completed between the headstage electrode and the reference electrode. The system is now able to measure the resistance (in Ohm) of the open patch pipette. For patch clamp experiments, we aimed to have pipettes with resistance between 3 and 4 MOhm. Good seals can be achieved with resistances between 2-10 MOhm. The stray potential between pipette and reference electrode was canceled out with the offset function of the amplifier. Offset voltage is usually measured in range between 0 and ± 20 mV. If the recorded offset value grows to ± 40-60 mV or more it indicates an impaired electrode coating or a stray current flow somewhere in the system. This could be caused e.g. by a bath chamber leak. If this happens solution and

surrounding metal components become connected and cause an electrical potential of several tens of mV. High offset values always need to be addressed.

The pipette is then guided down towards the area of interest using low magnification, and then to the selected cell of interest using high magnification and micromanipulators. As the tip of the pipette is brought in contact with cell membrane, the observed current at the pipette tip drops. This drop is caused by physical obstruction of the pipette opening caused by proximity to the cell membrane. This further limits the small opening at the pipette tip. At this moment, the pressure is quickly removed by switching a three way valve from the U-tube water column to a tube with a mouthpiece. The dimple in the pliable cell membrane that was created by outflow of solution under pressure shortly relaxes. Short sucking pulses bring the cell membrane in close contact with the tip of the pipette. The observed pipette resistance instantly increases by factor 10 to 100. Usually, the holding potential is switched at this moment from 0 mV to the desired holding potential of e.g. -70 mV for neurons or -80 mV for NG2-glia. The gigaseal, i.e. a resistance above 1 GOhm, is then achieved. This configuration is called “cell attached”. Since the procedure is done in the voltage clamp mode, the readout on the oscilloscope is a current in the nA range. The graph shows a large peak at the beginning and at the end of the 10 mV step. This peak corresponds to parasitic capacitance of glass patch pipette, which arises from conductors on both sides of insulating glass wall of the pipette. This conductance is then automatically canceled out by the amplifier function “C-Fast correction”. Parameters of the seal can now be recorded using a simple +10 mV step stimulation protocol to later estimate the quality of the seal before and after achieving the whole cell configuration.

After achieving stable gigaseal, cell is usually “opened” by repeatedly applying short suction pulses using the mouthpiece of the connected tube. These quick repeated suction pulses are applied to disrupt the patch of membrane inside the patch pipette without disturbing the adherence between cell membrane and glass capillary. With enough mechanical stress applied, the plasma membrane in the lumen of the pipette will rupture. This configuration is called “whole cell”. In whole cell configuration, the resistance between inside of the pipette and inside of the cell is called access resistance (R_a). R_a is relatively small compared to the resistance of cell plasma membrane that is called membrane resistance (R_m). The readout of the amplifier at this point is dominated

by cell-intrinsic parameters. In all experiments involving whole cell mode, a second "Artifact" stimulation protocol is recorded at this point, to be compared with the first "Artifact". Parameters such as R_a, R_m and C_m can be estimated using this difference.

This stimulation protocol is soon followed by a quick succession of voltage step-ups and step-downs that begin from the holding potential and go up to +20 mV and down to -170 mV in 10 mV incremental steps. The appearance of the readout from this stimulation protocol is determined by conductance typical for each type of cell. Together with other parameters such as membrane resistance, membrane potential, visual appearance and location, this conductance "fingerprint" allows instant identification of the type of cell currently patched.

Another important parameter is the resting membrane potential. It is measured in the current-clamp mode with zero current injection. The instant readout hints at the health of the cell patched. It is only meaningful if the membrane resistance is neither too high, like for skin or microglia cells, nor too low, like for astrocytes. In these cases additional adjustments are required to determine the correct value for the resting potential.

When all data is collected, the patch pipette is simply moved away from the cell, breaking the seal. The amplifier is set into the default state. The patch pipette is replaced with a newly-pulled one. A new cell is selected, and the cycle is repeated.

3.4.1.4 Patch-clamp principles and techniques.

Patch-clamp recording has many variations and subtypes, but the principle can be described as follows. The biological object – usually, an individual cell, but sometimes only a section of cell membrane, or a network of cells – is secured at the opening of the glass pipette. The pipette contains a 2^{nd} type electrode immersed into conductive salt solution. The solution is in contact with the cell at the pipette opening. The electrode is connected to headstage. Headstage is connected to amplifier for control and data readout. The cell is thus included in the electric circuit which begins and ends in the amplifier headstage. This circuit has the silver chloride-coated headstage electrode, the pipette solution, the glass pipette tip opening, the cell, the bath chamber of external solution, and the chamber-immersed reference electrode all connected in series (Fig 2(C), Fig 3(A)). Both the pipette electrode and the reference electrode have silver chloride (AgCl) at the interface between the silver wire and Cl^- ion-containing solution.

The difference between them is that pipette electrode is electro-plated and can withstand more wear-and-tear with day-to-day chlorination, while the reference electrode is a solid salt block (also sometimes called bridge) of AgCl. The purpose of completing a circuit with the cell included is the ability to detect the small changes in electric current which, ideally, originate from the biological object. This current is amplified and recorded, providing the information about the activity in the cell and cell membrane. While supplying negative and positive current is the only thing such circuit can physically do, the different interpretation of the change of the amount of this current over time creates the impressive multitude of patch-clamp technique variations.

The two main modes of patch-clamp are known as voltage-clamp and current-clamp modes:

In current-clamp mode,
the operator decides a fixed amount of current which is supplied to the cell at a given moment. The amount can be zero. The output of this mode of recording is **membrane potential, or voltage (mV)**. In this mode, the cell can be passively “listened to”, and changes (or lack thereof) in cell membrane potential are recorded. The current-clamp mode in this case is the way to record membrane potential in the way that is closest to physiological. If the operator then decides to specify a nonzero amount of current flowing through the circuit, the cell will find itself in the situation where it is dealing with what appears like a single, massively conducting ion channel, installed in its membrane – this “channel” being the opening of the patch pipette. The resulting electrical situation in the cell, which would be known to us through change in its membrane potential, will depend on the flow of current through this artificial “channel”. It will be added to the flow of ions through real biological membrane channels. The cell can also be made to act in certain manner. For example, it can fire an action potential, if an intrinsic capability to support an action potential is present in the cell, and other energy and sustenance conditions are met.

In voltage-clamp mode,
the amount of current which is injected into the cell is adjusted by a feedback loop of the operational amplifier. This circuitry acts in a sub-millisecond time frame. The output of

this mode of recording is **current (nA) through a membrane.** The membrane voltage is fixed at the desired amount during the whole measurement. In this mode, the decision on the operator side is to specify the desired membrane potential – voltage across membrane – that the cell will be maintained at (“clamped to”) by the amplifier. The amplifier achieves this by quickly working against the cell-intrinsic current sources (channels) fluctuating with physiological speeds (milliseconds), balancing them out at a greater than physiological speed (nanoseconds). The resulting membrane potential is maintained at the desired levels for any – physiological or unphysiological – amount of time, as long as cell keeps membrane integrity. Effectively, the cell can be subjected to a steady state at any desired value of its membrane potential. The value can be close to what is known to be physiological for a particular type of cell, or further away. This mode provides the ability to study cell's plasma membrane channels at any chosen value of cell's membrane potential. This allows the separation of the parameters of membrane channels using channel blocking substances. It also allows to take “fingerprints” from various cell types by recording the conductances over a spectrum of voltages, which will represent the collection of channels the cell type has. The so called “whole cell current pattern” is such an example.

Figure 3 lists the important parameters involved in conventional whole-cell electrophysiological experiments. R_a (also sometimes written as R_s – series resistance) is the access resistance. R_a consists of a combination of pipette resistance and the resistance imposed on the flow of ions by remaining plasma membrane inside the opening of the pipette. This value can vary depending on the amount of debris in the pipette opening. The smaller this value is, the better, however it is never lower than twice the amount of open pipette resistance which is usually around 3 MOhm for the largest usable pipettes. C_p is a sum of stray capacitances which arise from the glass pipette itself – this parameter is routinely negated by capacitance compensation which is a built-in function for modern amplifiers. R_m is a membrane resistance which is determined by membrane permeability typical for cell type and current state of the cell's ion channels and membrane. Finally, the C_m is the value of the membrane capacitance. Most of these parameters are interdependent and change over time within every experiment.

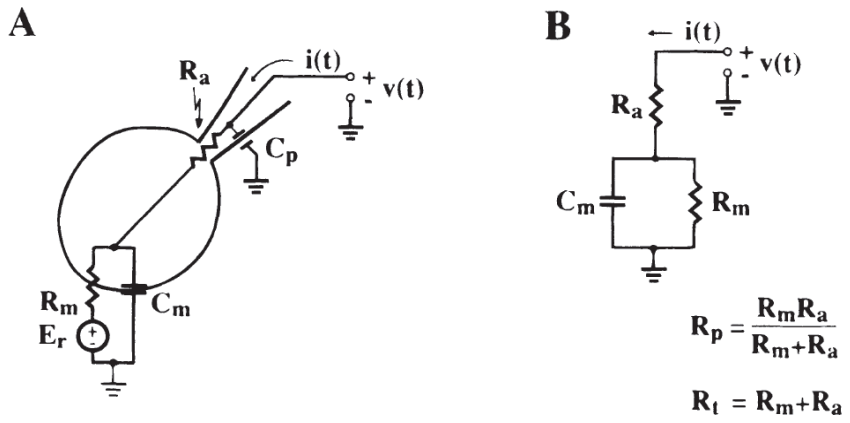

Fig. 3 (A) The equivalent circuit of a cell in the whole-cell or perforated patch recording configuration (Gillis, 1995) **(B)** Simplified three-component equivalent circuit. From (Gillis, 1995)

Electrically speaking, any biological cell has two distinct physical parameters that can be studied using electrophysiological methods. One of them is the cell membrane capacitance (C_m). The other is membrane resistance (R_m), an inverse of conductance.

All cells are surrounded by plasma membrane that consists of a lipid bilayer, separating two conductive water solutions of charged ions. The lipid bilayer itself is dielectric, it also restricts free travel of ions. In electrical engineering, a dielectric separating two conductors will have a property of electrical capacitance. The main characteristic of a capacitor is that it can store charge Q(Coulombs) proportional to the voltage across conducting sides Q = CV, where C is the capacitance (F, Farad) and V is the voltage (Barbour, 2021).

A capacitor has very low (zero) resistance, but only before any current is flowing through it. Following Kirchoff's circuit law, at a voltage divider (Fig. 3, B), the current will first flow through a capacitor (C_m), rather than the other components (R_m). However, as soon as the current begins flowing through a capacitor, it quickly charges it to its capacitance. The resistance of capacitor quickly grows to an infinitely large value, preventing further flow of charge through it. This introduces various time-related effects, or time constants, to each capacitor – in our case, to the cell membrane. The key contribution of capacitor to an electric circuit is that it allows current to flow at first, but then blocks the flow, making instantaneous change of voltage across capacitor terminals impossible. Measuring the parameters of this time constant imposed on current response makes it

possible to record cell's capacitance.

In practice, capacitance readout in patch clamp experiments provides information related to the area of the capacitor (plasma membrane), which, biologically, translates into the area of cell's plasma membrane, which can be used, for example, to estimate cell size, depending on cell shape. The area-independent specific capacitance of most biological membranes needed for this estimation is accepted as a constant of 1 μF cm^{-2} (Gillis, 1995).

3.4.1.5 Principles of membrane capacitance recording

The plasma membrane capacitance recording is a set of methods that, most popularly, are based on a variation of **voltage-clamp** mode of patch-clamp. The method is based on the property of the plasma membrane to have measurable electrical capacitance. Measured capacitance depends on the amount of electrically-controlled plasma membrane (Gillis, 1995). In most cases, this is related to surface area of plasma membrane. Therefore, an increase in the plasma membrane area under voltage clamp control causes an increase in measured cell capacitance. Such an increase is likely to occur as the result of inclusion of more membrane from an intracellular space into the PM. An inclusion of a vesicle causes an increase in measured capacitance. The amount of increase represents the amount of membrane that the vesicle added to a total area of the plasma membrane. This value can be used for the calculation of the vesicle diameter if the geometry of the vesicle is assumed to be a sphere, which it usually is. The measured capacitance decreases if plasma membrane is recycled into a newly formed intracellular vesicle. Capacitance recording alone it is not able to tell whether the addition of membrane was caused by arrival of membrane from intra- or extracellular space. It is also not possible to decide whether capacitance decrease was due to release or budding of vesicles towards inside or to outside of the cell. Because of this limitation, capacitance measurement is sometimes coupled with amperometric measurements. Budding vesicles will burn on a high-voltage carbon electrode and cause deflections in the measured current. However, this method also has its own set of limitations.

In this work, we used a sine-wave lock-in capacitance measurement approach. It

leverages fast alternating current to get the highest possible time resolution achievable for capacitance recordings. The physical principle behind the method is the same as described above, however, alternating current is used in this approach (Fig. 4).

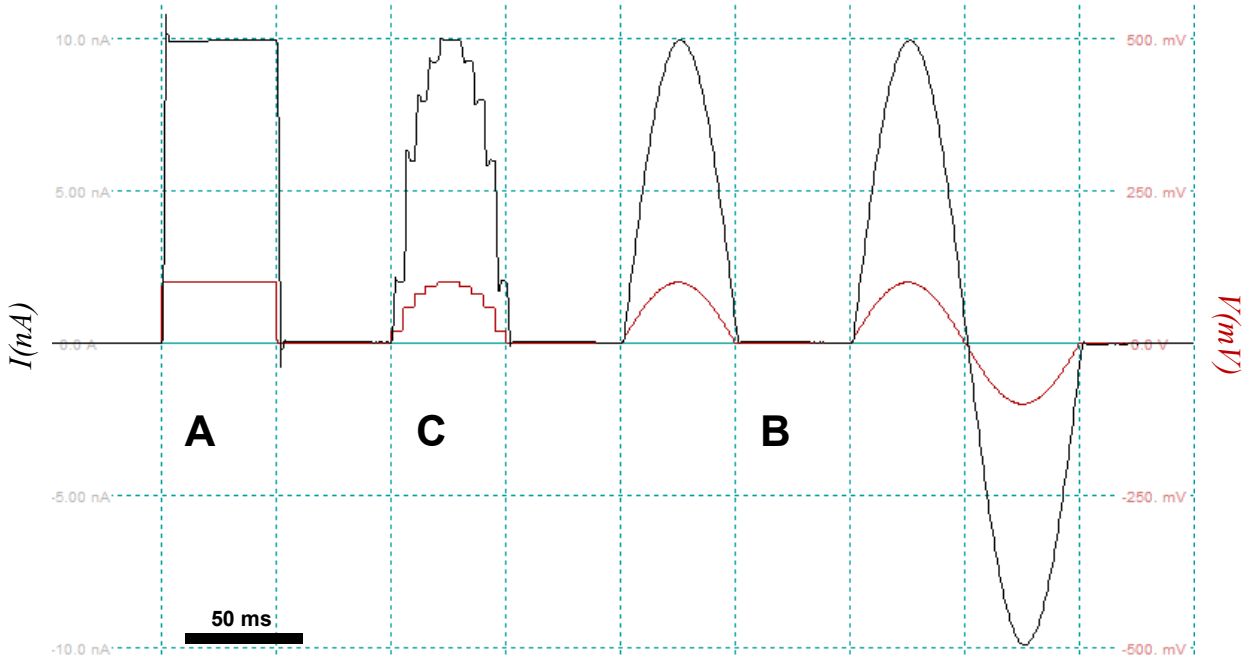

Fig. 4 (A) rectangular voltage step (in red), rectangular current response (in black) in a resistor-only circuit; behavior typical for direct current. **(B)** a sine wave segment; typical for alternating current. **(C)** an approximation of sine wave segment with rectangular voltage steps – an in-between situation.

In the trace above, note the coincidence of phases of the red applied voltage sine wave and the black current response sine wave. The peaks of both sine waves are coinciding in time, they are in-phase. This is the case if the circuit contains only ohmic resistance and no capacitors or coils. Living cells have both an ohmic resistance and a capacitance, both changing in time. What happens when capacitance is introduced into the system, along with more significant resistance, typical for a living cell (Fig. 5)?

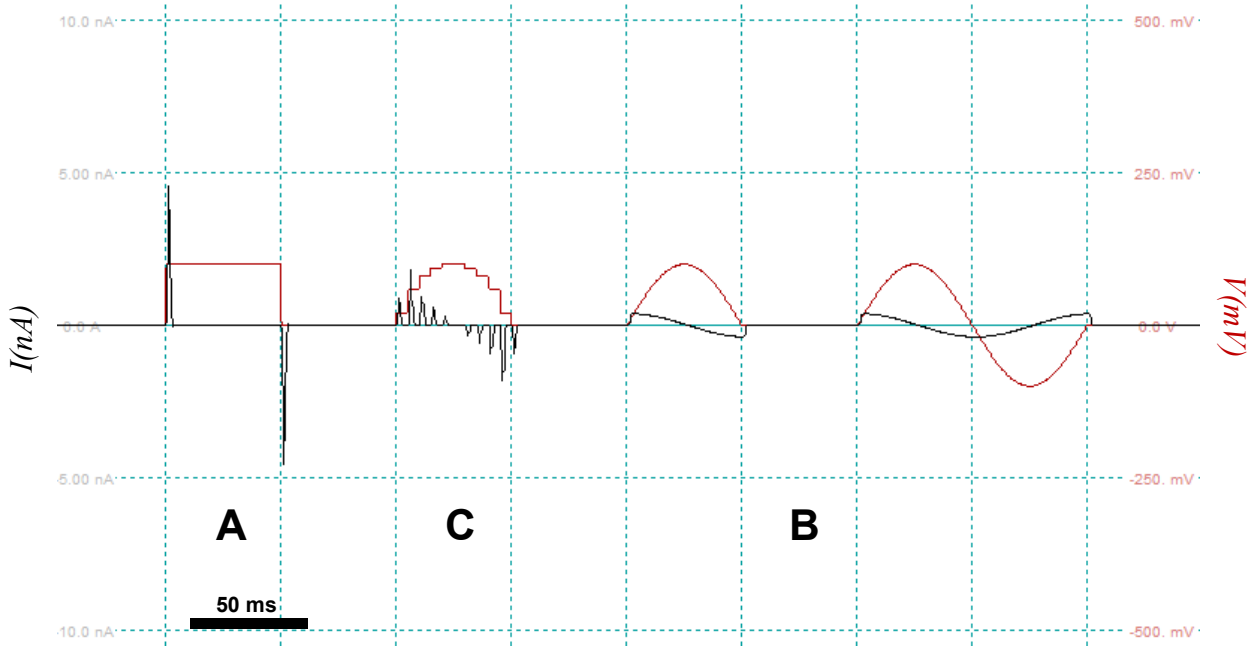

Fig. 5 (**A**) rectangular voltage step (in red), current response typical for high-resistance cell (in black). Note the sharp capacitance artifact. (**B**) a sine wave (alternating current) segments (in red), with corresponding cell response (in black). (**C**) an approximation of sine wave segment with rectangular steps.

In the above trace, note the decreasing amplitude of the capacitance artifacts in (C) as the collection of rectangular voltage steps is approximated to a sine wave. Further approximation to a continuous set of points creates another sine wave (in black) of lower amplitude. The resulting sine wave contains the information about both the membrane resistance R_m of the cell, mixed into sine wave's amplitude, and about cell's membrane capacitance C_m, mixed into the sine wave's phase. Note that peaks of voltage sine wave and peak of current sine waves no longer correspond in time. The difference is known as “phase shift”, and its amount describes the C_m of the system. Tracking phase shift allows for continuous recording of cell's membrane capacitance at very high time resolution (given high enough frequency of alternating current, and high enough sampling rate of the amplifier, which in our case was up to 2 kHz and 20 kHz respectively). In our work, this was achieved using software-based phase-sensitive detection which is a function of EPC10 amplifier.

One important requirement for phase-tracking is to know the initial state of the system, i.e. the phase to which the response sine wave is already shifted by electronic

components of the amplifier itself. Since the EPC10 has a well-characterized circuitry the phase shift calibration is carried out automatically by Lock-in function of EPC10 (“Calculated calibration”).

High resolution of such a recording also depends on the distance between sine wave peaks. The less the distance between every next wave of alternating voltage, the higher is the time resolution. This parameter is the frequency measured in Hertz (Hz). We used sine wave frequencies from 2 kHz for whole cell to 10 kHz for our cell-attached recordings. The amplitude of the commanded voltage sine wave must also be adjusted in accordance to the frequency. The amplitude of the voltage change is set higher for higher frequencies, and decreased for lower frequencies. A combination of low frequency and high amplitude would damage the cell by acting on the cell's conductances in a same way as repeated direct-current voltage steps of high amplitude, and low amplitude at high frequency would be harder to resolve. In perforated patch experiments, we used the amplitude of 70 mV around a baseline of -80 mV of holding potential, i.e. 70 mV peak-to-peak or +/-35 mV above and below -80 mV. For a series of experiments, these parameters would be set once and kept constant.

A more detailed explanation can be found in the literature (Gillis, 1995; Neef et al., 2007a; Rituper et al., 2013)

3.4.1.6 Cell-attached mode of capacitance recording

A variation of the above-described capacitance recording method, known as cell-attached membrane capacitance recording, was also performed. In this mode, a much higher frequency together with much higher amplitude is used to record the capacitance changes that originate only at the interface between a cell and patch pipette. This method does not require the electrical access to the whole cell, however it precludes gathering of the information from the regions of the cell that are outside the patch. No information can be gathered from membrane that is not inside the patch pipette. The upside is a much higher sensitivity and resolution. In theory this allows to record vesicular fusions of single vesicles, but at the cost of decreased chance of observation of an event. The requirements for reducing/avoiding ambient electric and thermal noise and potential artifact sources are also very high, therefore a very careful interpretation of the results is needed.

Calibration in this mode is different and requires an internal control. The internal control was provided by amplifier-driven pneumatic system. The system consisted of the low-pressure vessel and an amplifier-controlled valve which opened and closed upon receiving a TTL pulse from an amplifier, for the duration of 10-30 ms. Duration could be chosen depending on the seal quality. The opening of valve linked the low pressure vessel with the back of the patch pipette, creating a short suction pulse. The pulse slightly unfolded and tensioned the membrane inside the patch pipette, exposing more of the membrane to the internal volume of the patch pipette, and leading to a momentary increase in recorded capacitance. After valve is closed the membrane relaxes and capacitance value returns to initial value. The result is a short (10-50 ms) non-destructive increase in recorded capacitance, without corresponding increase in conductance. The calibration is considered correct when the suction pulse results in small upward deflection of capacitance (C_m), while membrane conductance (G_M) remains the same.

3.4.1.7 Recording in perforated patch mode

The technique described in 3.4.1.4 was implemented in a perforated patch variation. The electrical access to the cell in this mode was achieved by adding an antibiotic Gramicidin to a patch pipette solution. Over the course of tens of minutes to an hour, Gramicidin would insert itself in the exposed section of the plasma membrane patch. This forms pores between the inside and outside of the cell, providing transport for Na+ and K+ ions, but not the Cl- ion (Kyrozis and Reichling, 1995). In effect, this provides an access to the whole cell that is more stable and longer lasting. The relatively small internal volume of the cell is not washed out into the large volume of patch pipette solution. This preserves internal composition of the cell better, compared to mechanically destroying the membrane patch to gain whole-cell electric access. The trade-off is severely increased time of experiment per-cell, up to an hour and a half, of which most is dedicated to waiting for Gramicidin to act and R_a to drop low enough for recording to be meaningful. R_a value of 40 MOhm was considered acceptable, but most recording were not started until R_a dropped to 30 MOhm or less. The recordings were stopped if R_a experienced a sudden sharp drop of few MOhm or to less than 10 MOhm – in most cases this indicated a spontaneous mechanical breakage of cell's membrane inside the pipette, which would

transform a perforated patch configuration into a whole-cell configuration, with associated cytosol dialysis effects. Cells which did not react to Gramicidin or never reached the threshold R_a range were also discarded. R_a was monitored using online analysis function of Patchmaster during each experiment. The online analysis was done by of sending a 50 ms +10 mV voltage step every second, calculating the current at the highest point of capacitance artifact compared to baseline, and dividing 10 mV by this value.

To achieve perforated patch, the internal solution was supplemented with Gramicidin or Gramicidin-A in the concentration between 50 and 100 µg/ml. In this case, each pipette was first front-loaded with normal internal solution by dipping the tip into a tube of normal internal solution, and then back-loaded with micro-loading pipette with Gramicidin-internal solution mix. Filamentless pipettes were used for all perforated patch experiments, because dip front-loading could not be achieved in filamented pipettes, and double back-loading increased time to access beyond usability.

3.4.2 Immunolabeling experiments

Immunolabeling experiments included immunofluorescent microscopy and immunoelectron microscopy. They were carried out using animal models.

3.4.2.1 Trans-cardiac Perfusion and slice preparation.

Trans-cardiac perfusion was carried out as the beginning phase of immunofluorescent labeling experiments, in cases where acute drug application was not needed. In comparison to fixation of acute brain slices, trans-cardiac perfusion enables better preservation of brain tissue that is also achieved much sooner after blood circulation is stopped. The result is cells not sustaining any razor damage or asphyxiation damage while alive, providing a microscopic image that is largely undisturbed by tissue reactivity to injury or asphyxiation. Perfusion-fixated brain can also be sliced much thinner than the fresh brain, down to 40 µm compared to 150-200 µm of acute brain slice.

For perfusion, the animals were anesthetized with intraperitoneal injection of a 1:2:3 mixture of 2 % Xylazine, 10 % Ketamine and normal saline, in volumes 0.5:1:2 ml of substances per animal. The reflexes were controlled by pinching of the paws. Procedure was not started until a reaction could not be observed anymore. Depending on the animal activity and heart rate after the injection, this could take from 1 to 10 minutes.

The mouse was affixed on a working surface on its back, and front side of ribcage was exposed by cutting off the skin. Transverse cut through the front side of upper abdominal cavity and diaphragm were made, followed by side cuts along the lateral surfaces of the ribcage. The front of the ribcage was then mobilized and flipped upward, exposing the heart. A needle was placed inside the tip of the heart, aiming at the brighter left ventricle, to gain access to *aorta*. Simultaneously, a cut on the *vena cava inferior* was made and perfusion of 30 ml of filtered ice-cold PBS started. The PBS circulated through the system, draining outside through cut in *vena cava*, washing out blood cells and preventing clotting. After PBS washout, the system was switched to deliver 30 ml of ice-cold 4 % PFA solution in PBS, instantly killing and fixating cells in all the tissues that can be reached through capillaries. If the perfusion was carried out for subsequent electron microscopy, 150 ml of fixative solution was used instead of 30 ml, with the addition of glutaraldehyde. At this point in the procedure, successful perfusion was indicated by general stiffness of cadaver. The animal was then decapitated and whole brain was harvested into a container with 4 % PFA for postfixation at 4°C on a rocker. Postfixation continued for at least 6 hours, but in most cases no less than 16 hours. After postfixation, the brain was rinsed with PBS, dissected, glued to vibratome mounting plate, and sliced at 40 or 50 µm. The slices were stored in PBS-NaN3 solution in 24-well plates, at 4°C, for up to 2 months. Labeling after longer period was not done as the slice antigenicity would decrease, resulting in less fluorescence.

3.4.2.2 Immunofluorescent labeling

Indirect immunofluorescent labeling of tissue antigens was used in the course of the project (Fig. 6). We used a collection of commercial antibodies, each generated as a recombinant antibody or as a monoclonal antibody to have high affinity against a protein of interest. The antibodies themselves are complex proteins. Each antibody molecule has a region which binds to target protein with high specificity. This region is termed antigen-recognizing site. Another region on an antibody normally identifies the molecule to surrounding tissues of a host animal. While the antigen-recognizing site enables targeting of different structures of the studied tissue sample, the antibody host information of each molecule allows to target these antibodies themselves. This targeting was achieved by application of so-called secondary antibodies. Each

secondary antibody molecule is conjugated to a fluorescent dye particle, and the antigen-recognizing site of the secondary antibody is trained to bind only to first antibodies that have host information of a particular animal, such as rabbit, rat, goat, chicken or other. As an example, by applying a rat-derived antibody against a protein of interest first, and then applying a secondary dye-conjugated anti-rat antibody, information about location of protein of interest can be obtained. Secondary antibodies are commercially-available, coupled to a wide selection of fluorescent dyes of different emission spectra. Normally, two to four different colors identifying up to four different antigens/structures are workable for a modern confocal microscope within one sample, three being the safe choice.

Care must be taken to prevent overlapping of fluorescent signal at different dye emission wavelengths. This requires careful planning of dyes to be used in experiment. As a rule of thumb, it is better to use dyes emitting in colors which are far from each other on a spectrum, e.g. blue, green and red, and to track less markers at the same time, if possible.

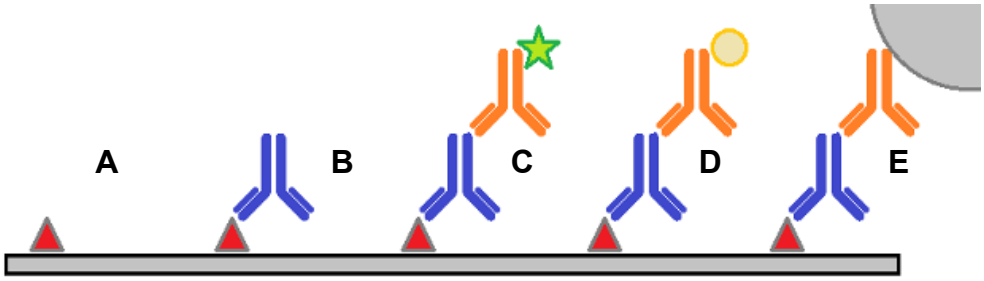

Fig. 6 Immunolabeling (**A)** antigen, (**B**) first antibody (**C**) second antibody with conjugated fluorophore (**D**) second antibody with conjugated gold particle (**E**) second antibody with gold particle layered with silver for increased visibility in EM.

The **exemplary immunofluorescent labeling protocol** is as follows. The protocol spans two days, with two-three days after mounting for samples to settle down under the coverslip. It begins with application of epitope unmasking agent, if antigen retrieval is required. The base medium for immunofluorescent staining is PBS. The washing step which follows is universal for every step of the protocol and consists of three washes with PBS, for 10 min each, on a shaker. The base volume for most operations is 250ul per well, if 24-well plate is used, and the samples are as large as coronal mouse brain slices. The washing is followed by unspecific blocking step, which is included to prevent

unspecific binding of first antibodies to the tissue, and to improve signal-to-noise ratio. This step takes two hours at room temperature (RT). The unspecific binding agent may vary, but normal serum is considered one of the best options. It is believed that host animal for neutralizing serum should be the same as the host animal for secondary antibodies. This is not a strict requirement however the serum must not be of the same host animal as the host animal for first antibodies. Small amount of detergent (0.25 % of Triton X100) is added to the blocking mixture to begin membrane permeation. In most experiments, we used normal horse serum at 10 %. The step is followed by application of 1st antibodies in a PBS solution of 5 % normal serum and 0.1 % Triton X100. The amount of antibody needed was determined experimentally for each kind. Concentrations between 1:100 and 1:500-1:1000 were used for first antibodies. The samples were incubated with the appropriate mixtures of antibodies at 4°C overnight. This was followed by application of secondary antibodies using the 5 % normal serum and 0.1 % Triton X100 in PBS, for two hours at RT. 1:500 volume:volume was used for secondary antibodies. This step was followed by washing. After this, usually a nucleus staining dye was applied for 10 minutes in case of Hoechst stain. This, again, was followed by washing. To finish, the brain slices were placed on the sample slides. Mounting medium was applied on top of slices, and glass coverslip carefully placed on top of the medium drop. Best results are achieved if samples are allowed to solidify for several days in the fridge.

3.4.2.3 Immunoelectron microscopy

Pre-embedded immunogold labeling was used in immunoelectron microscopy experiments. The same first antibody was applied initially as was in preparation for immunofluorescent microscopy. This first antibody was then bound by the secondary antibody conjugated to a nanoparticle of gold. In the process of tissue polymerization, the nanoparticles were made to grow in size by layering gold with enough silver atoms, up to a point where particles are big enough to be visible as high-contrast spot in a field of view of electron microscope. With this approach only one antibody can be used per sample. The signal from two different antibodies after silver-enhancement would present itself as dots of same size, preventing meaningful identification. The SNR of this method is high and comparable to that of immunofluorescent microscopy.

3.4.2.4 Microscopy principles and microscopes involved.

Few different modes of microscopy were used in this study. Bright field microscopy and epifluorescent microscopy were used in the patch-clamp experiments, where a patch pipette must be guided to a cell of interest. Bright field microscopy is the oldest known method of microscopy. It depends on the light from the light source that is behind the sample passing through the sample and into the detector. The contrast in this case is created by densities in the sample that absorb some, or all, of the passing light – such as membranes, organelles, debris, glass of the pipette, etc. There are different methods that allow to enhance the contrast. These include limiting the spectrum of the detected light to deep red and infrared wavelengths, or by using polarized light (Nomarski optics).
Epifluorescent microscopy, on the other hand, as well as other fluorescent microscopy modes, depends on creating contrast from light sources that are within the tissue itself. In the patch-clamp experiments of this project, the fluorescent light source in the tissue was usually the enhanced yellow fluorescent protein (EYFP), which is excited by blue-green light, and emits in yellow.
Fluorescence in practical sense can be described as the ability of matter to emit light in certain wavelength, after being subjected to excitation by light of a different wavelength. Unlike phosphorescence, the fluorescence ceases as soon as the excitation light stops. The emission wavelength in almost all cases, except for few very rare substances, has lower energy compared to excitation wavelength, therefore the spectrum of emitted light is shifted towards longer wavelength, compared to excitation light (Stoke's shift). In simple terms, this would usually mean that, for example, orange excitation light might cause an emission of red light, but not the green light, while blue excitation light might cause an emission of green or yellow or red light, but not UV light. This emitted light is usually filtered before it is registered by a detector. This removes the undesired light of excitation wavelength or ambient light being reflected from the sample. Usually, this is done with dichroic filters. In case of more advanced systems, by a combination of dichroic filtering and splitting of light beams using prisms.
To a degree, most, if not all, biological substances have the property of fluorescence – as well as many minerals, organic chemistry compounds, dyes – however, the particular excitation and emission spectra and energies involved make some substances better fluorescence sources than others. During patch-clamp experiments, NG2-glia was localized in the brain slices taken from NG2-EYFP or hGFAP-EGFP transgenic animals by its emission in the epifluorescent light.

3.4.2.5 Confocal microscopy

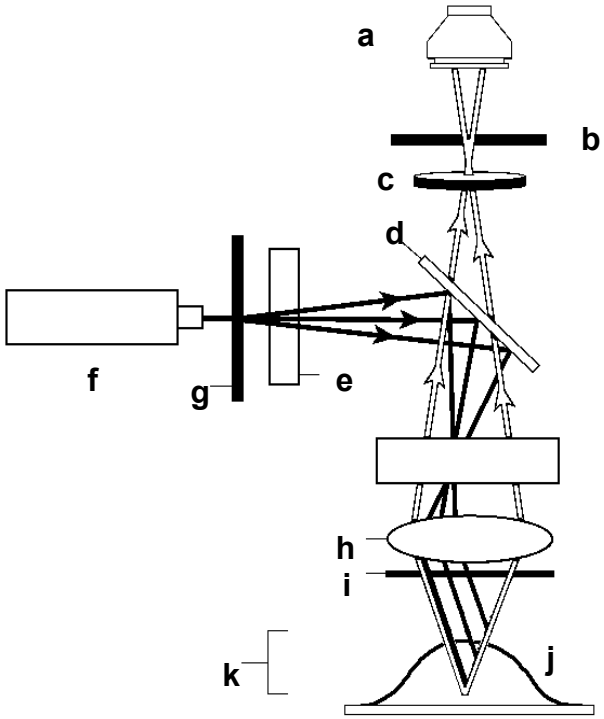

Fig. 7 Confocal microscope, an overview, from (Paddock and Eliceiri, 2014) **(a)** Photomultiplier detector, **(b)** Pinhole aperture, **(c)** Barrier filter, **(d)** Dichromatic mirror, **(e)** AOTF, **(f)** Laser, **(g)** Scanning unit, **(h)** Objective, **(i)** Coverslip, **(j)** Specimen, **(k)** Focal planes.

Confocal microscopy is a subtype of fluorescent microscopy. The advantage of confocal microscopy when compared to epifluorescent microscopy is its ability to visualize a thin plane of tissue within the sample. This enables collection of data that is differentiated along the top-bottom axis of the sample (Z-axis). This is done by preventing light from the sources above or below the focal plane from reaching the detector. This greatly increases the resolution of resulting images and enables three-dimensional visualization. It comes at a cost of decreased total amount of light that reaches the detector, increasing the requirements for tissue luminescence and illumination quality. The main modification to a microscope that allows confocal imaging is the addition of a pinhole diaphragm at the focal point in the light path (Fig. 7). This diaphragm cuts off light from above and below the focal plane. Only “paraxilar” light from a thin section can pass through. A fully opened pinhole effectively turns a “confocal” microscope into an “epifluorescent” one.

While in an epifluorescent microscope all of the tissue is excited and emits at the same time, creating a lot of stray ambient light, a scanning laser only excites tissue which is within the width of a narrow laser beam. This has a number of advantages, from preventing the excessive bleaching of fluorescent dyes, to improving the resolution and preventing light aberration, to providing a mono-frequency excitation for better control of the emission. A microscope combining both approaches is typically called a laser confocal microscope.

A laser confocal microscope that was used in this study was a Leica SP8 LSM. The system includes an inverted microscope with an air 10x objective and water-immersion 63x objective mounted on a vibration-free table. Immunolabeled brain slices were mounted on standard 76x26 mm glass slides and covered with 0.13-0.18 mm thick cover glass held together by a mounting medium. The slide was installed in the holder in the microscope light path. The holder was motor-actuated and controlled in all three axis by a computer, allowing for automated imaging of large areas, such as whole hippocampus, in three dimensions. The SP8 system includes three lasers with eight emission lines for excitation of fluorescent dyes or proteins. The wavelength range is 405 nm to 647 nm. The detection of emitted light is possible anywhere in the spectrum between 380 and 800 nm using any combination of two photomultiplier tube detectors and two hybrid detectors. In practice, no more than two channels were collected simultaneously to prevent cross-excitation and bleed-through between channels. (i.e. 488 nm emission of Alexa488 together with 647 nm emission of Alexa647, but not 488 with 555). The DAPI channel was always collected separately from other channels, due to high emission intensity of the dye across the spectrum. LAS-X software package of the SP8 system provides data-handling, microscope, laser and detector controls, basic analysis and visualization. The system also includes specialized software packages, one of which enables deconvolution of collected data. Deconvolution can increase signal-to-noise ratio in the resulting images using post-processing. Another protocol enabled automated merging of individual view panes into larger tiled images.

3.4.2.6 Electron microscopy and Correlated Light-Electron Microscopy (CLEM)

Any microscopy method is fundamentally limited by the wavelength of electromagnetic radiation that is being used. It is possible to enhance the performance of light microscopy in terms of resolution by using different workarounds – for example, by using light which is more towards shorter ultraviolet wavelength. The light waves themselves can be modulated in case of super-resolution microscopy. The size of the sample can be increased using expansion microscopy. All of these workarounds are still limited in situations where two light sources are so close together that the wavelengths from these light sources are comparable to the distance between them. This ambiguity presents itself at different two-point distances depending on the wavelength being used, but in all

cases it is still referred to as diffraction limit. In practical terms, this prevents resolving structures which are less than 150-300 nm in size – at least in case of a conventional non-superresolution laser confocal microscopy. To this day, the only way to meaningfully resolve structures smaller than the light diffraction limit – which is most subcellular structures – is to use electron microscopy.

Electron microscopy (EM) is a technique which is altogether different from the microscopy techniques mentioned above. While the contrast in the electron microscope is formed – similarly to a bright field microscopy – in dependence on the density, shape and thickness of the tissue being observed, the method uses a scanning beam of electrons accelerated in vacuum rather than a light of certain wavelength (which consists of photons). The electrons act like very small particles and, while they do have a certain wavelength which depends on the energy of the particle, it is few hundred times smaller than that of photon at the same energy level, and is usually in sub-nanometer range. This enables forming images on a scale which can be as small as few picometers, but routinely the scale of 1-2 nm per pixel is used for biological samples. The electrons either fly right through the sample (in case of Transmission Electron Microscopy, TEM) or are reflected by the tissue surface at an angle and into a nearby detector (for Scanning Electron Microscopy, SEM). Modern electron microscopes can combine both methods to a degree, however the requirements for sample preparation are stricter compared to that of light microscopy. Most importantly, for TEM the tissue must be sliced extremely thin – in the order of several nanometers – which is few orders of magnitude thinner than the slices used for immunofluorescent labeling or patch-clamp; in a thick slice all the electrons would be withheld by the tissue and the image would be completely black. A biological tissue in its native state, even after formaldehyde fixation, cannot be sliced this thin without being destroyed. As the result, samples for TEM are prepared in multiple sequential steps which involve dehydration in spirits, infusion of heavy metals for contrast enhancement and conductivity, polymerization in resin and liquid-phase slicing using a diamond-edged knife (ultramicrotomy). Nevertheless, the result provides a morphological ground truth on a subcellular level, including structures as thin as single lipid bilayers or individual ribosomes. This level of performance is, to this day, unattainable for light-microscopy methods. The trade-off, in most cases, is the laboriousness of the EM sample preparation, as well as tremendous complexity of the

observed tissue, with all the subcellular features being visible at the same time over the large area. Recently, this is being addressed by operational linking of fluorescent microscopy with electron microscopy, often called correlated light-electron microscopy (CLEM). This approach aims to provide the best of both worlds, in terms of morphology and comprehensiveness.

In our project, the CLEM approach was possible thanks to availability of NG2-EYFP mice, in which the native signal of EYFP could be collected together with DAPI-stained cell nuclei before application of any antibodies and resin embedding of slice. The fluorescent dataset that contains the full tiled stack through a hippocampus on one side was collected and stored. The tissue then underwent further processing, losing fluorescence, but gaining the immunogold signal. The thick slice, which was used for collection of fluorescent data (40-50 μm) was flat-embedded into a block of resin. The face of the block was re-sliced using ultramicrotome to EM-compatible thickness of 50-80 nm. The EM data was then collected using Zeiss Crossbeam 550 electron microscope, to form an EM-tilescan of block face. The two datasets were then manually correlated using major features of tissue such as large vessels and notable cell nuclei.

3.4.2.7 Image analysis and colocalization.

Image analysis was carried out using ImageJ Fiji software. Fiji is a user interface shell for ImageJ package, which itself is a collection of scripts and macros designed for an advanced image manipulation. The project is mostly community-driven, offering both a large selection of analysis tools and high customization. The package allows analysis automation with scripts written in a number of software languages. In the present study, scripts containing code snippets taken from the public sources, as well as original code, were used for image manipulation and analysis.

Colocalization testing was carried out using a Coloc2 plugin version 3.0.5 implemented in Fiji/ImageJ (v.1.53i). The plugin uses automatic thresholding algorithm by Costes (Costes et al., 2004). The article also describes a bespoke colocalization test that uses this algorithm. While the thresholding algorithm by Costes is commonly accepted as one standard approach to the first step of analysis pipeline, the test itself, while popular, remained a matter of discussion (Bolte and Cordelières, 2006). In a review by Dunn (Dunn et al., 2011), several approaches are described, with no single approach being a

one-size-fits-all universal method for establishing colocalization. In fact, the very necessity of carrying out numerical colocalization testing is questioned, unless the test involves comparison of two conditions (i.e. control vs. treatment) and thus requires a numerical answer. Still, the final decision is left for investigator's discretion, and it is advised to keep in mind the scientific question at the basis of the test, for example to not miss an interaction which can't be boiled down to pixel-by-pixel coincidence. Other conditions such as background noise level, smoothing, the availability of deconvolution packages, amount of background, offsetting, masking, usage of stacks vs. a MIP – may dramatically influence one test while making little impact on the other. After comparing few representations of the same data using coloc2 plugin of Fiji/ImageJ, we decided to use MIPs rather than z-stacks, because region of interest masks in the tissue could only be specified for one z-level, and not for a collection of z-levels. To address the issue of spurious signal from above or below a cell in the MIP, the data was first filtered to only include signal delimited by EYFP-positive cytosol of NG2-glial cells. This limits the colocalization tests to interactions observed within NG2-glia only. This preliminary filtering was only done for CD63/Alix and CD63/Flotillin-1 pairs but not done for EYFP/Flotillin-1 colocalization test. The results are presented as a panel of coefficients. Most of them range from zero to one. One usually indicates perfect colocalization or an otherwise high degree of relationship. We omitted Costes test from the results because, contrary to other coefficients in the output, Costes test always produced a perfect correlation score. This output deviated away from this high value only in case of extreme data masking, which also resulted in a failure of automatic thresholding step.

3.4.2.8 Flotillin-1 positive granule count analysis.

To quantify the affinity of Flotillin-1 positive granules to NG2-glia, data was collected as a 5 µm-thick tiled stacks of mouse hippocampus. The area included CA1, parts of CA2, CA3 and DG. To enable semi-automatic analysis of the data, we took advantage of high signal-to-noise ratio of EYFP expressed in NG2 cells of NG2-EYFP mice. The EYFP intensity was enhanced using immunolabeling with Alexa-488 dye. Anti-Flotillin-1 antibody was used together with a secondary antibody coupled to Alexa-647 dye. Simultaneous collection of two channels was possible due to chosen dyes having emission spectra non-overlapping and far enough from each other. Third channel (405 nm) was collected independently to prevent cross-excitation and emission leak, but in

short succession with 488 nm and 647 nm channels. After collection, the tile stacks were merged using LAS AF software. Resulting volumetric stacks were then converted into 8-bit MIP three-channel hyperstacks. The images were then analyzed using ImageJ/Fiji v1.53i software.

For the initial analysis, densely packed neuronal sections of the hippocampus, namely Pyramidal layer (PL) and Dentate gyrus (DG), were masked with zero data across all channels. This excluded a large portion of principal neurons from the analysis. However, it enabled a unified approach to defining per-cell regions of interest within the data. This wouldn't be possible with too many smaller cells packed close together. The NG2-glial cells are also usually not present within these neuronal layers. The hilus of DG, despite having an increased number of NG2-glial cells compared to other layers, was also masked due to higher background intensity of Flotillin-1 signal (perhaps indicating higher uniform content of the protein in this layer), to prevent artifacts during the thresholding. Areas above or below hippocampus (i.e. corpus callosum) were masked as well. Large vessels were not masked (Fig. 8).

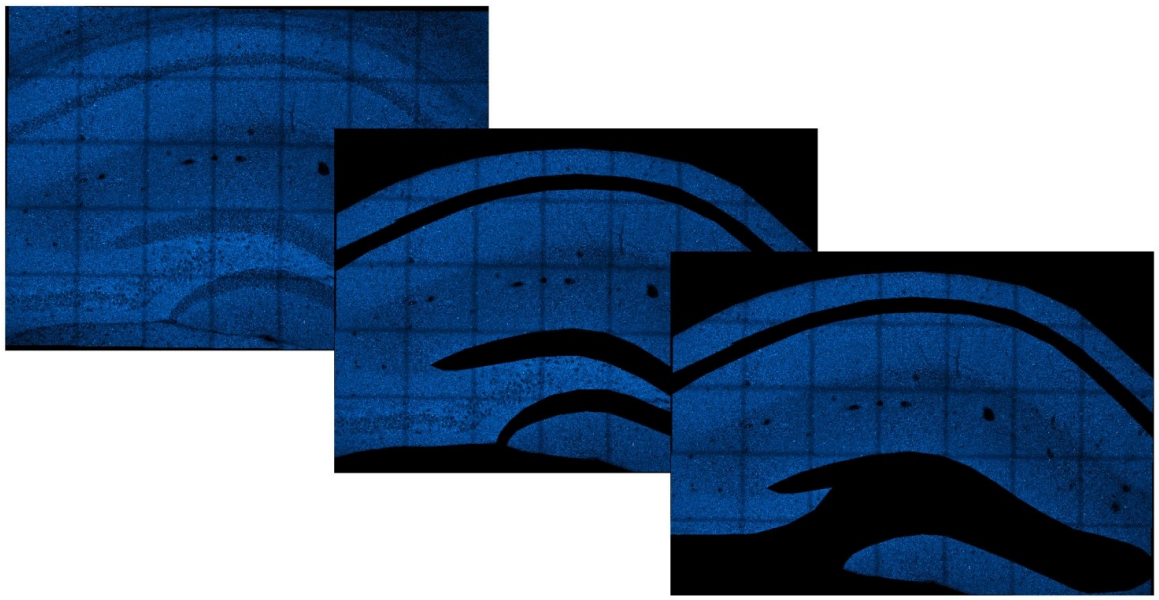

Fig. 8 Tileset masking. The MIP of a tileset was masked through all channels. The visible sections of *corpus callosum*, pyramidal layer, and granular layer of dentate gyrus were blanked. This prevents inclusion of Flotillin-1 binding from those areas. PL and GL are largely devoid of NG2-glial cells. The full masking which was used in the analysis also obscured the hilus and adjacent pyramidal layer of CA3. This was due to high background intensity of Flotillin-1 in these areas, which interfered with automatic thresholding.

The segmentation for all cells in the analysis was carried out using a uniform circular region of interest (ROI). The diameter of each ROI was 220 pixels, or 18.14 µm. This was done to prevent misdetection of Flotillin-1 positive granules as pertaining to a cell or being just outside of it around the ROI edges. This might occur if a simple threshold-based approach would be used. The cells also present themselves in different three-dimensional orientations within a relatively thin (5 µm) plane of tissue. Some NG2-glial cells have their largest dimension within a plane of tissue, while others are oriented perpendicularly to it. These cells only present a cross-section of two smallest dimensions. The overall shape of cells might be elongated or spherical. The size of 18.14 µm was selected based on the collection of several elongated NG2-glial cells representing the extreme cases. In these cells the visible Flotillin-1 positive granules were manually annotated. The circular ROI was then grown with a step of 10px, using a centroid derived from a cell outline. The centroid, in most cases projected within the boundaries of projection of cell's nucleus. The resulting diameter of ROI which accounted for most of the annotated Flotillin-1 positive granules for those elongated cells was measured at 220 pixels. This size of ROI was used for all comparisons (Fig. 9). The circular ROI positioning around cell's centroid required little adjustment in terms of thresholding for initial shape-finding, despite the brightness of the EYFP varying across the animals of different litters, ages, and sample preparation runs. The same approach was also easily implemented for (I) nuclei of the DAPI-stained cells, (II) natively fluorescent EYFP cells, and (III) cells marked with other antibodies, such as CC1. The NG2-antibody, however, being mostly membrane-associated, proved difficult for automatic segmentation. This was due to ambiguity of defining a dominant cell shape for centroid placement. Wildtype animals were therefore segmented manually.

In rare cases in which circular ROIs of two adjacent NG2-glial cells overlapped, the manual survey was sufficient to verify that no single Flotillin-1 marked granule was within two distinct ROIs. We can exclude any misleading double counting of Flotillin-1 marked granule in this way. Manual survey also helped to prevent counting of EYFP-positive pericytes together with NG2-glial cells. Partial cell shapes that were cropped by masked areas or by edges of the tilescan were excluded in most cases. The faintly-EYFP positive spherical cells which represent NG2-cells that undergo or just previously

underwent differentiation into oligodendrocytes were also not included with the NG2-cells. This observation was verified with anti-CC1 labeling (see section 4.2.12 for full details). The resulting subset of ROIs is EYFP-derived.

The DAPI-derived circular ROIs represent all nucleus-containing cells in the hippocampus. No correction was performed for overlapping ROIs of adjacent cells. In some cases, it may be that a Flotillin-1 positive granule that pertains to a NG2-glial cell was also accounted for the closest neighbor of this particular cell. Small inflation of total numbers of Flotillin-1 positive granules in “all cells” subset might be the result. This difference was not significant. This was proved by comparison of two DAPI-derived ROI sets. Both sets contained 1314 ROIs. The first set contained default circular ROIs, all equiareal, circular and sometimes overlapping. The second set with same set of ROIs but now broken up at all overlaps, resulting in no overlapping ROIs. The Flotillin-1 positive granule counts of both groups were tested with a two-tailed paired t-test. The p-value of $p = 0.3473$ proved no significant difference.

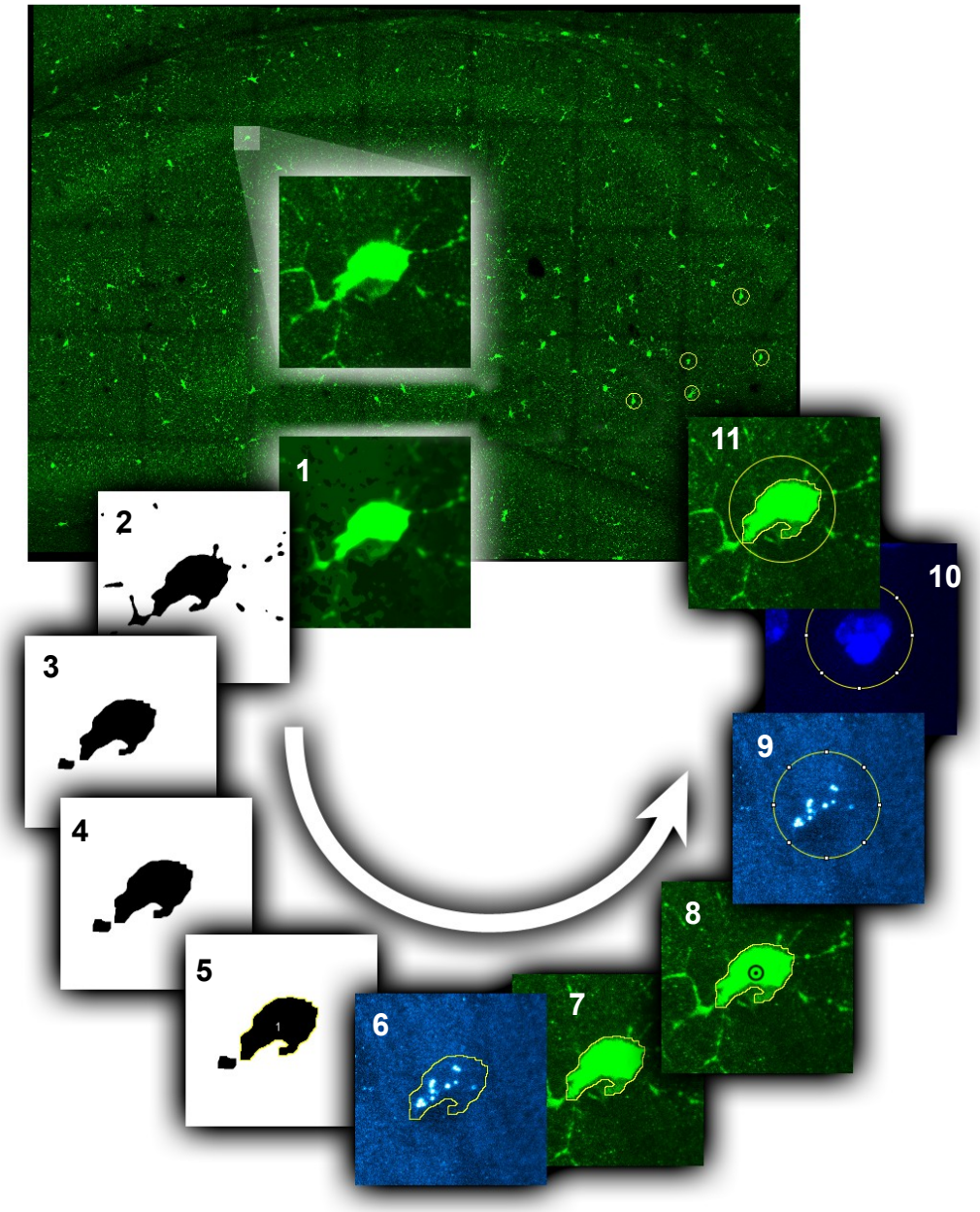

Fig. 9 Basic semi-automated algorithm for segmentation for NG2-glial cells. Starting from the top, counter-clockwise, in sequence: (1) median filter (6 px), (2) threshold (parameters vary, but consistent within slice as well as within a sample slide), (3) erosion of binary image (clears away small shapes, while preserving large shapes), (4) open binary (erodes thin circle-shaped objects, preventing any “donuts” or closed loops), (5) dilate binary (grows remaining shapes, to try and connect to remaining adjacent objects, usually a cell and its process), (6) area-filtered particle detection (defines remaining large shapes into traced ROIs, omitting smaller shapes),(7) quick manual survey of the resulting shapes, (8) centroid, (9-11) circle-shaped ROI created from centroid, in three channels.

After generating both of the ROI subsets described above, a third subset was calculated by subtracting the EYFP-derived subset from DAPI-derived subset. The ROIs which overlapped (to any degree) between the two subsets were excluded, resulting in “All-except-NG2-glial cells collection” (Fig. 10). This way, cells which were neighboring to NG2-glial cells were also often excluded. As the result of overlap detection, the “all cells” subset is not equal to sum of NG2-derived and all-except-NG2 subsets. Instead, this sum of “All except” and “EYFP-derived” is 92.6 % of the “all cells” count on average.

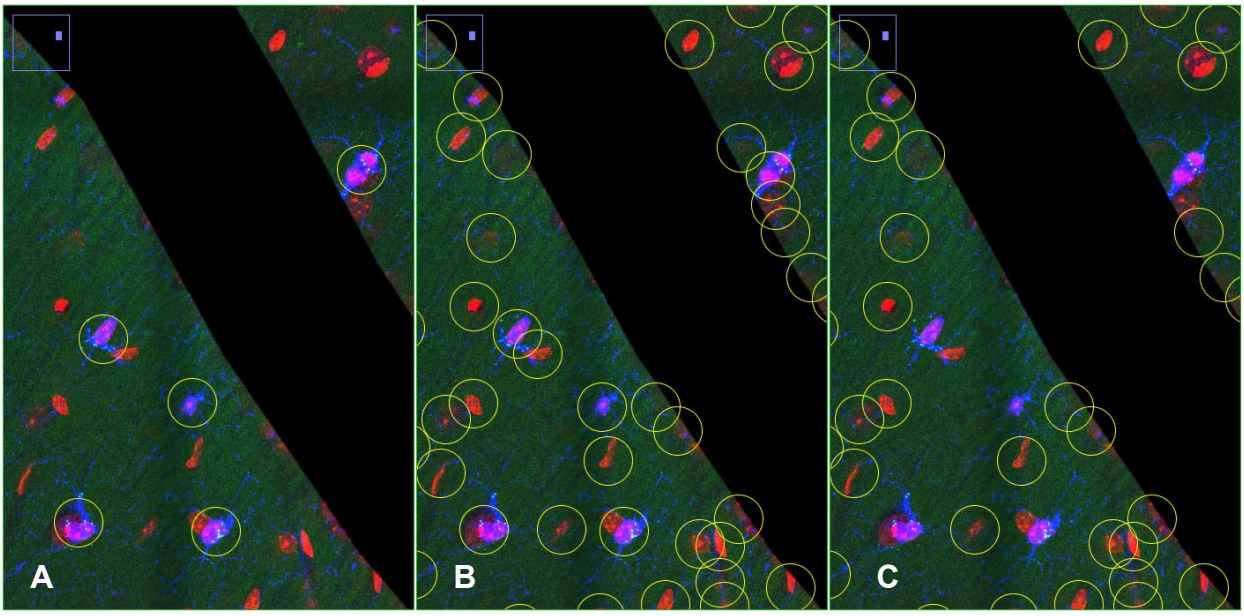

Fig. 10 Circular ROI subsets, EYFP (blue), DAPI (red), Flotillin-1 (green). **(A)** – EYFP-derived collection, **(B)** – DAPI-derived collection (“all cells”), **(C)** – “All cells except NG2-glia”.

Regardless of the source channel used for determining ROI positions, the accompanying Flotillin-1 channel was then analyzed to find the number of Flotillin-1 positive granules within each ROI. A simplified algorithm is shown in Fig. 11. Only granules which were found inside the resulting circular ROIs were accounted for.

We therefore evaluated the number of Flotillin-1 positive granules in three groups: NG2-glial cells, all cells, and all cells except NG2-glial (Fig. 10).

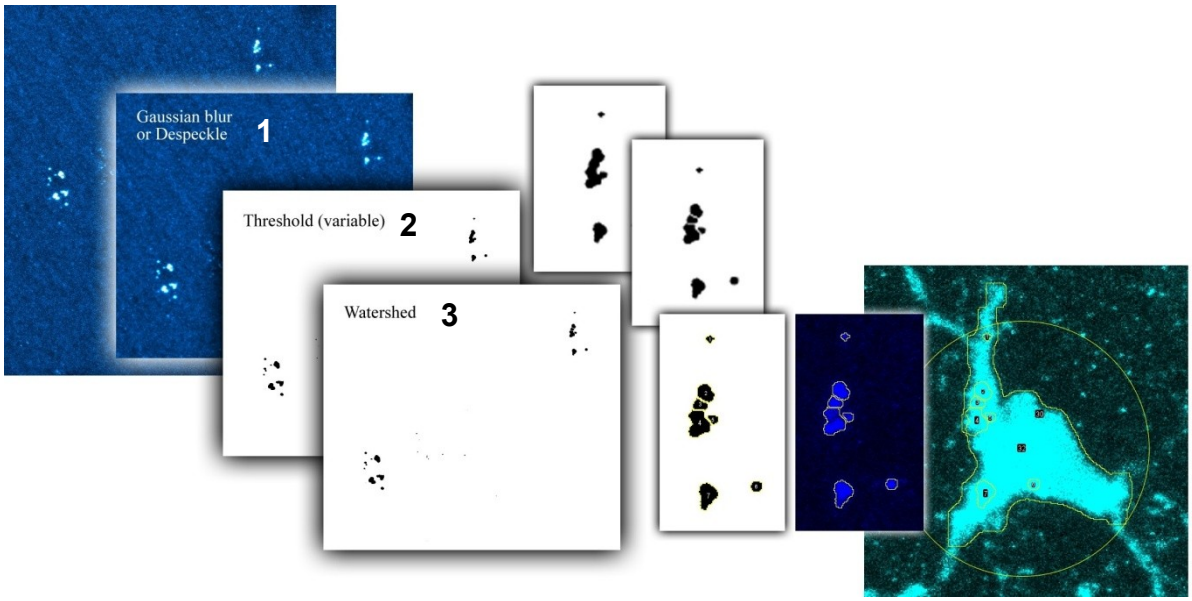

Fig. 11 Flotillin-1 positive granules particle analysis, from left to right: (1) Gaussian blur (1px), (2) threshold (manual, varying according to labeling intensity, but unchanged within experiment/slide/comparison pair), (3) watershed (attempts to fracture the elongated “pearl-necklace” structures into individual “beads”).

3.5 Statistics

Statistical analysis was carried out using R v.4.0.4 and RStudio v.1.4.1106.

Where applicable, data was tested for normality using Shapiro-Wilk test. Variance distribution was tested using Levene test. The α-value used was 0.05. The α-value, also known as significance level, is the probability of wrongly rejecting the null hypothesis (the absence of real difference) when it is true. A significance level of 0.05 or 5 % indicates a 5 % possibility of concluding that there is a difference in a comparison when there isn’t one. Smaller than 5 % α-values are a requirement in some fields of science, for example, in particle physics, where a significance level of 6×10^{-7} is the convention.

Due to non-normal distribution of data for Flotillin-1 counts (the distribution was found to be close to zero-inflated Poisson distribution) a non-parametric Kruskal-Wallis test was used with Dunn test for pairwise comparisons. The post-hoc tests were carried out using Bonferroni Procedure. The clustering was performed using K-means procedure. A-priori sample sizes were determined using GPower v.3.1 software.

4. Results

4.1 Electrophysiological experiments with capacitance measurements in whole-cell mode

4.1.1 PC12 cell line – establishing the capacitance recording technique and analysis procedure.

PC12 cell line was used to establish the method for membrane capacitance recording. This was done because chromaffin cells and cell lines are often used to study neurosecretion, and membrane capacitance recording is often involved in these studies (Harkins and Fox, 1998; Lindau, 2012; Moser and Neher, 1997; Neher and Marty, 1982). Perforated patch recordings were used in order to prevent the cytosol from washing out into a much larger volume of the patch pipette. An exemplary trace of R_a decreasing over time under the influence from Gramicidin is shown in Fig. 12:

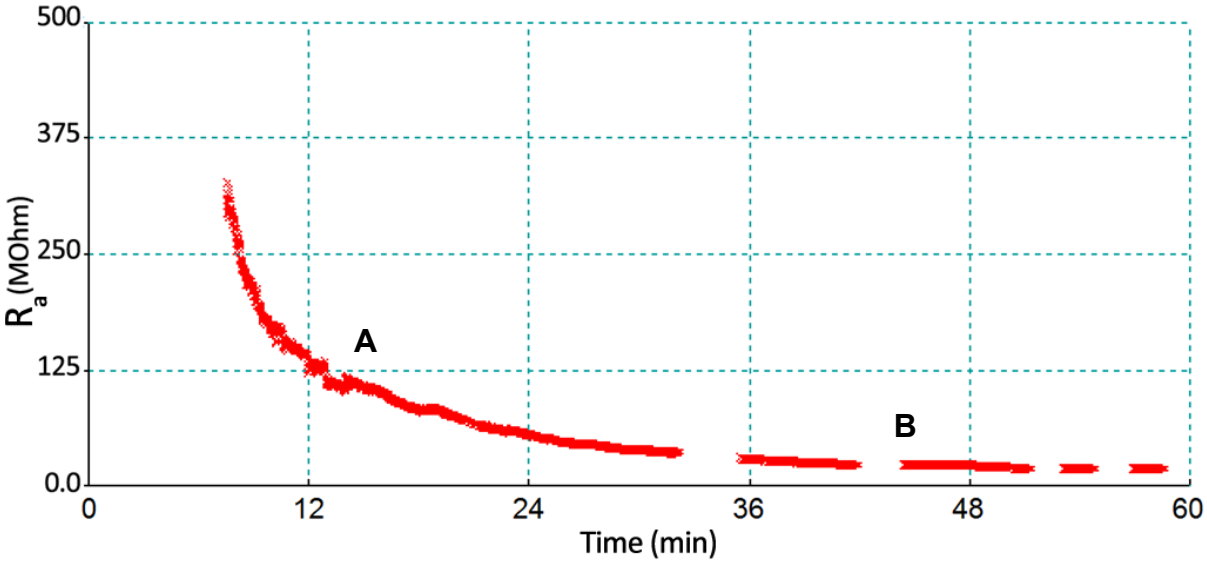

Fig. 12 Perforated patch, access resistance (R_a), in PC12 cell. (**A**) R_a sampled every second until access is achieved. (**B**) Experiment segment.

Sharp drops in R_a indicated a mechanical breakdown of patch membrane and transition to whole-cell configuration. The membrane breakdown could usually be verified upon visual inspection of membrane patch within a patch pipette under high magnification. Such recordings were discontinued (Fig. 13):

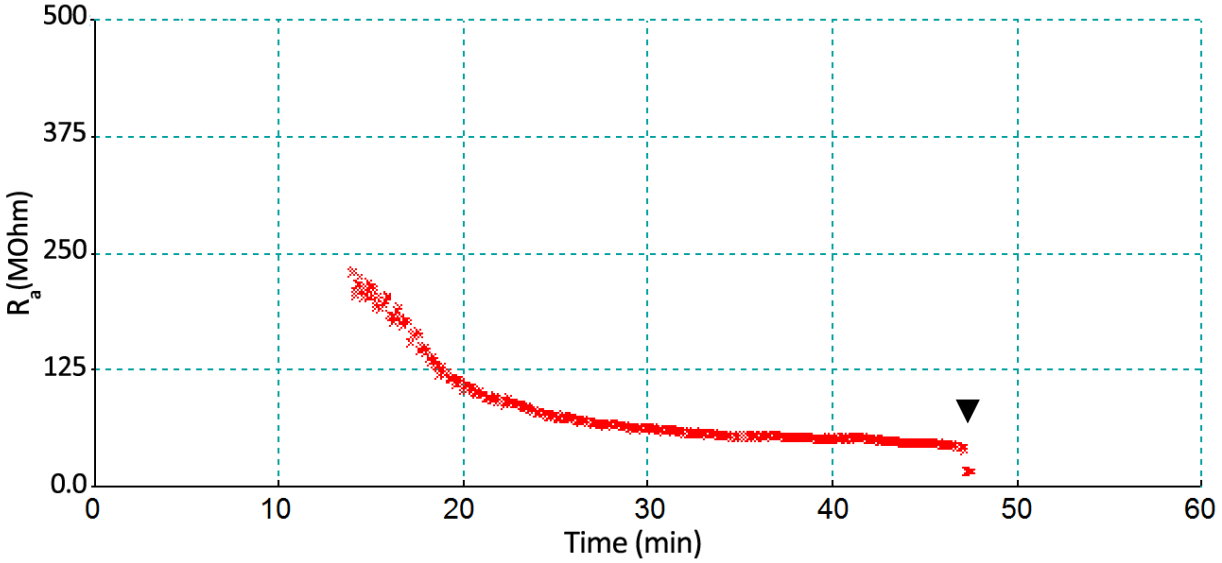

Fig. 13 Patch membrane breakdown during perforated patch (at ▼ mark), in PC12 cell.

Traces above were collected using a quick but a more comprehensive estimate of R_a from the amplitude of the capacitance artifact peak at the beginning of a 50 ms*10 mV voltage step. Within each second of the recording one such voltage step was recorded, providing one data point. In parallel to the rectangular 50 ms voltage step, a 100 ms sine wave segment was collected within the remaining 950 ms of each second. This parallel recording was started only when R_a value approached 40 MOhm. Both sine wave and rectangle pulse provided R_a estimates every second, but following a different algorithm. Each of 100 ms sine wave segments also provided three readouts: G_S, G_M and C_m (Access conductance, membrane conductance and membrane capacitance) (Fig. 14). Access conductance (G_S) is inversely proportional to R_a:

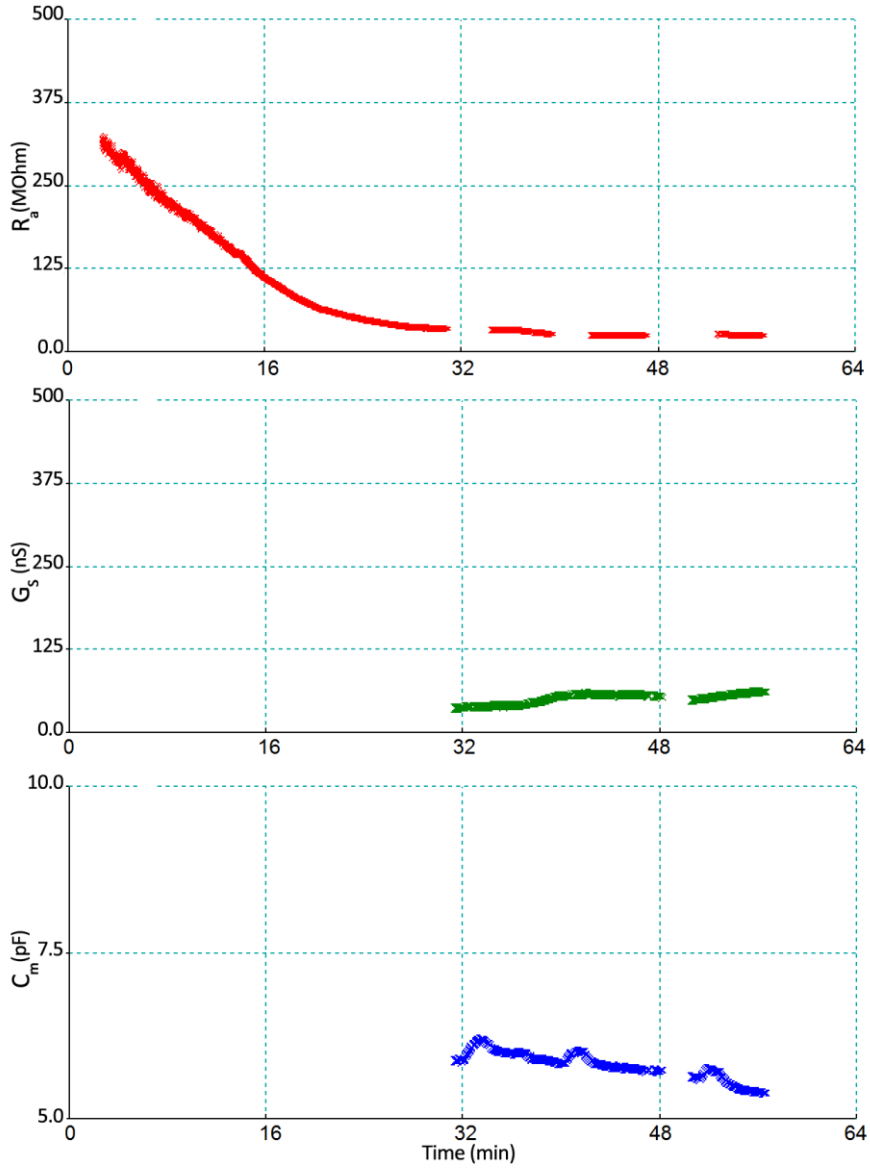

Fig. 14 Parallel recording of Access resistance (R_a, red), Access conductance (G_S, green) and Capacitance (C_m, blue), overview. Overlapping sections of R_a and G_S traces were collected simultaneously at a sampling rate of 1Hz for R_a and 2000Hz for G_S and C_m. Above data is resampled at 1Hz for both modes.

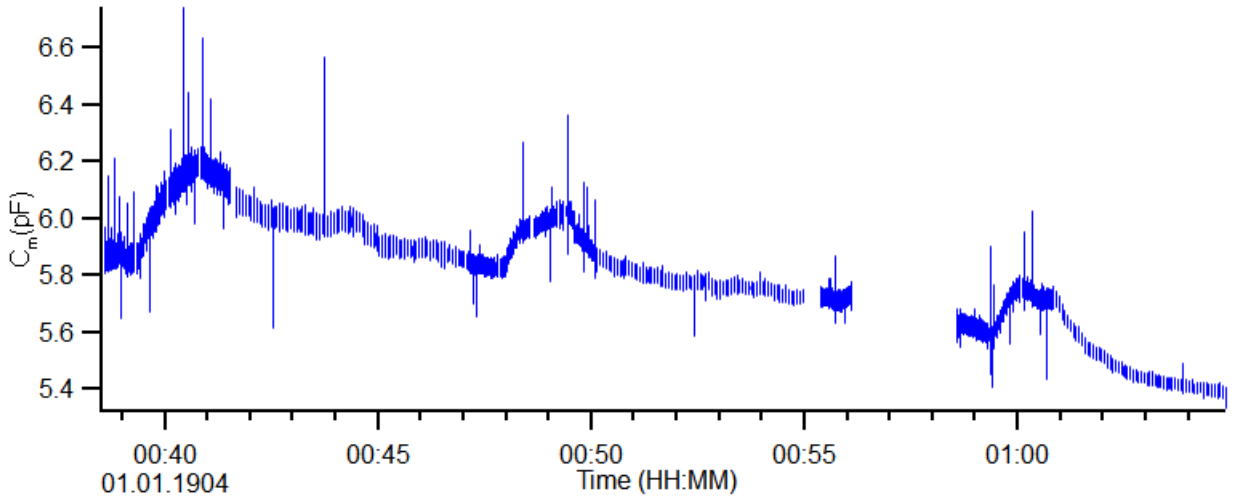

Fig. 15 A magnification of high-resolution capacitance (C_m) recording from Fig. 14, at 2kHz

Data collection was not continuous, even though all sine wave-derived data was collected at 2 kHz. This is because a single-channel amplifier cannot generate a sine wave and a rectangular voltage step simultaneously. Spaces in the trace of Fig. 15 contain either rectangular voltage steps used for R_a estimation or indicate a time skip. In the data gaps no observation of cell state was made. The cell however was kept at holding potential of -80 mV throughout the experiment.

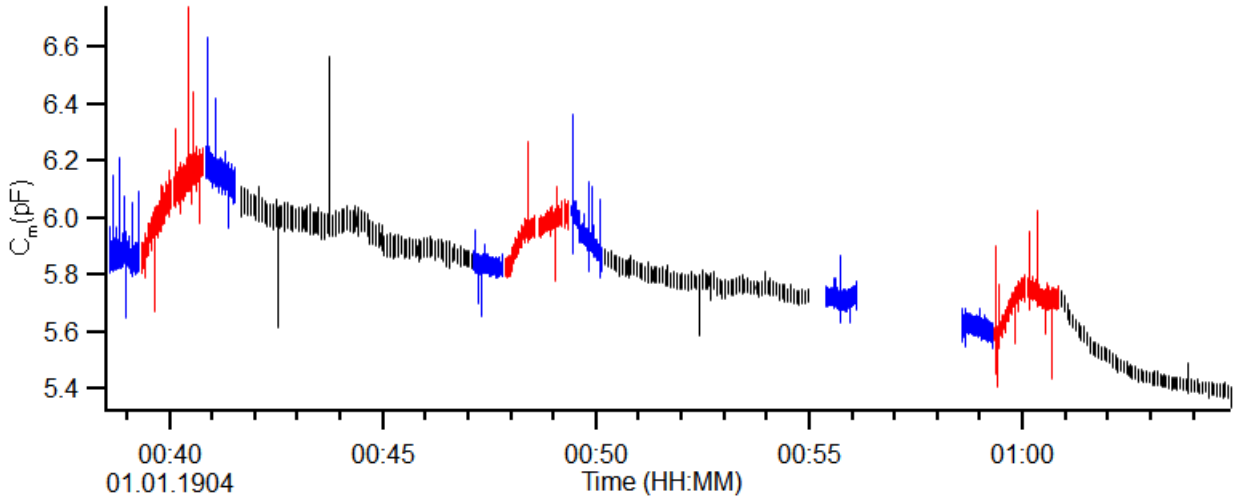

Fig. 16 Exemplary 2kHz capacitance data recording. Color-annotated by type of data collection: see text below for details

Colors in Fig. 16 indicate different kinds of recording segments. Membrane capacitance was always recorded by application of the sine wave protocol. Data segments that

contained 10 ms depolarization step to +20 mV holding potential are annotated in red. In blue are the areas of higher data density (2 s of continuous data per 4 s of real time) while black indicates lower data density (100 ms of data per 1 s) (Fig. 17):

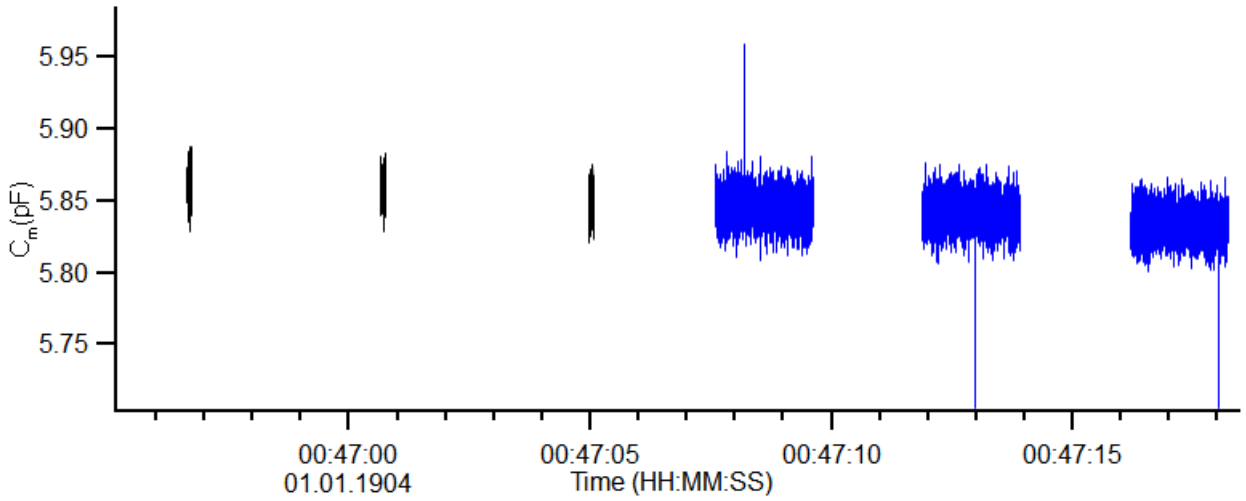

Fig. 17 2kHz capacitance data, segment of Fig. 16. Transition from lower (black) to higher (blue) density data collection modes.

Blue and red segments in Fig. 16 and Fig. 19 differ only in red segments containing a 10 ms depolarization step to +20 mV (Fig. 18,B), while blue segments simply keep membrane potential at holding level of -80 mV. In this way, blue segments are an internal control for the depolarization step containing segments.

Figure 18 is a zoom-in of a trace segment shown in Fig. 19. The time point is denoted by the triangle (▼). Note the 10 ms gap in the middle of capacitance trace, below current peak.

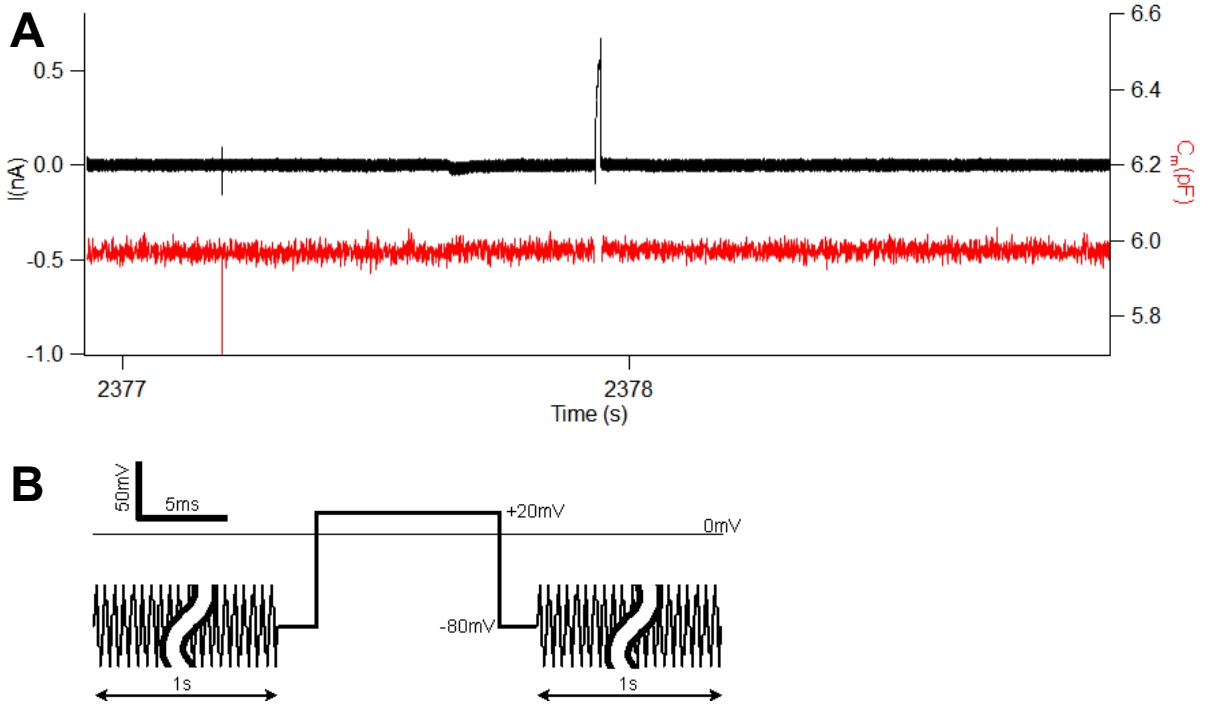

Fig. 18 Zoom in of 2kHz capacitance data, segment of Fig. 19: 10 ms depolarization pulse. (**A**) Black trace is the sine wave current (nA) interrupted by a 10 ms voltage step in the middle. Red trace is membrane capacitance (pF) derived from above sine wave using phase-sensitive software lock-in. Note the lack of data in the red capacitance trace during the voltage step response in the middle of the traces. (**B**) Command voltage protocol.

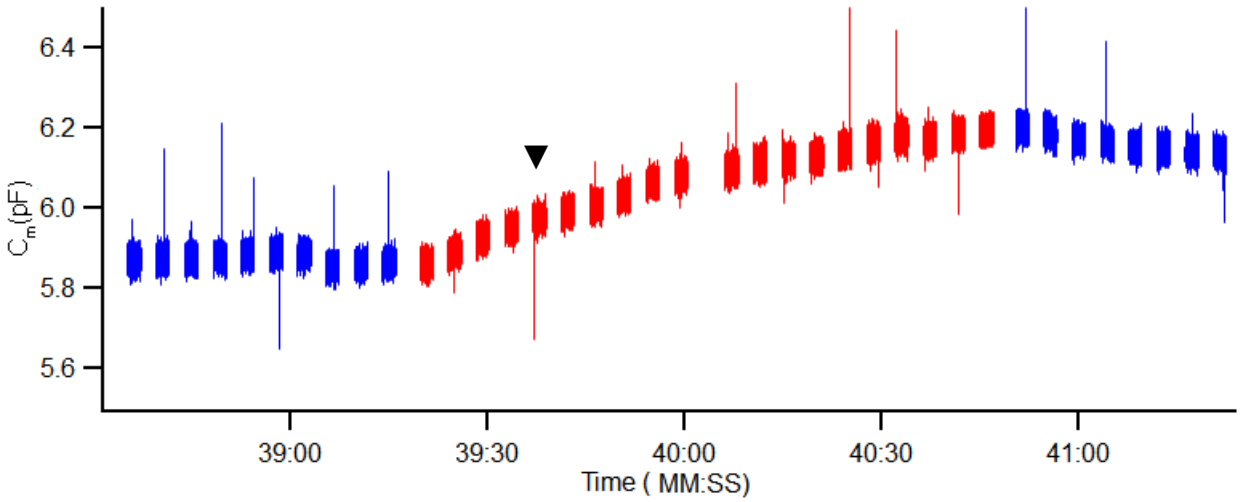

Fig. 19 2kHz capacitance data, changes during depolarization train segment (red). (▼) indicates the location of details shown in Fig. 18A.

Baseline capacitance rises in response to a train of 10 ms depolarization steps (Fig. 19, red segments). The increase stops, as soon the depolarization pulses were discontinued

(right blue segments).

High resolution C_m data (Fig. 18) was collected in all experiments in the anticipation of observing a sharp increase of capacitance on a scale of few milliseconds to a second. Such an increase could be quantified in regards to number or size of vesicles fusing with plasma membrane. However no such sharp increases were observed when comparing the traces before and after each depolarization step. Still, when comparing every trace to the next one a clear difference in capacitance between the steps was seen. For analysis, each high-resolution capacitance trace was line-fitted to produce a single value. This provided a low-time resolution capacitance recording for each depolarization train (Fig. 20):

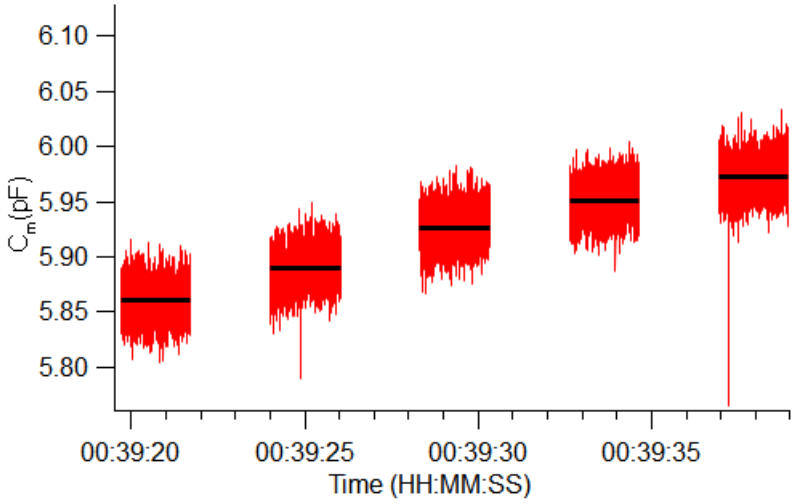

Fig. 20 2kHz capacitance data, segments of Fig. 19. Line-fitting of depolarization train segment (black).

In the Figures 15 and 16 there's a trend of total membrane capacitance decrease. It is observable over the course of several minutes to tens of minutes. This trend is reversed only upon depolarization. The slope of this trend differed among cells but it was present in all recordings. We believe that this downward trend in capacitance is a result of combination of electrostatic and/or pressure effects that each cell is subjected to during patching. It may also be related to membrane reuptake. The portion of the cell that remained exposed to extracellular solution after typical 60-120 minutes of patching became visibly smaller compared to initial state. The portion of the cell that was sucked into the patch pipette increased. Visible membrane patch “creeps” into volume of the pipette, away from pipette opening. This “creep” was not stopped even when switching from ambient pressure to overpressure inside the patch pipette. As the result, the area of

the cell's membrane which remained exposed to extracellular solution decreased. This decreased the effective area of the capacitor under voltage clamp control. Because the slopes of this trend from cell to cell were different, the linearization of traces around the point of 1st depolarization step was necessary. Otherwise, the absolute values of C_m change between each trace could not be directly compared. The slope of each recording was estimated from capacitance recorded in the passive non-depolarizing segment, just before the first depolarization step of the train (Fig. 21):

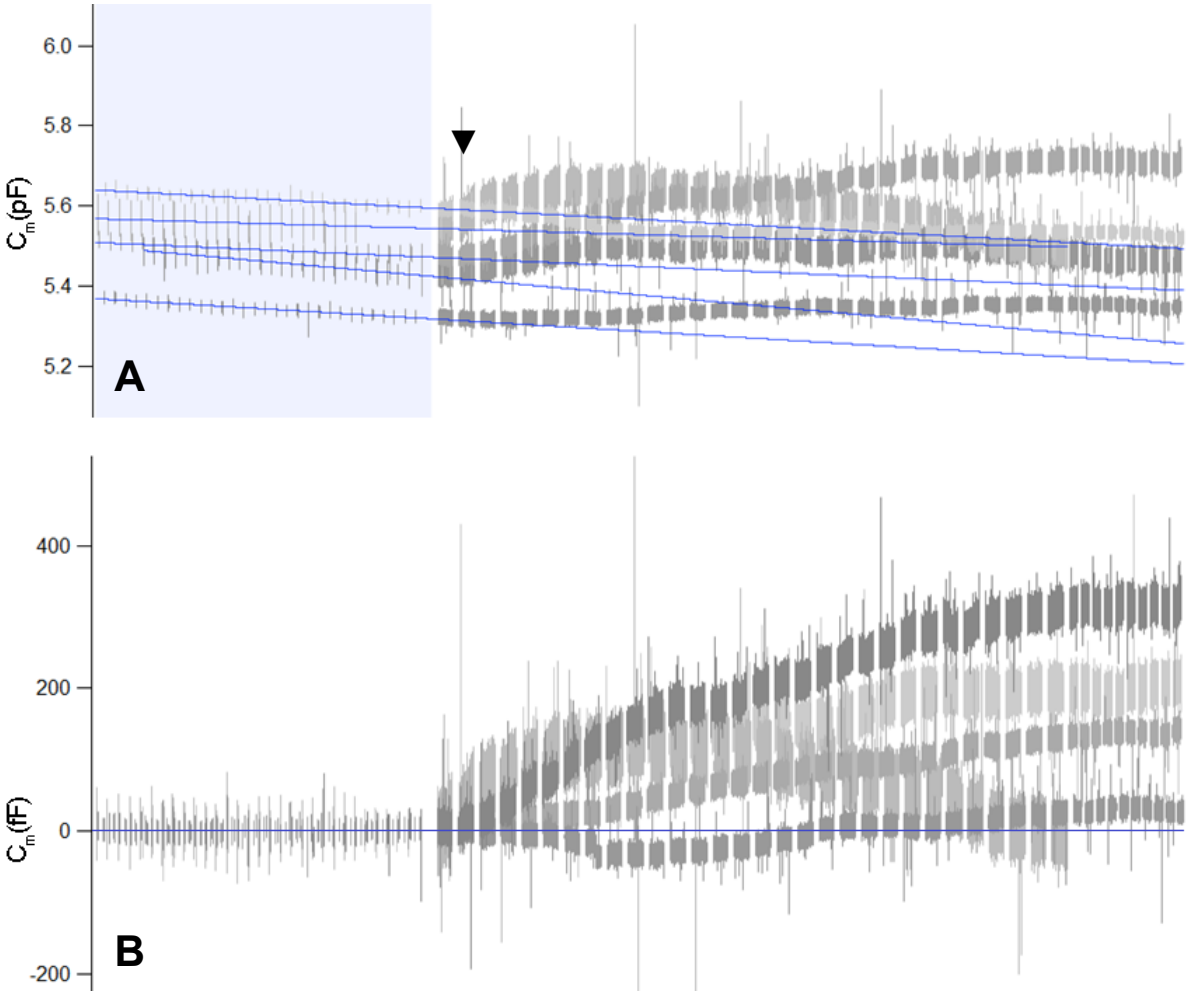

Fig. 21 Local capacitance data linearization. (**A**) A collection of traces from 5 different PC12 cells with comparable baseline capacitance values. Depolarization trains start at the marked position (▼). Slope of data within the light blue box is used for linearization. (**B**) Resulting data after linearization.

The response of PC12 cells to twenty 10 ms depolarization steps was quantified according to line fitting and slope linearization procedures mentioned above (Fig. 22):

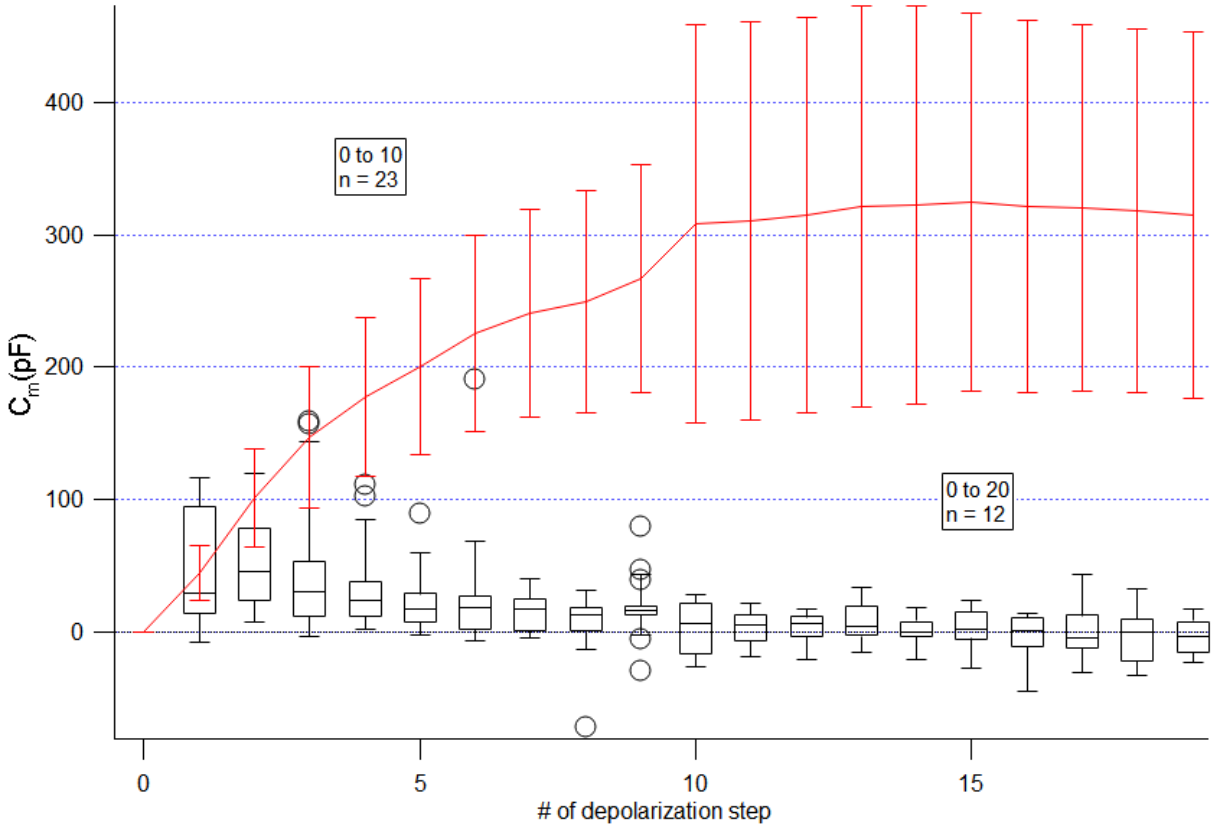

Fig. 22 Averaged C_m response of PC12 cells to first 20 consecutive depolarization pulses of 10 ms, linearized, in red. Size of each next C_m value compared to the value in the previous step (delta step), in black. Time between each depolarization step within the first 10 and second 10 pulses was 4.3 s on average. 23 cells were subject to at least 10 pulses, of which 12 were subjected to 20 pulses. Time between pulses #10 and #11 varied, but remained small (under 10 s). Error bar is standard error.

The duration of depolarizations was increased, since 10 ms depolarization pulses did not always produce a visible response. For subsequent experiments, each depolarization segment was modified to include five 100 ms depolarization steps from -80 mV to +20 mV. This was done to maximize the impact of a depolarization train on each cell. The number of segments in each depolarization train was increased from 20 to 30. Most cells were subjected to two depolarization trains with a total of 60 segments. The individual trains were separated by varying amount of time (513 s on average, n_c = 7).

This was done to (I) probe the potential for a strong repeated depolarization-induced influx of Ca^{2+} to exhaust the releasable pool of vesicles in each cell, and (II) to maximize the number of cells with depolarization-induced changes in C_m.

In retrospect, the magnitude of responses of best-responding PC12 cells subjected to 10 ms depolarization pulses every 4.3 s appeared larger than typical responses to 5x100 ms depolarization trains every 7.8 s. One of the explanations to this might be a decrease in PC12 cells secretory capability as the culture progressed through passages during culturing. While all data was collected from the same run of PC12 culture, last recordings from a 5x100 ms protocol were collected 15 weeks later compared to last recordings of 1x10 ms protocol. Another explanation might be the inhibition of Ca^{2+}-permeable voltage gated channels by cumulative 500 ms depolarizations to +20 mV every 7.8 s., compared to single 10 ms depolarizations every 4.3 s.

Nevertheless, all further measurements were conducted using a 30x5x500 ms depolarization protocol.

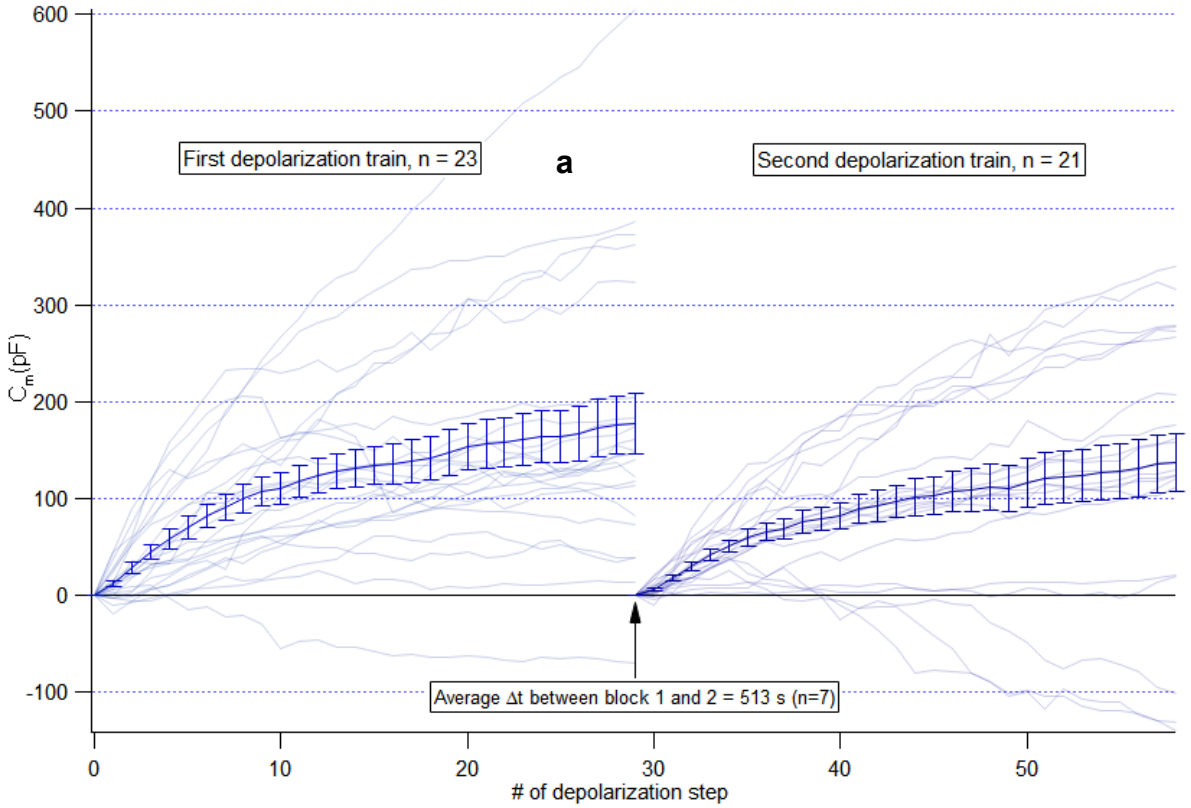

Fig. 23 Averaged C_m response of PC12 cells to the first and the second train of depolarizations (30x5x100 ms), linearized. All cells which were subjected to the second depolarization train did experience the first depolarization train. Time between first and second train was 513 s on average. The duration of each depolarization train was 235 +/-2 s. Time between each depolarization step within a train is 7.8 s. Error bar is standard error.

With the changed depolarization protocol, the PC12 cells reacted similarly with increase in C_m (Fig. 23). The total increase of membrane capacitance by the end of depolarization train was in the range of 100-200 fF, in some cases up to 400 fF (Fig. 23, a). Some cells still did not respond to depolarization. While the general trend of C_m decrease remained present, the cells could recover between the first and the second depolarization trains. Some responded with C_m increase even during the third depolarization train (not shown). In all cases, within one cell, the total capacitance increase was smaller for every next depolarization train.

With this result, we established the method of sine-wave capacitance recording and confirmed the capacitance response of PC12 cells to depolarization. The PC12 cell line was discontinued. In the next step, we focused on the capacitance responses of the Oli-neu cell line.

4.1.2 Oli-neu cell line – capacitance recording in NG2-glia model cells

Oli-neu cells were cultured and subjected to the same 30x 5x 100 ms depolarization pulse protocol as were the PC12 cells. The resolution of passive (non-depolarizing) segments was also increased. This was done to provide more information about what is happening with the cells before and after the depolarization train, and to provide internal control. The passive recording segments that flank the central depolarizing segment have the same duration and amount of data points as central depolarizing segment (Fig 24):

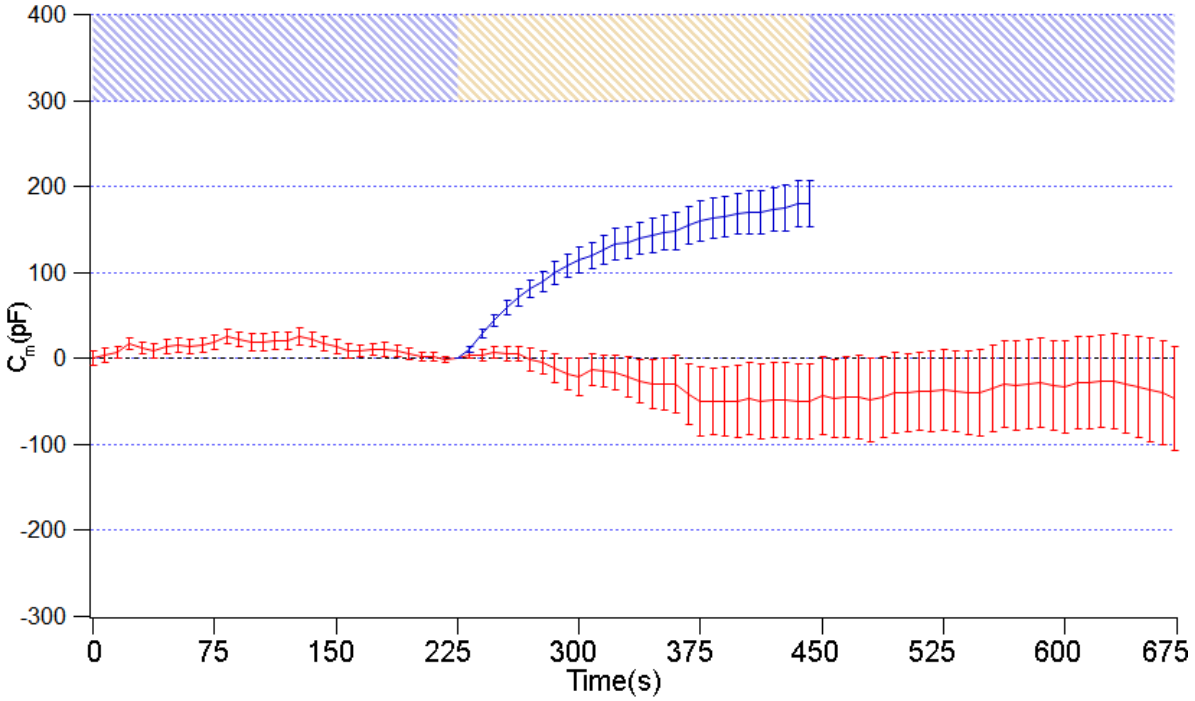

Fig. 24 Averaged C_m response of Oli-neu cells to the first train of depolarization (30x5x100 ms), **red** (n_c = 25). PC12 response to the same stimulation protocol, **blue** (n_c = 32), for comparison. Dashed areas in light blue indicate the passive (non-depolarizing segments), while the dashed area in yellow indicates the time when cell was subjected to a depolarization train. The duration of each depolarization train was 235+/-2 s. Time between each depolarization step within a train was 7.8 s. Error bar is standard error.

No increase of recorded C_m was observed during or after the depolarization of Oli-neu cells.

With this result, Oli-neu cell line was discontinued, and remaining experiments were carried out in NG2-glial cells *in situ,* using acute brain slices.

4.1.3 Capacitance recording from NG2-glial cells in acute brain slices.

Using the same depolarization protocol, NG2-glial cells were analyzed *in situ*, using acute brain slices obtained from 5 male and 5 female NG2-EYFP mice aged P7-P13 (Fig. 25).

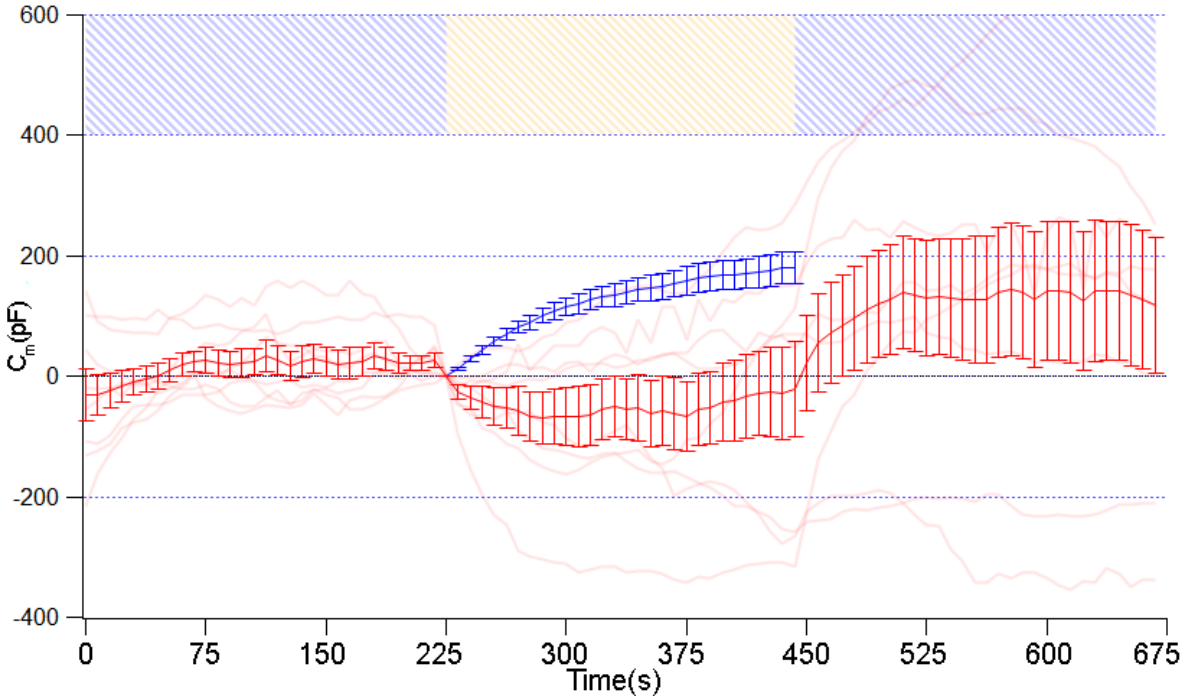

Fig. 25 Averaged C_m response of *in situ* NG2-glial cells to one train of depolarization (30x5x100 ms), in **red** (n_c = 8). PC12 response to the same stimulation protocol, in **blue** (n_c = 32), for comparison. Error bar is standard error.

Subjected to depolarization trains, the NG2-glial cells did not demonstrate the increase in membrane capacitance similar to PC12 cells. The decrease in baseline capacitance during depolarization train may be attributed to voltage gating artifacts. However, the capacitance baseline increase above the zero level in the post-stimulation segment was not due to this kind of artifact.

To trigger the fusion events without involving the voltage-gated channels, 1 µM dihydroxyphenylglycine (DHPG) was applied via bath wash-in. No amplifier depolarization was used during recordings in DHPG solution. Instead, all three segments were replaced with passive capacitance recording with cells clamped at the holding potential of -80 mV. The application of DHPG solution was timed to follow the

end of first recording segment (Fig. 26):

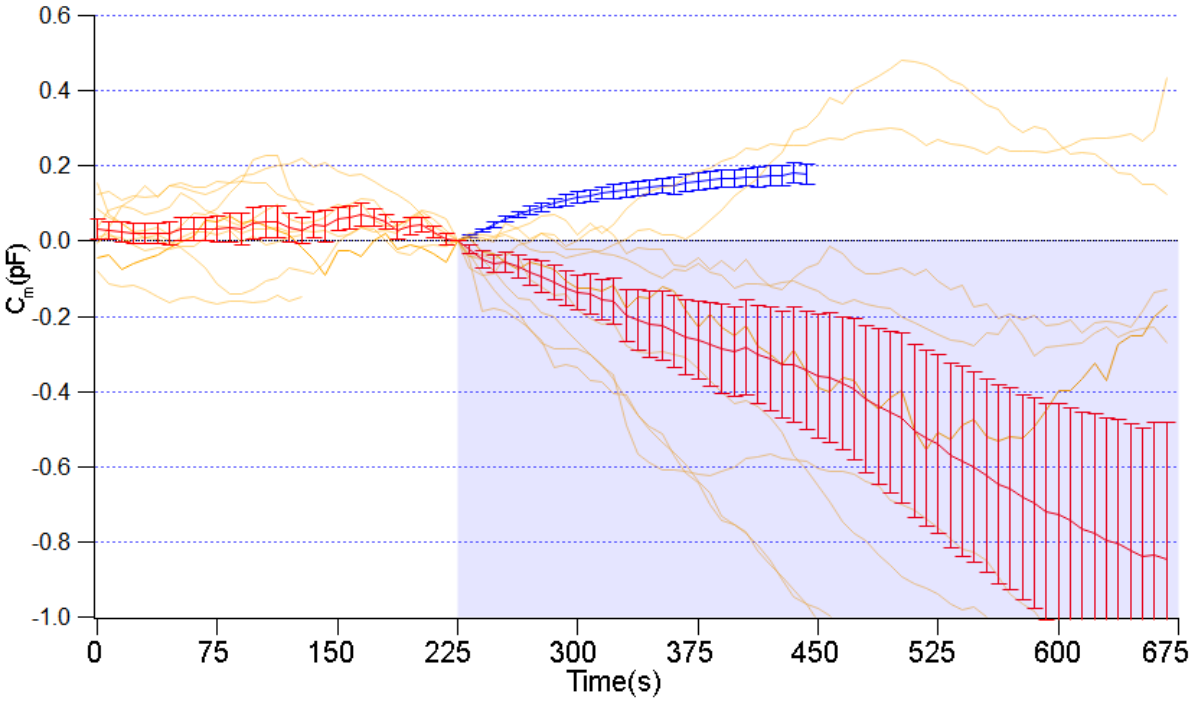

Fig. 26 Averaged C_m response of *in situ* NG2-glial cells to bath application of DHPG at 0.1 µM, in **r**ed (n_c = 7), without membrane depolarization. Light blue filled area indicates the presence of DHPG in the extracellular solution. PC12 response to the depolarization train protocol (no DHPG wash-in), in blue (n=32), for comparison. Error bar is standard error.

We assumed that whole cell current noise might mask small C_m changes caused by fusion of small intracellular vesicles. Capacitance recordings in whole-cell perforated-patch configuration were discontinued for this reason. Next, we tested whether the results change if we employ the cell attached mode configuration.

4.1.4 Cell-attached capacitance measurement in NG2-glia – important caveat revealed

The next recordings were performed in cell-attached mode. This method improves the signal to noise ratio and therefore the resolution of C_m recordings. However, C_m measurements in this mode are collected only from the small area directly underneath the patch-pipette. Information about the rest of the cell plasma membrane is missing in the cell-attached mode. For necessary calibration of sine wave phase, an amplifier-controlled suction pulse was automatically applied to patch pipette. These suction pulses are marked with a black arrowhead (Fig. 27).

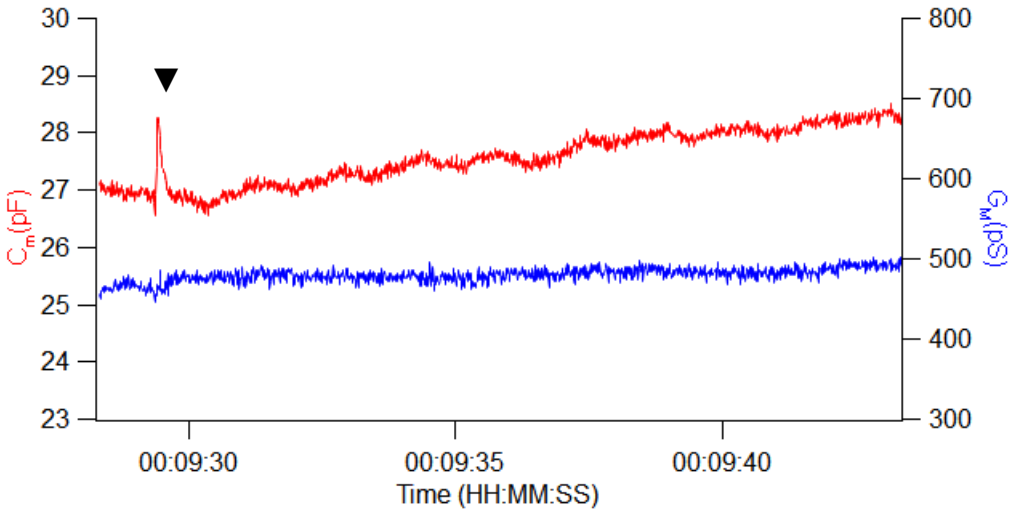

:

Fig. 27 Cell-attached mode recordings from NG2-glial cells of acute brain slices. C_m recording (**red trace**, left axis) with corresponding observation of the membrane conductance (G_M, **blue trace**, right axis). The protocol duration is 15 s. The suction pulse is issued after 1 s. Note: The test pulse response occurs only in C_m trace.

The recording protocol consisted of 15 s segments repeated 25 times, adding up to a total of 375 s. Suction pulses were applied at the beginning of every segment for phase quality control. The phase was calibrated correctly if the suction pulse occurred only in the capacitance trace. Membrane fusion events were triggered by activation of G_Q coupled metabotropic receptors. Specific ligands were washed-in the bath solution. The time point of wash-in was determined during previous experiments.

Upon wash-in of DHPG, on several occasions we observed a stepwise increase in recorded C_m (Fig. 28):

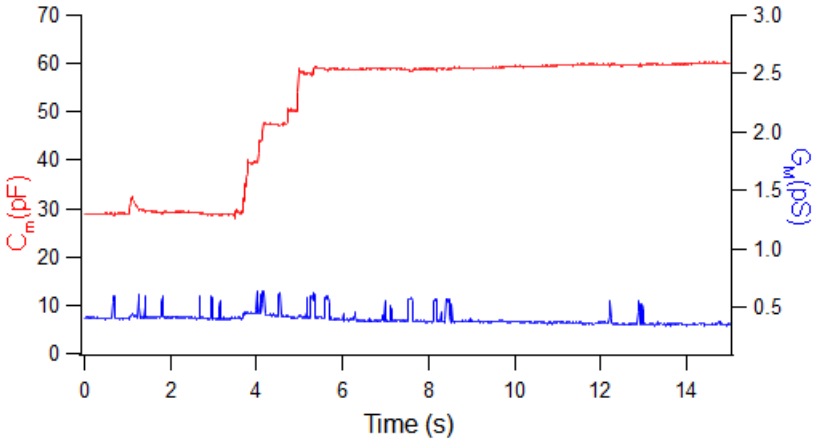

Fig. 28 Cell-attached C_m recording (red, left axis), with corresponding membrane conductance (G_M) trace (blue, right axis), in NG2-glial cell. Recording during wash-in of DHPG (1 µM).

The spike-like transient changes in the accompanying conductance trace (blue) might correspond to groups of individual ion channels spontaneously opening and closing within the confined area of membrane patch. The conductance changes were not reflected in the capacitance trace, and *vice versa.* This indicates the correct phase parameters.

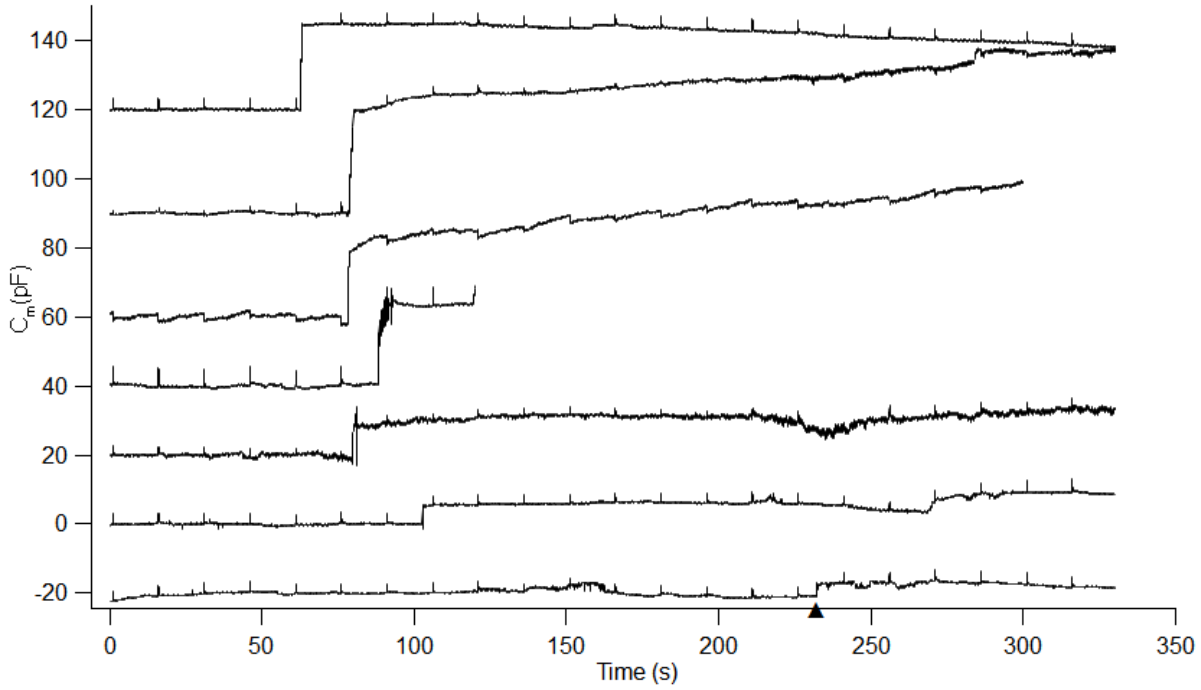

Fig. 29 Cell-attached C_m recordings, from 7 different *in situ* NG2-glial cells. Expected time of wash-in of 1 μM DHPG in the bath chamber is after around 70-75 s. Traces truncated on the right side represent cells that experienced a membrane breakdown during recording.

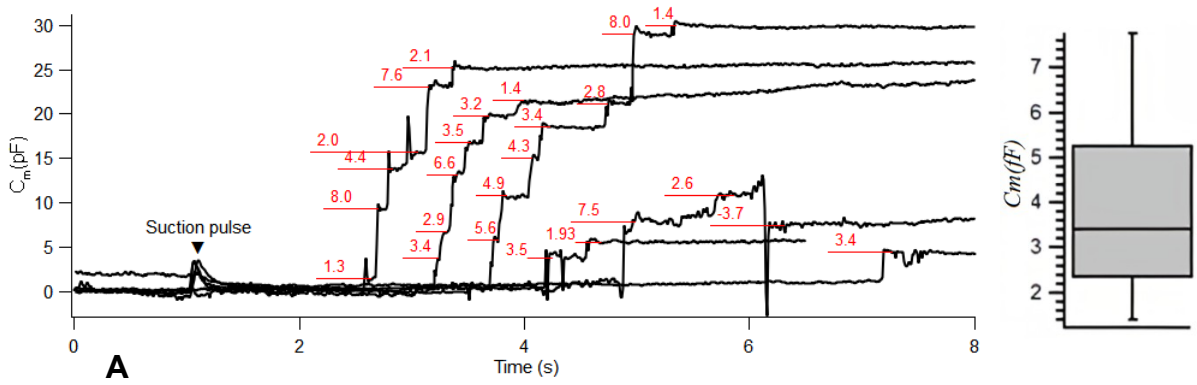

Fig. 30 Cell-attached C_m recording, *in situ* NG2-glial cells. (**A**) Recording during application of 1 μM DHPG. Differences in C_m between every next discernible step in **red** (fF). (**B**) Box plot of individual C_m step sizes.

B

Assuming the difference between each individual step within the staggered trace corresponds to an individual vesicle fusing with the membrane, the average size of steps in selected traces from Fig. 30 amounts to 3.87 fF. This corresponds to expected diameter of 0.351 μm that a fusing vesicle might have.

However, in some of the control recordings with drug-free ACSF wash-in the characteristic staggered response was also observed. The time to capacitance deflection was somewhat longer, from 195 s to 255 s (i.e. 2-3 min later than the timepoint of drug application)(Fig. 31):

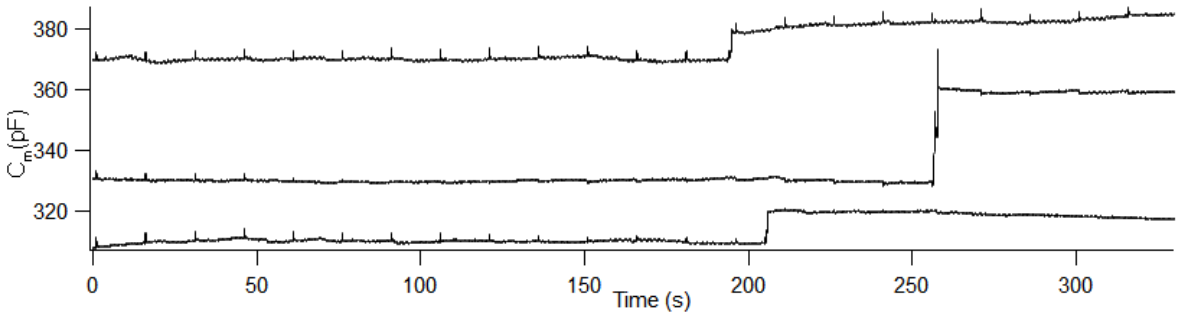

Fig. 31 Cell-attached membrane capacitance (C_m) recording, in NG2-glial cells (control recording). Drug-free ACSF is arriving at the same time (around 70-75 s after beginning of recording).

Another interesting observation was that, in line with the expected rarity of putative fusion events, most events were observed during the first hour of the recordings performed at the specific day. This was observed independently of the applied substance, i.e. ACSF or DHPG (Fig. 32).

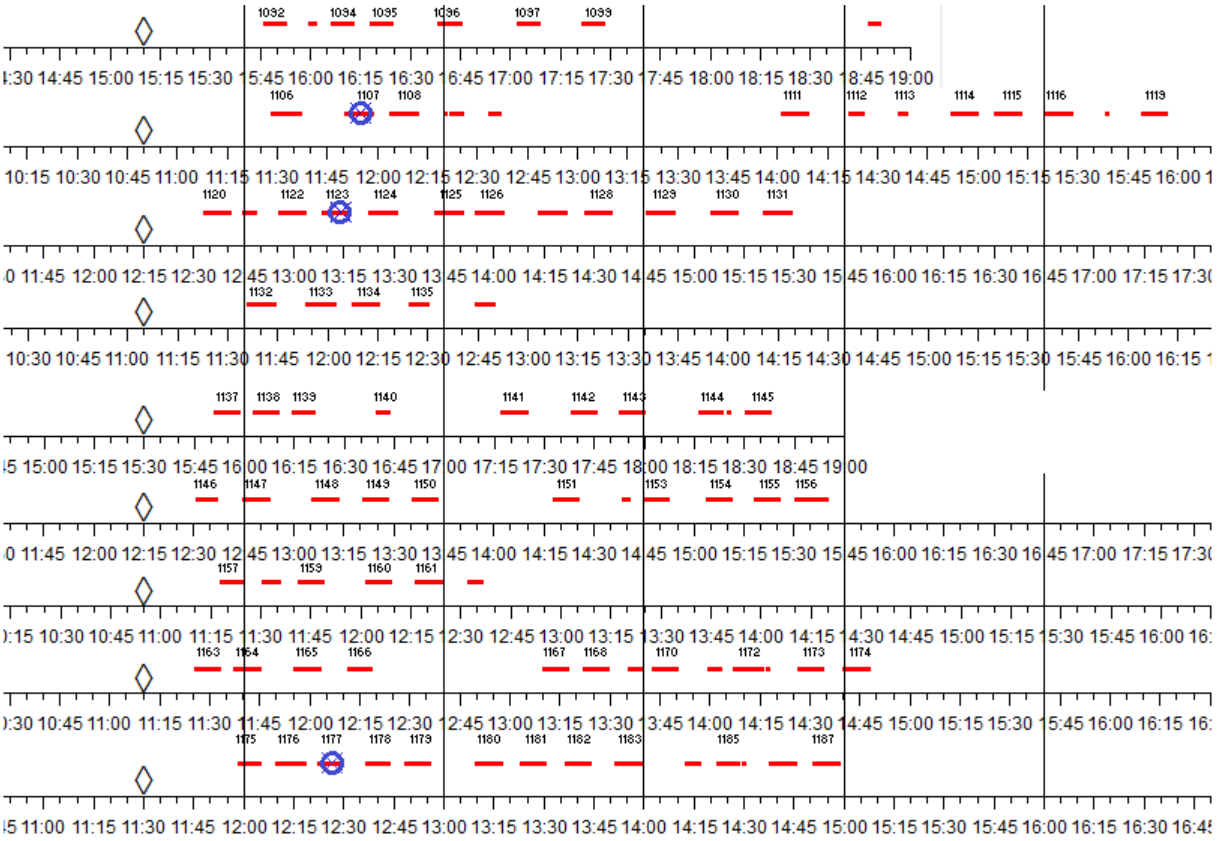

Fig. 32 Day time during cell-attached C_m recordings (in **red**), in NG2-glial cells (control data). The diamond indicates the time when the slice preparation was completed. Vertical lines show 1 h marks. Red dashes indicate recordings from individual cells and their duration. Blue crossed circles indicate the observed staggered events in C_m trace.

In the effort to identify the source of the capacitance changes the tubing delivery system was replaced. This was done to exclude the probability of drug substances depositing in the tubing and contaminating the control data. The following observation revealed the fact that capacitance recordings are subject to extreme changes in case the flow of delivered ACSF is disturbed by air bubbles in the system (Fig. 33):

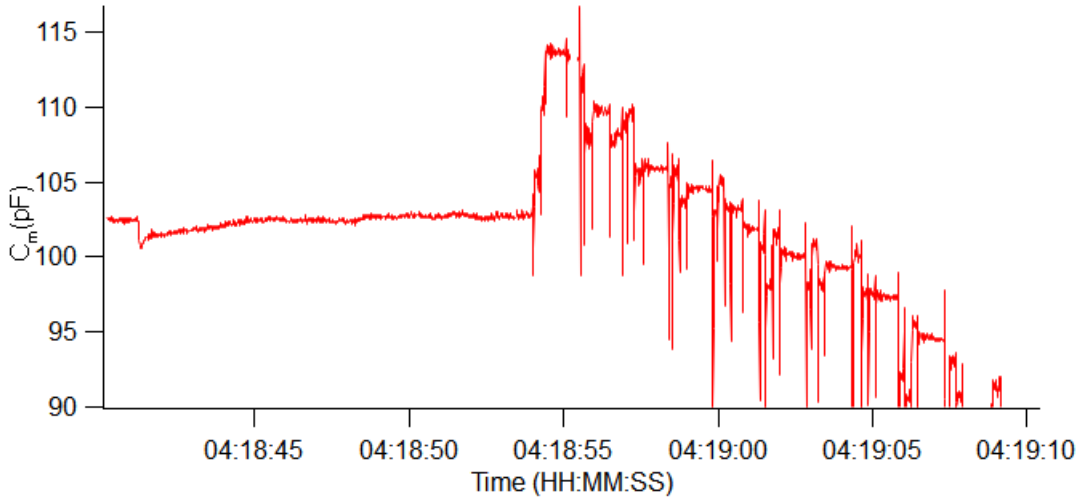

Fig. 33 Air-liquid mixture in the delivery system due to faulty fitting.

The familiar staggered appearance of capacitance trace change in this recording implicated the data previously collected as potentially erroneous. In subsequent observations, small air bubbles were purposefully injected into the ACSF delivery system (Fig. 34):

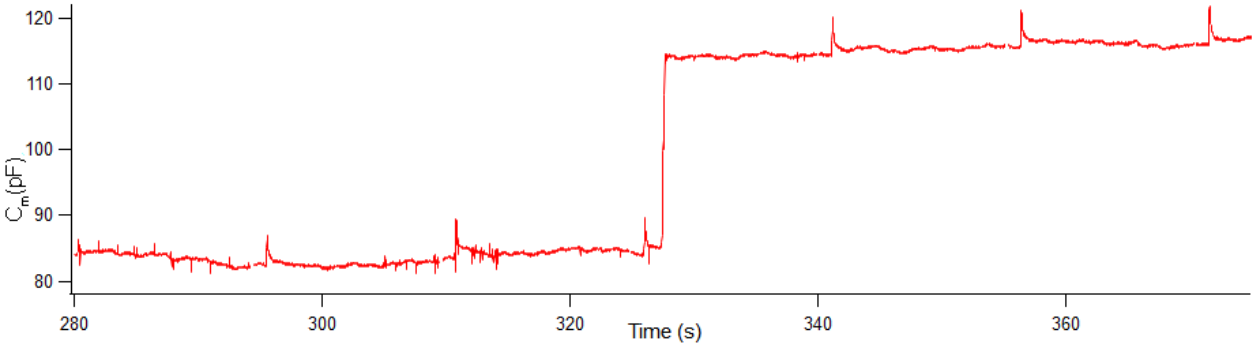

Fig. 34 Singular injection of an air bubble in the delivery system causing a persistent capacitance deflection in a recording from an NG2-glial cell.

Unexpectedly, the injection of the first bubble in the delivery system changed the baseline of the recorded capacitance. The change was not transient, unlike the bubble itself. To rule out the possibility of real fusion event being triggered by cells being disturbed by mechanical effects of a gas bubble bursting nearby, the patch pipette was sealed onto a submerged ball of Sylgard. This silicon elastomer can be used to simulate a gigaohm seal (Fig. 35):

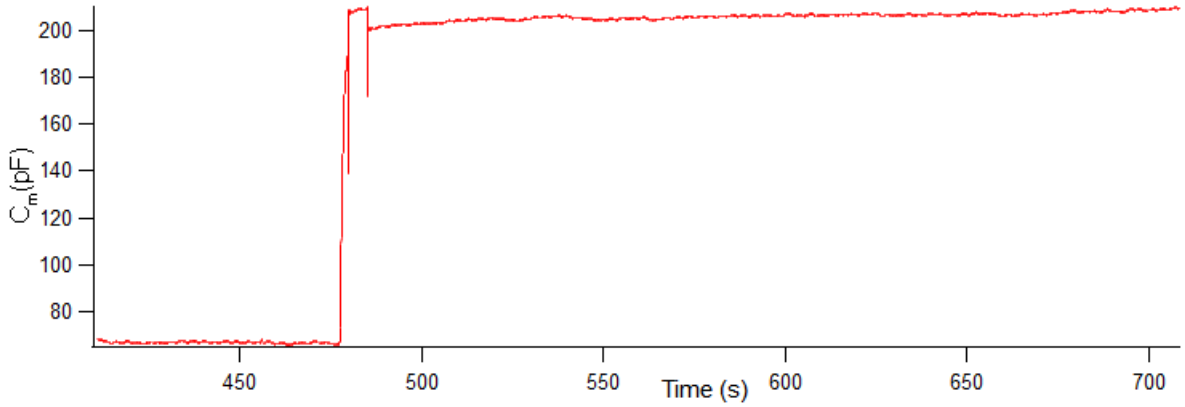

Fig. 35. Singular injection of an air bubble in the solution delivery system causing a persistent capacitance deflection in a recording from a submerged Sylgard ball.

With this result all previously observed presumed capacitance change events recorded in cell-attached configuration were obviously artifacts. Since the observed events fully corresponded to expectations of the real fusion event qualitatively, yet were artifacts, the real events, if any were registered by us, should then be different only in the quantitative sense. I.e., the parameters of real membrane fusion events can, perhaps, be distinguished from artifact events by their measurable parameters, for example duration, speed, absolute size, total number of events per cell, e.t.c. These parameters, however, are likely flexible across different cell types.

Outside of the implicated data segments, other segments of data collected did not demonstrate any other quantifiable class of C_m events.

4.2. Imaging experiments

Sets of imaging experiments were conducted as a second line of investigation into the potential for exosomal function in NG2-glial cells. The experiments involved immunofluorescent labeling of brain slices that were later extended with immunoelectron microscopy and correlated light-electron microscopy (CLEM).

4.2.1 Choice of imaging antibodies

Most of the experiments were conducted with NG2-glial cells of NG2-EYFP mice, since these animals provided the highest signal-to-noise ratio. The green channel was reserved for EYFP fluorescence, while two other channels were available for visualization of other markers.

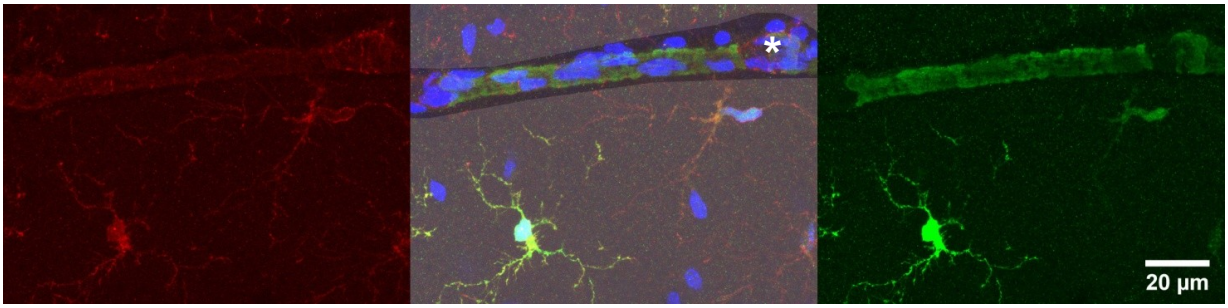

Fig. 36 An NG2-glial cell in *stratum oriens* of an NG2-EYFP mouse hippocampus. Maximum intensity projection (MIP), 20 planes, 5.48 µm in total. On the **left** – antibody labeling against an NG2 protein (red), on the **right** – antibody labeling against EYFP (green), in the **center** – composite image indicating a large vessel (*). Cell nuclei are labeled with DAPI (blue).

EYFP was found to be uniformly distributed through NG2-glial cells (Fig. 36). Relative thickness of cell soma compared to processes creates a strong localized signal. This and the tendency of NG2-glial cells to spread away from each other created a picture where individual NG2-glial cells were easily identifiable (Fig. 37). On occasions, some NG2-glial cells were visible in close proximity to each other, indicating an ongoing division, or division which was completed recently.

It should be noted that EYFP expression sometimes failed in NG2-EYFP cells completely, or EYFP was under-expressed (Fig. 38). In original publication by Karram (Karram et al., 2008), the number of these cells was estimated at around 1 %. In our

work, we estimate the number of cells which fail to express EYFP at around 5 %, however no study of EYFP expression versus NG2 expression was made in more than few samples due to added complexity of using third or fourth channel to visualize NG2 on top of EYFP and a putative exosomal marker protein. Nevertheless, the NG2-glial cells that failed to express EYFP have to be considered as a potential source of spurious signal when identifying features pertaining to NG2-EYFP-glial cells, if EYFP alone is used as guidance.

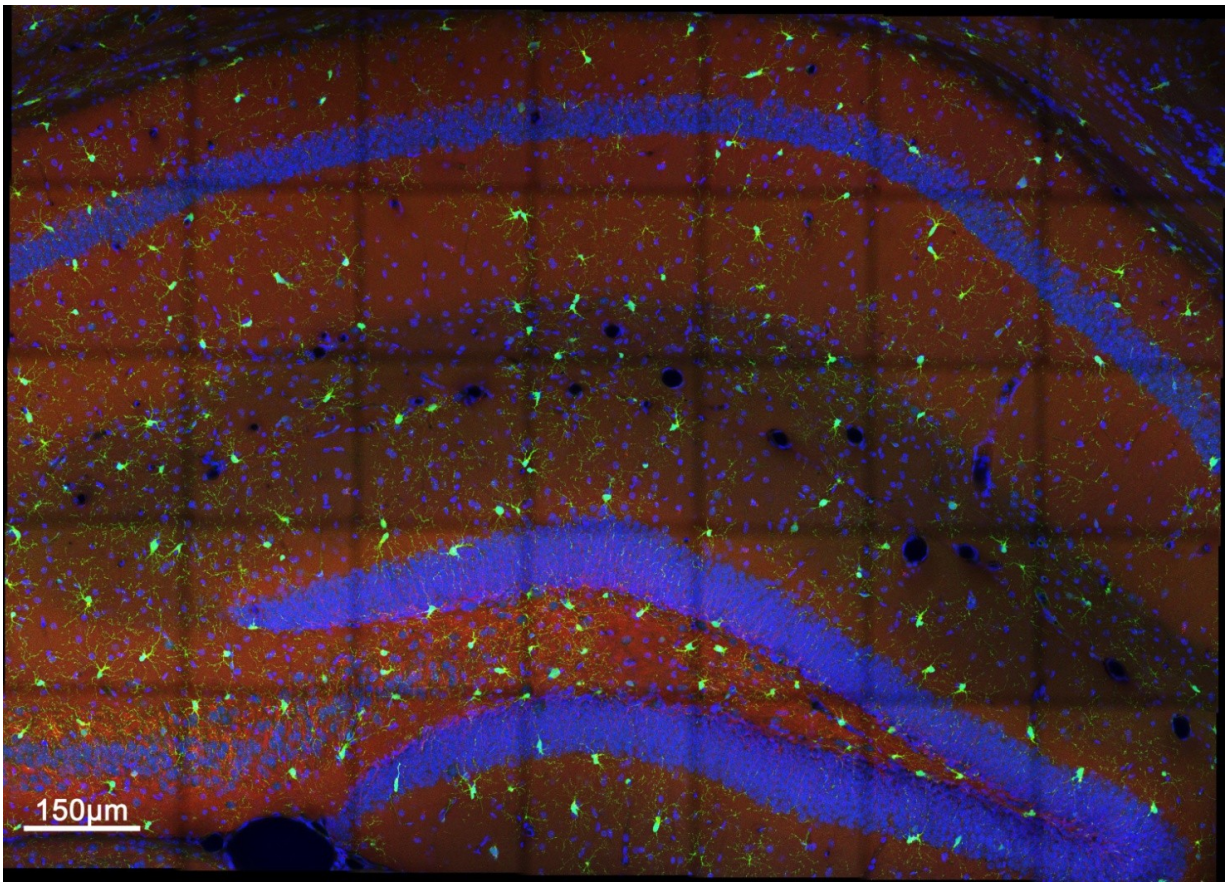

Fig. 37 Mosaic image of NG2-EYFP fluorescence in the mouse hippocampus, MIP. Each square tile has a side of about 220 µm. The total image stack is 1.54 mm x 1.1 mm x 5 µm and was recorded in 20 equidistant z-planes with 250 nm focal depth. Blue – Hoechst labeling, antibody staining: green – anti-EYFP, red – anti-Flotillin-1. The dark grid over image is the result of mosaic stitching.

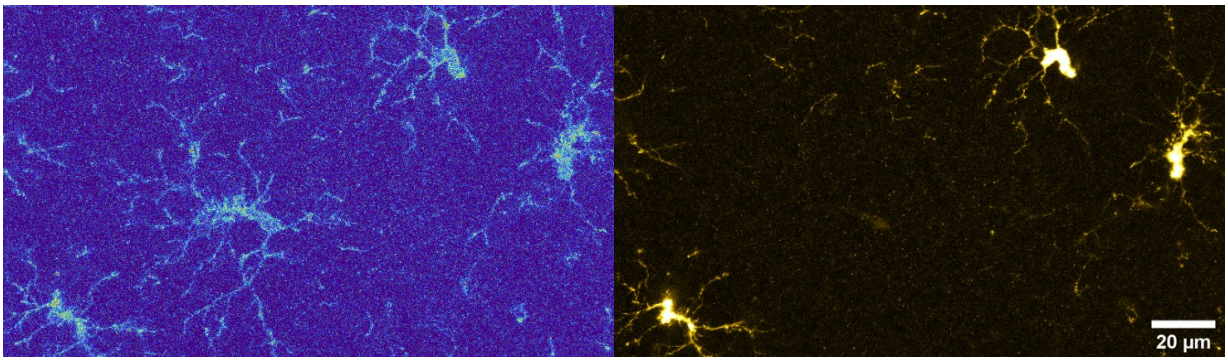

Fig. 38 NG2-glial cells in *stratum radiatum* of an NG2-EYFP mouse hippocampus, MIP, 5 µm over 20 planes. On the **left** – antibody labeling against an NG2 protein, on the **right** – antibody-enhanced labeling against EYFP. Note the cell in the center is largely missing EYFP.

Initial imaging experiments were made using pairs of antibodies against known markers of exosomes or exosome pathways. In particular, those were co-labeling with CD63 and Alix, and CD63 and Flotillin-1.

4.2.2 CD63 co-labeling with Alix and Flotillin-1

We co-labeled brain slices using pairs of antibodies against markers previously described as related to exosomes. Co-detection of both markers would indicate potential presence of exosomes in NG2-glial cells. Since the anti-Alix and anti-Flotillin-1 antibodies that were available for purchase were both made in rabbit host, co-labeling of these two markers in one sample was not carried out. Pairs of CD63 and Alix, or CD63 and Flotillin-1 were imaged together, without overlap of secondary antibody signals.

4.2.3 Co-labeling of Alix and CD63

The anti-Alix labeling in hippocampus featured intense granular background. Most of the signal was associated with apical dendrites of pyramidal neurons (Fig. 39, A). Apical dendrites featured a fine granular pattern along the whole length of process in the *stratum radiatum.* Some neurons were upregulated in terms of Alix signal. A close spatial association was observed between an NG2-glial cell and an Alix-enriched neuron (Fig. 39, B). No dependency or direction of interaction was identified.

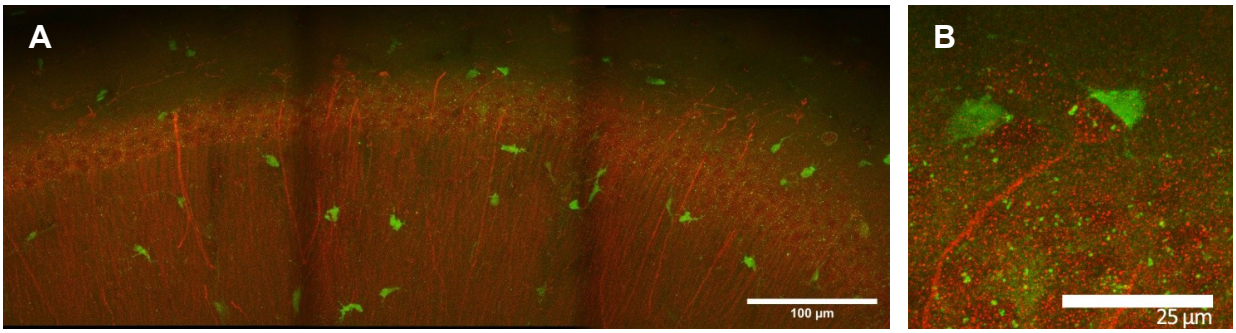

Fig. 39 (A) Overview of anti-Alix (red) labeling in an NG2-EYFP mouse hippocampus CA1 area. EYFP signal was not enhanced by antibody staining (green). **(B)** Detail of NG2-glial cell and an Alix-enriched neuron in close contact. Granular signal in the green channel in the projection of pyramidal layer is lipofuscin auto-fluorescence in the EYFP channel.

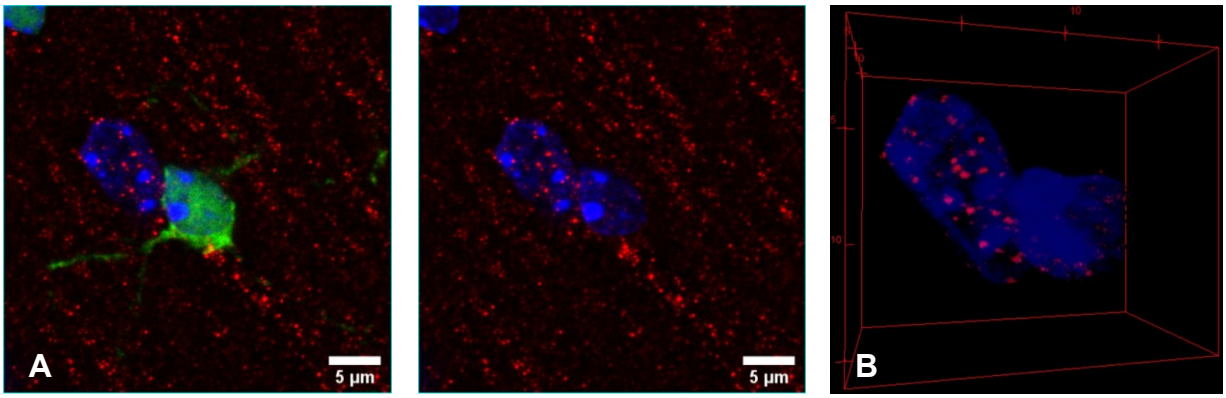

Fig. 40 An EYFP-positive (green) NG2-glial cell in *stratum radiatum* of an NG2-EYFP mouse hippocampus. MIP (24 slices over 8.54 µm) and a 30x30x10 µm, volumetric render of DAPI-stained nuclei. (**A**) The Alix-enriched apical dendrites can be seen in the surrounding tissue. The NG2-glial cell appeared downregulated in terms of Alix binding, when compared to neighboring cells in *stratum radiatum*. However a comparison of Alix-positive granule content in nuclei of EYFP-positive ($n_c = 9$) and EYFP-negative cells ($n_c = 42$) did not reveal significant differences. Alix-positive particle counts per nucleus and Alix-positive particle size of granules were not significantly different as assessed by two-tailed T-test of independent means. The p-values amounted to 0.26 and 0.95, respectively (**B**) 3D volumetric render of DAPI-stained nuclei. The volume was 30 µm x 30 µm x 10 µm. Render was constructed without EYFP channel data.

Unlike Alix and Flotillin-1, anti-CD63 labeling did not reveal any visible anatomical organization. CD63 did not delimit layers of tissue, shape of cells or any notable extracellular features. No clear dependence between CD63 and NG2-EYFP glia was observed. An unidentified subtype of hippocampal cells may feature enrichment in CD63 label (Fig. 41 C). Three-dimensional imagery of double stainings against both Alix and

CD63 did not reveal a significant colocalization between the markers. Quantification is given in Table 1.

Table 1. Quantification of colocalization of Alix and CD63 in EYFP-positive NG2 glial cells. Values close to 1 or close to 0.5 for Li's ICQ indicate significant colocalization (Dunn et al., 2011). Data outside of NG2-glial cells was masked in each plane individually prior to MIP. See Materials and Methods section for details. Data is a two-channel MIP (31 planes over 30 µm) of a part of CA1 SR of NG2-EYFP mouse, thresholded using Costes algorithm (Costes et al., 2004).

Pearson's R value (no threshold)	Pearson's R value (below threshold)	Pearson's R value (above threshold)	Li's ICQ value	Spearman's rank correlation value	Spearman's correlation t-statistic	Manders' M1 (Above zero intensity of Ch2)	Manders' M2 (Above zero intensity of Ch1)	Manders' tM1 (Above autothreshold of Ch2)	Manders' tM2 (Above autothreshold of Ch1)	Kendall's Tau-b rank correlation value
0.17	0	-0.14	0.135	0.271559	74.0588	0.85	0.809	0.244	0.382	0.1981

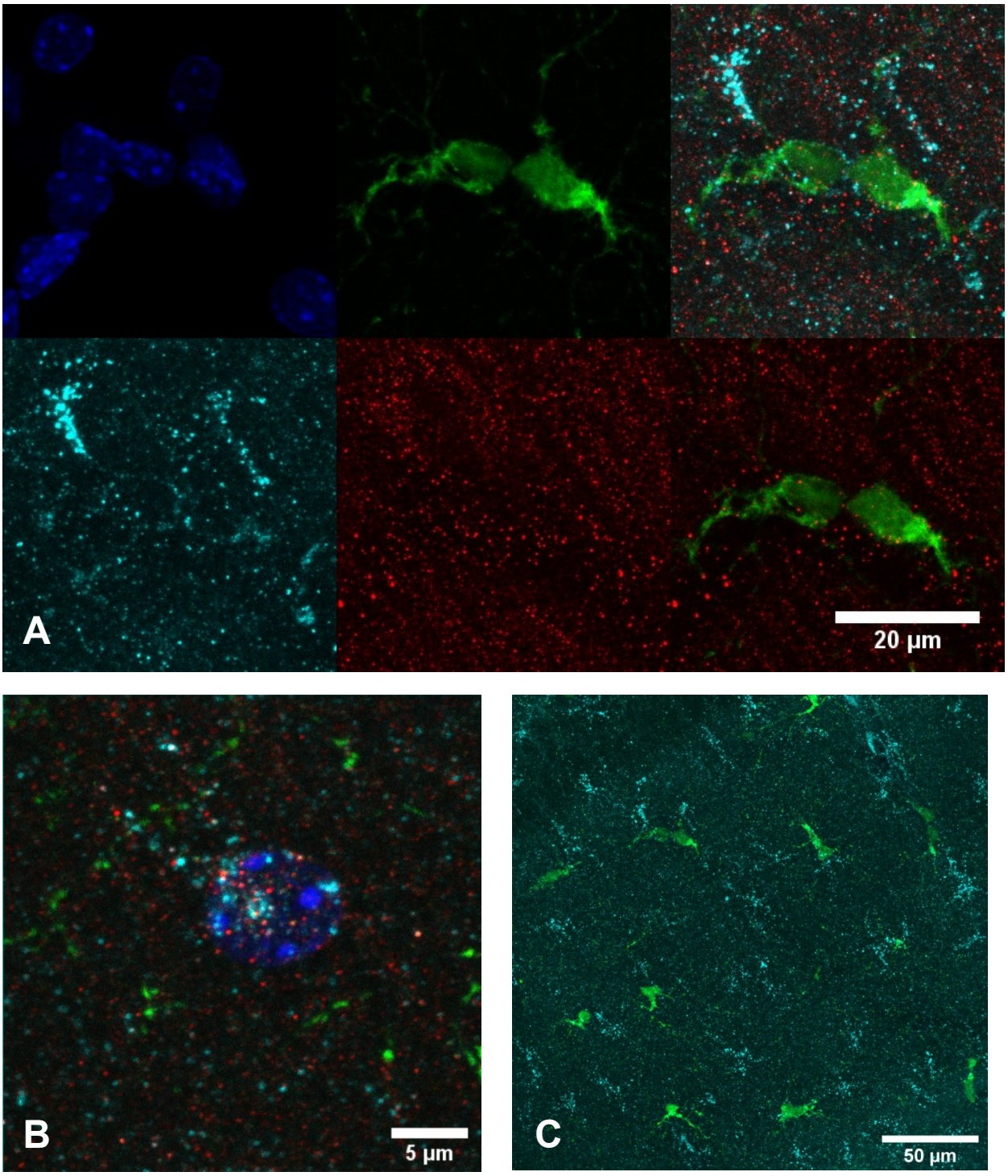

Fig. 41 Alix/CD63 labeling in mouse hippocampus **(A)** An EYFP-positive (green) NG2-glial cell in *stratum radiatum* of an NG2-EYFP mouse hippocampus. MIP, 30 µm x 30 µm x 9.6 µm over 27 slices. Alix (red), CD63 (cyan), Hoechst (blue). **(B)** An EYFP-negative cell in *stratum radiatum* of an NG2-EYFP mouse hippocampus (MIP, 30 µm x 30 µm x 10 µm over 28 slices). The illustrated cell of unknown type appeared enriched in Alix (red) and CD63 (cyan). Labeling against Alix and CD63 did not colocalize in three-dimensions. **(C)** CD63-enriched cells and NG2-EYFP positive cells, MIP(246 µm x 246 µm x 30 µm over 30 slices)

4.2.4 Co-labeling of Flotillin-1 and CD63

CD63 was observed in close proximity or colocalized to some Flotillin-1 positive granules in some NG2-EYFP cells (Fig 42.). Quantification of the observation produced intermediate results. This result appears to be representative of the staining. Some of the Flotillin-1 positive granules occasionally colocalize with portions of CD63. Both markers share a cytosol subdomain, possibly indicating stages of modification of subcellular structures along a common signaling pathway (Table 2).

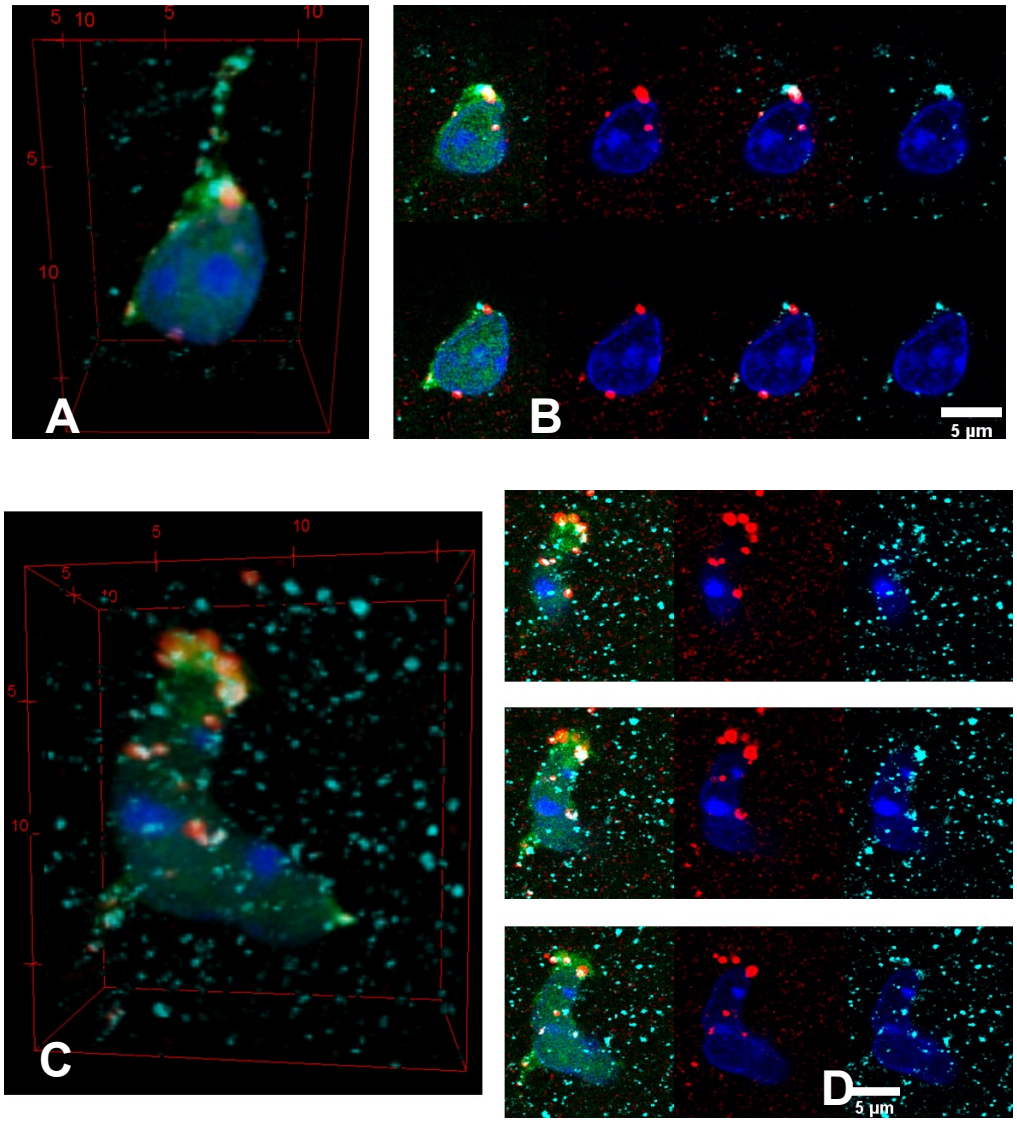

Fig. 42 CD63 (cyan) and Flotillin-1(red) in a heterozygote NG2-EYFP mouse (p53, female). EYFP fluorescence was not amplified by antibody staining (green). **(A,C)** – 3D reconstructions. **(B,D)** –1 µm MIPs (3 planes each) slicing through the cell.

Table 2. Quantification of colocalization tests, Flotillin-1 and CD63 in EYFP-positive NG2 glial cells. Values close to 1 (or 0.5 for Li's ICQ) indicate significant colocalization (Dunn et al., 2011). Data outside of NG2-glial cells was masked in each plane individually prior to MIP. Data is a two-channel MIP (35 µm deep over 110 planes) of a section of CA1 SR of an NG2-EYFP mouse, automatically thresholded using Costes algorithm (Costes et al., 2004).

Pearson's R value (no threshold)	Pearson's R value (below threshold)	Pearson's R value (above threshold)	Li's ICQ value	Spearman's rank correlation value	Spearman's correlation t-statistic	Manders' M1 (Above zero intensity of Ch2)	Manders' M2 (Above zero intensity of Ch1)	Manders' tM1 (Above autothreshold of Ch2)	Manders' tM2 (Above autothreshold of Ch1)	Kendall's Tau-b rank correlation value
0.41	-0.01	0.19	0.203	0.449816	200.4767	0.998	0.997	0.534	0.543	0.3178

Besides occasionally finding colocalization of CD63 with Flotillin-1, another observation was made. In hippocampus, Flotillin-1 positive granules were observed almost exclusively within NG2-glial cells, for reasons unknown (Fig 43). This warranted a closer look into Flotillin-1 as potential exosomal marker in relation to NG2-glial cells.

Table 3. Quantification of colocalization tests, Flotillin-1 and EYFP. Values close to 1 (or 0.5 for Li's ICQ) indicate significant colocalization (Dunn et al., 2011). Data is a two-channel MIP (35 µm deep over 110 planes) of a section of CA1 SR of an NG2-EYFP mouse, median-filtered and automatically thresholded using Costes algorithm (Costes et al., 2004).

Pearson's R value (no threshold)	Pearson's R value (below threshold)	Pearson's R value (above threshold)	Li's ICQ value	Spearman's rank correlation value	Spearman's correlation t-statistic	Manders' M1 (Above zero intensity of Ch2)	Manders' M2 (Above zero intensity of Ch1)	Manders' tM1 (Above autothreshold of Ch2)	Manders' tM2 (Above autothreshold of Ch1)	Kendall's Tau-b rank correlation value
0.14	0	-0.11	0.085	0.33597	2156.2421	1	1	0.545	0.212	0.2417

The standard approach to quantification produced intermediate results for colocalization of Flotillin-1 and EYFP in NG2-glial cells (Table 3). This was likely due to significant background noise in the Flotillin-1 channel, while a higher integrated count of EYFP across the studied area was not balanced by the similarly abundant Flotillin-1. A more detailed approach to quantification was necessary.

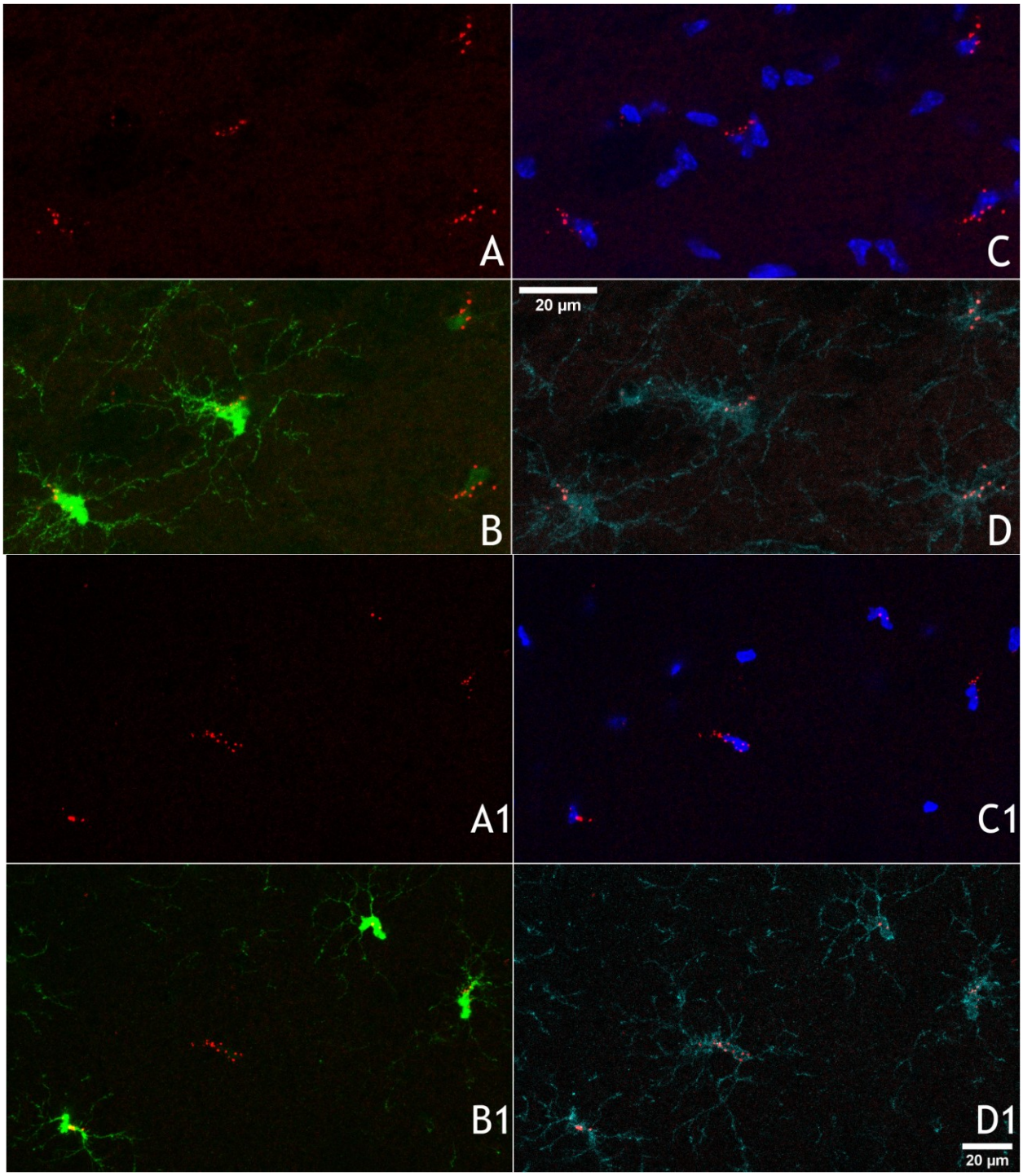

Fig. 43 Flotillin-1 is enriched in NG2-glial cells, independently of EYFP expression. **(A,A1)** Flotillin-1 (red). **(B,B1)** EYFP (green) and Flotillin-1. **(C,C1)** DAPI (blue) and Flotillin-1. **(D,D1)** NG2 (cyan) and Flotillin-1. NG2-EYFP P63(f), MIP 5.48 µm over 20 slices.

4.2.5 Enabling of Flotillin-1 visualization

We found that successful immunofluorescent labeling for Flotillin-1 in brain slices after PFA fixation requires an additional antigen retrieval step. This was done initially by dipping each brain slice in a 1:1 methanol and acetone mixture for 10-15 s prior to unspecific blocking. Later on, antigen retrieval was achieved by using commercial Thiol-based antigen unmasking L.A.B. solution (Polysciences) with incubation for 5-15 minutes. Both methods produced similar results. Omission of antigen retrieval leads to poor binding of anti-Flotillin-1 antibody and almost complete loss of signal (Fig. 44).

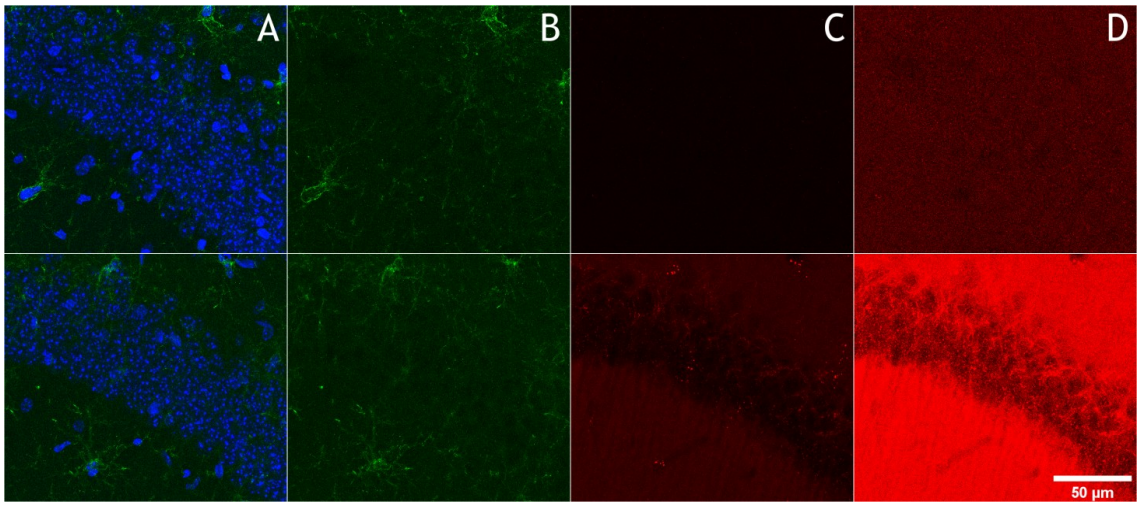

Fig. 44 Effect of epitope unmasking in a P47(F) C57BL6J mouse hippocampus. Top row – no antigen retrieval, bottom row – methanol-acetone antigen retrieval. **(A)** NG2 (green) and DAPI (blue) overlay. **(B)** NG2 channel **(C)** Flotillin-1 channel. **(D)** Overexposure of the brightness of the Flotillin-1 channel by factor five. Flotillinin-1 signal is masked by saturated pixel brightness in the lower panel. MIP 26 µm over 26 slices.

4.2.6 Quantification of Flotillin-1 cell type specificity

Flotillin-1 positive granules were imaged and analyzed as described in section 3.4.2.8 (Fig. 45).

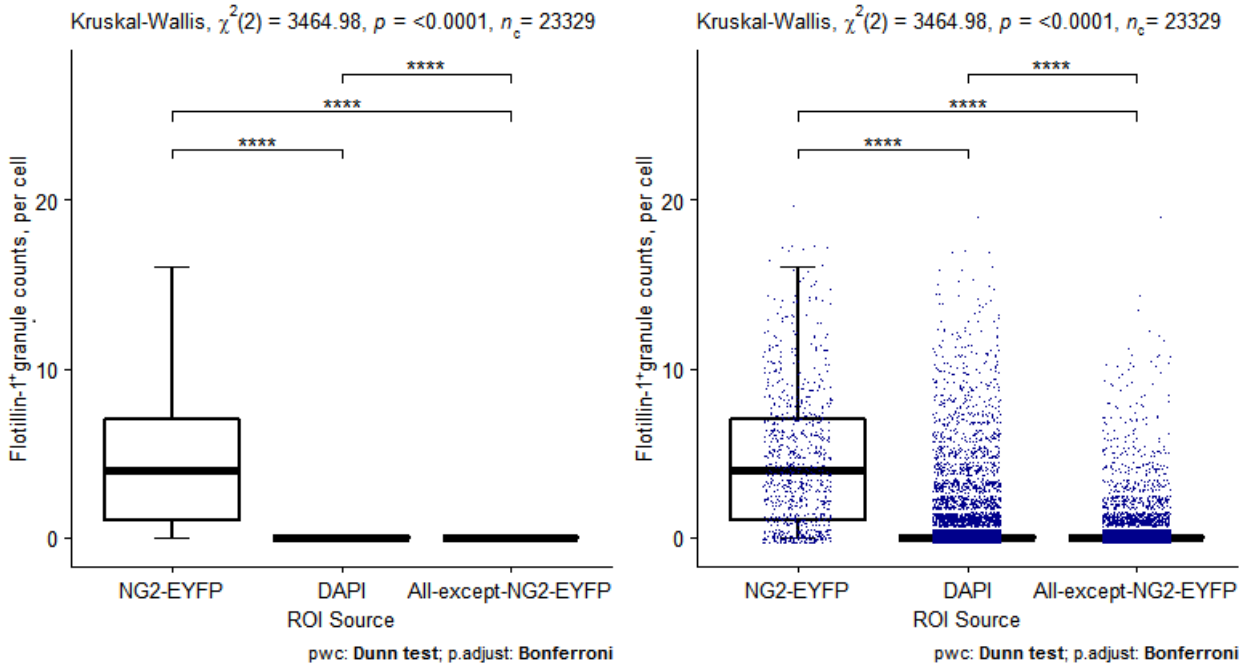

Fig. 45 Flotillin-1 positive granules count, per cell. Data is shown without (left) and with (right) individual data points (blue dots). Each dot represents the number of granule counts per one cell. The scatter plot forms bins along the Y-axis, since all counts are integers. n_c – number of cells, n_g – number of granules.
EYFP group includes all NG2-glial cells that did not fail to express EYFP; n_c(NG2-EYFP) = 857. DAPI group includes all cells with successfully labeled nucleus; n_c(DAPI) = 12120. The last column contains all (DAPI positive) cells that did not express EYFP; n_c(All-except-NG2-EYFP) = 10352. Data from seven hippocampal slices of four NG2-EYFP mice. A total of 6290 individual Flotillin-1 positive granules were detected across all slices: n_g(NG2-EYFP) = 3792, n_g(DAPI) = 6290, n_g(All-except-NG2-EYFP) = 2233.

The binarized MIP of individual granules inside every ROI has parameters such as area, circularity, dimensions, angularity and so on. The total and average areas of these granules between cell groups were compared (Fig. 46).

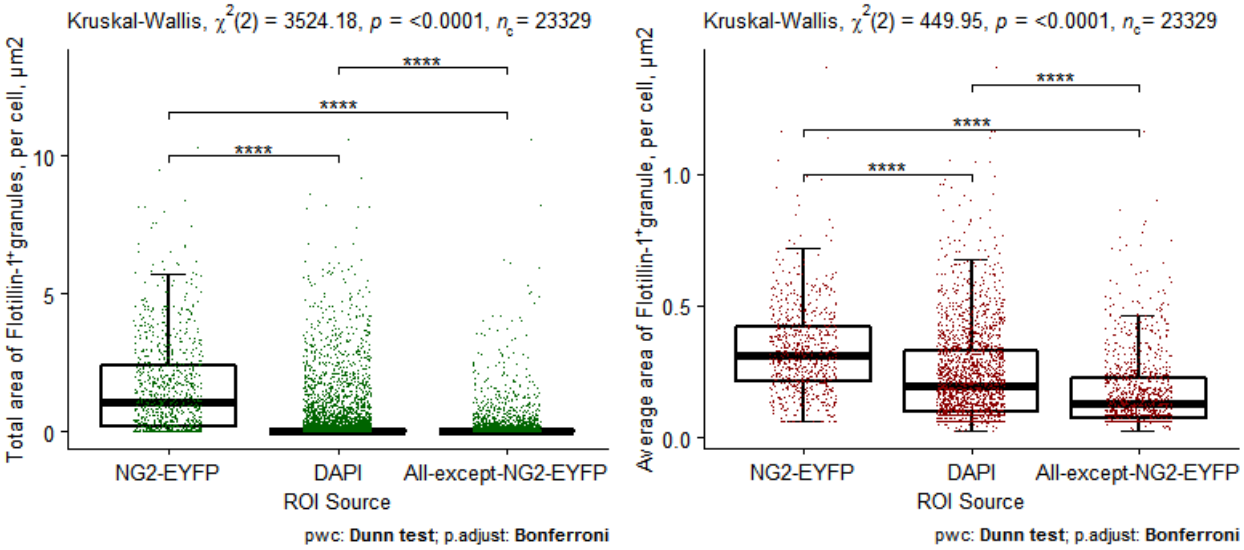

Fig. 46 Total area (left, green) and average size (right, brown) of Flotillin-1 positive granules per cell. Data points are real numbers, y-axis is continuous. Groups and sample sizes same as in Fig. 45

Most Flotillin-1 positive granules were found in EYFP-expressing NG2-glial cells. The granules found in NG2-glial cells were the largest within the data set.

NG2-EYFP mice are genetically modified. EYFP-expressing cells of heterozygous animals which were used in the analysis miss one copy of the NG2 proteoglycan. The NG2-glial cells also artificially contain EYFP. We decided to verify our finding using wildtype animals, to rule out side effects caused by the performed genetic manipulations (Fig. 47).

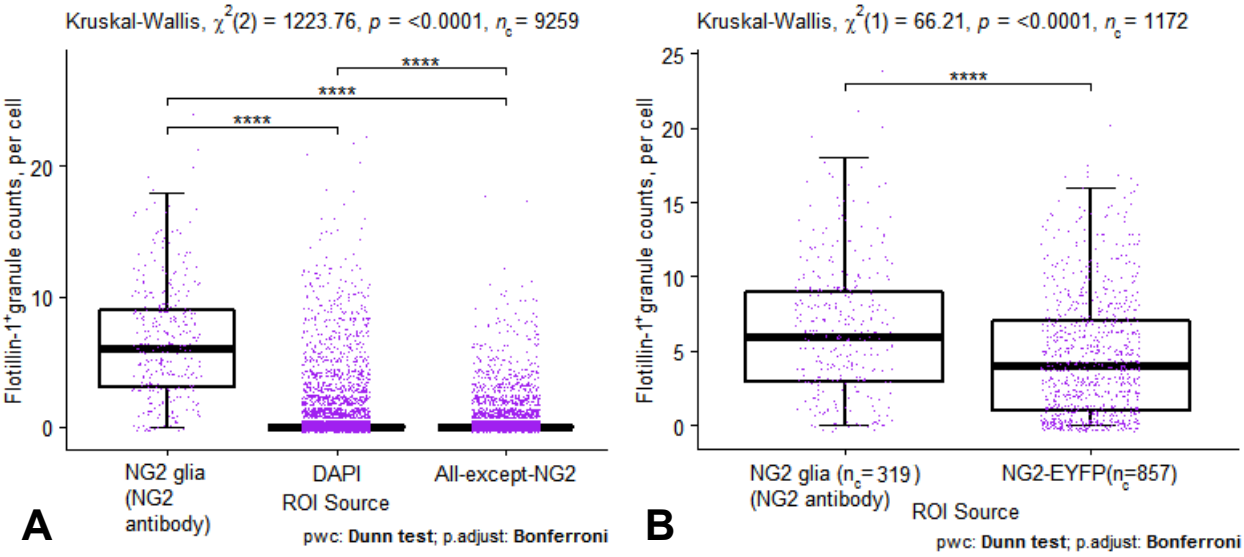

Fig. 47 (A) Flotillin-1 positive granules count, per cell, from three slices of a female P40

C57BL6J mouse hippocampus. Slices were stained with anti-NG2 antibody. n_c(NG2) = 319, n_c(DAPI) = 4760, n_c(All except NG2) = 4180. 4115 granules tracked in “All cells”(DAPI) group: n_g(NG2) = 2142, n_g(DAPI) = 4115, n_g(All except NG2) = 1917. **(B)** Flotillin-1 positive granules count, per cell, in P40 wildtype mouse and in four NG2-EYFP mice.

The properties of Flotillin-1-marked granules of wildtype mice resembled those of transgenic NG2-EYFP mice. The absolute count per cell was higher in wildtype animals, compared to NG2-EYFP. This result however must be taken with caution as the comparison is made between independent experiments which scope was to carry out comparisons within slices. The imaging parameters between the experiments were not intentionally kept consistent, which may have introduced variability.

4.2.7 Functional experiments with Flotillin-1 as an MVB candidate marker

We expected that the count of the granules may be altered under different conditions. Flotillin-1 positive granules may represent the releasable pool of multivesicular bodies inside the NG2-glial cells in the form of MVBs. If this is true, then the count of the granules may change in a fusion event. During fusion of an MVB with outer cell membrane, the membrane of a spherical MVB unfolds into plane of plasma membrane. One might expect that if this occurs, the visibility of Flotillin-1 antibody, whether it marks the content of a vesicle or the MVB surface, will be altered. In this case it may no longer be visible as a granule. The count of granules per cell, therefore, would change as a consequence of fusion events.

We tried to force vesicular fusion events in Flotillin-1 positive granules of NG2-glial cells to test this hypothesis. A good trigger is the alteration of intracellular Ca^{2+}. All known MVB fusion mechanism depend on $[Ca^{2+}]_i$ (Glebov et al., 2015). The number of Flotillin-1 positive granules should change upon $[Ca^{2+}]_i$ increase even though the observation of vesicular release is a matter of balance between MVB fusion and membrane reuptake to the cytosol. Short- and long-term effects are possible.

4.2.8 Acute treatment of hippocampal slices to influence Flotillin-1 appearance.

Acute slices from three NG2-EYFP(+/-) P36 mice were prepared to elicit a $[Ca^{2+}]_i$ increase in NG2-glial cells. Slices were incubated for 30 minutes either with DHPG (1 mM, 4 slices from 2 animals, Fig. 48) or with ATP (10 mM, 8 slices from 3 animals, Fig. 49). Neighboring slices were used as control tissue. Tilescans were imaged with identical optical parameters and to equal depth and thickness from slice surface. The analysis settings were same for drug-exposed and control slices and analyzed, as described previously.

The resulting data were non-normally distributed. Kruskal-Wallis test was used. Dunn test with Bonferroni-adjustment was used for the pairwise comparison.

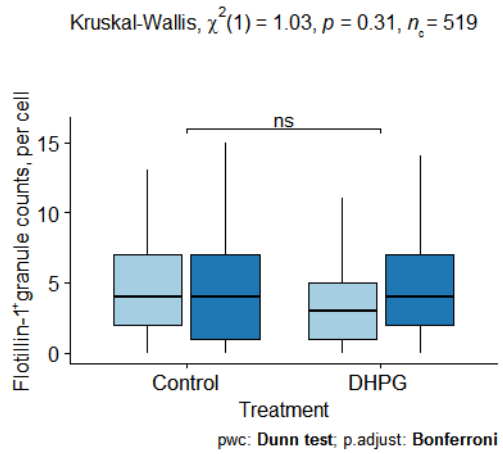

Fig. 48 Flotillin-1 positive granule counts per EYFP-positive cell. Acute slices from two male P36 mice treated with 1 mM DHPG for 30 min. Alternating coronal slices treated with ACSF served as control. n_c(Control) = 269, n_c(DHPG) = 250. All comparisons are within same animal.

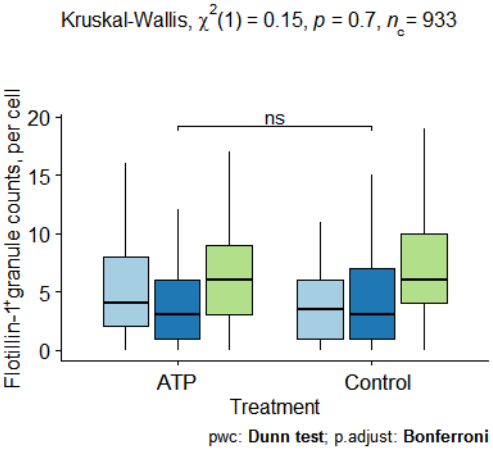

Fig. 49 Flotillin-1 positive granule counts, per EYFP-positive cell. Acute slices, from three male P36 mice treated with ATP 10 mM for 30 minutes. Alternating coronal slices treated with ACSF served as control. n_c(Control) = 465, n_c(ATP) = 468. All comparisons are within same animal.

The effect size was found to be small for both ATP and DHPG treatment (-0.000915 and 0.0000524 generalized η^2). The test power was small (0.05 for ATP and DHPG). To reach a power of 0.8 at the given effect size the sample sizes would need to be increased 10^4 to 10^6 times.

The differences between numbers of Flotillin-1 positive granules in some pairs of slices may be attributed to variation in imaging parameters. We aimed to keep these parameters constant within pairs of tilescans for all experiments. Another reason might be variation of Flotillin-1 content per cell that is related to relative position of coronal slices in the brain.

4.2.9 Age influence on Flotillin-1 positive granule content.

Flotillin-1 is involved in cell cycle (Gómez et al., 2010; Santamaría et al., 2005). Therefore, it may be affected by age. We compared young adult (P40) and middle-aged (P200) mice in terms of Flotillin-1 positive granules content (Fig. 50)

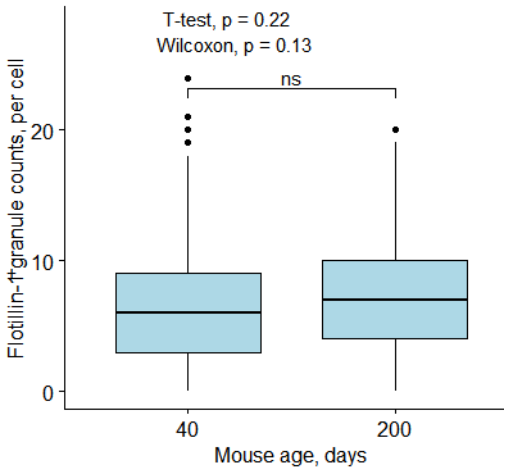

Fig. 50 Flotillin-1 positive granule count, per NG2-positive glial cell. Fixated slices from three C57BL6J female mice of 40 and 200 days old. n_c(P40) = 315, n_c(P200) = 290 cells.

No significant difference was found between Flotillin-1 positive granule counts in NG2-glial cells of aged and younger animals.

4.2.10 Conditional knockout of Kir4.1 channels in NG2-glial cells.

Long-term effects on NG2-glia innervation could influence the content of Flotillin-1 positive granules. A long lasting depolarization might influence fusion probability of MVB. The total count of Flotillin-1 positive granules might change as the result. We compared three P67 NGCE and three P62 Kir4.1 conditional knockout mice 36 days after tamoxifen injections (Fig. 51). See section 3.3.9 for mouse model details.

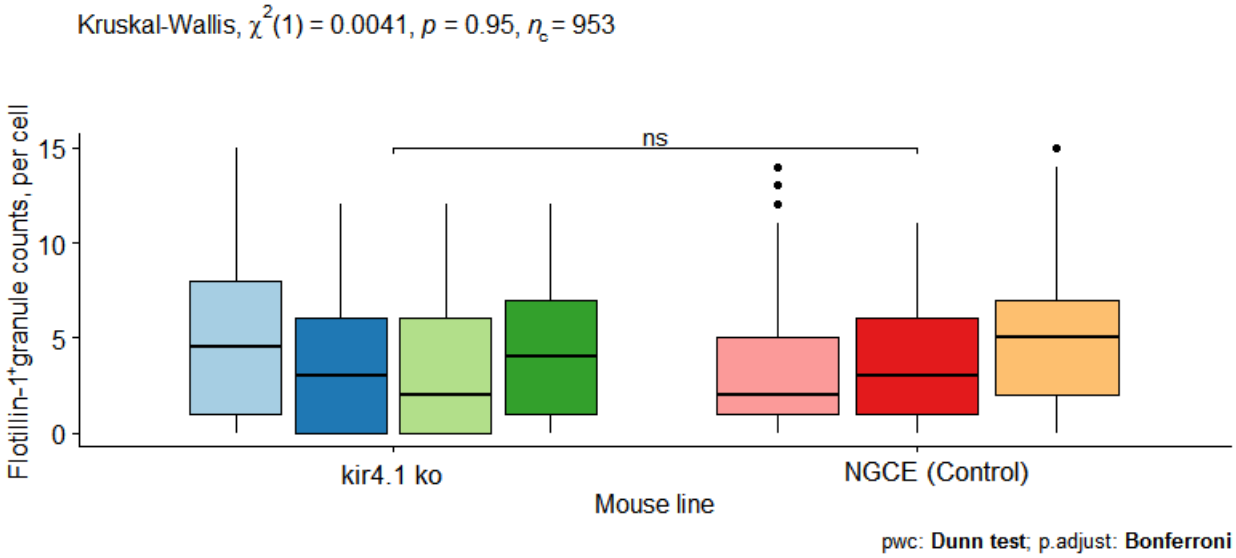

Fig. 51 Flotillin-1 positive granule count, per EYFP-positive glial cell. Fixated slices from NGCE and Kir4.1ko mice (individuals are color-coded), 5 weeks after tamoxifen injection. n_c(Kir4.1 ko) = 429, n_c(NGCE) = 524 cells.

The effect size was found to be small (0.00105 generalized η^2). The test power was small (0.05). To reach a power of 0.8 at the given effect size the sample sizes would need to be increased $7*10^3$ times.

Since the comparisons were made between brain slices of many animals the perfusion quality could vary. Additionally, the animals had different genetic background. This is in contrast to comparisons that were made within a slice, between cell groups within one animal, or within one mouse line at different ages. Out of 12 randomized slice pairs made, only five had comparable background fluorescence levels in Flotillin-1 channel, enabling comparison without changing of analysis parameters within a pair. Perfusion parameters, levels of EYFP expression and variability across individuals and/or mouse lines further complicates data comparability.

4.2.11 Oligodendrocyte lineage progression effect on Flotillin-1

If NG2-glial cells contain Flotillin-1 positive granules, what happens to the granules if an NG2-glial cell differentiates into an oligodendrocyte? We evaluated the possible fate of Flotillin-1 positive granules by analyzing populations of EYFP-positive NG2-glial cells and CC1-positive cells in a single P28 mouse. CC1 is a marker for mature oligodendrocytes (Bin et al., 2016) often used when labeling of myelin is not required. Fully unmasked tilescan of hippocampus in a coronal slice was used.

The cells in CC1 channel and in EYFP channel were visually identified. The regions of interest were created around each cell. Both sets of ROIs were combined into one, and the resulting set was sorted according to CC1 signal intensity, from highest to lowest (Fig. 52, C). Since each ROI retained information from all three channels, the signal in remaining two channels was reordered accordingly to CC1-imposed ordering.

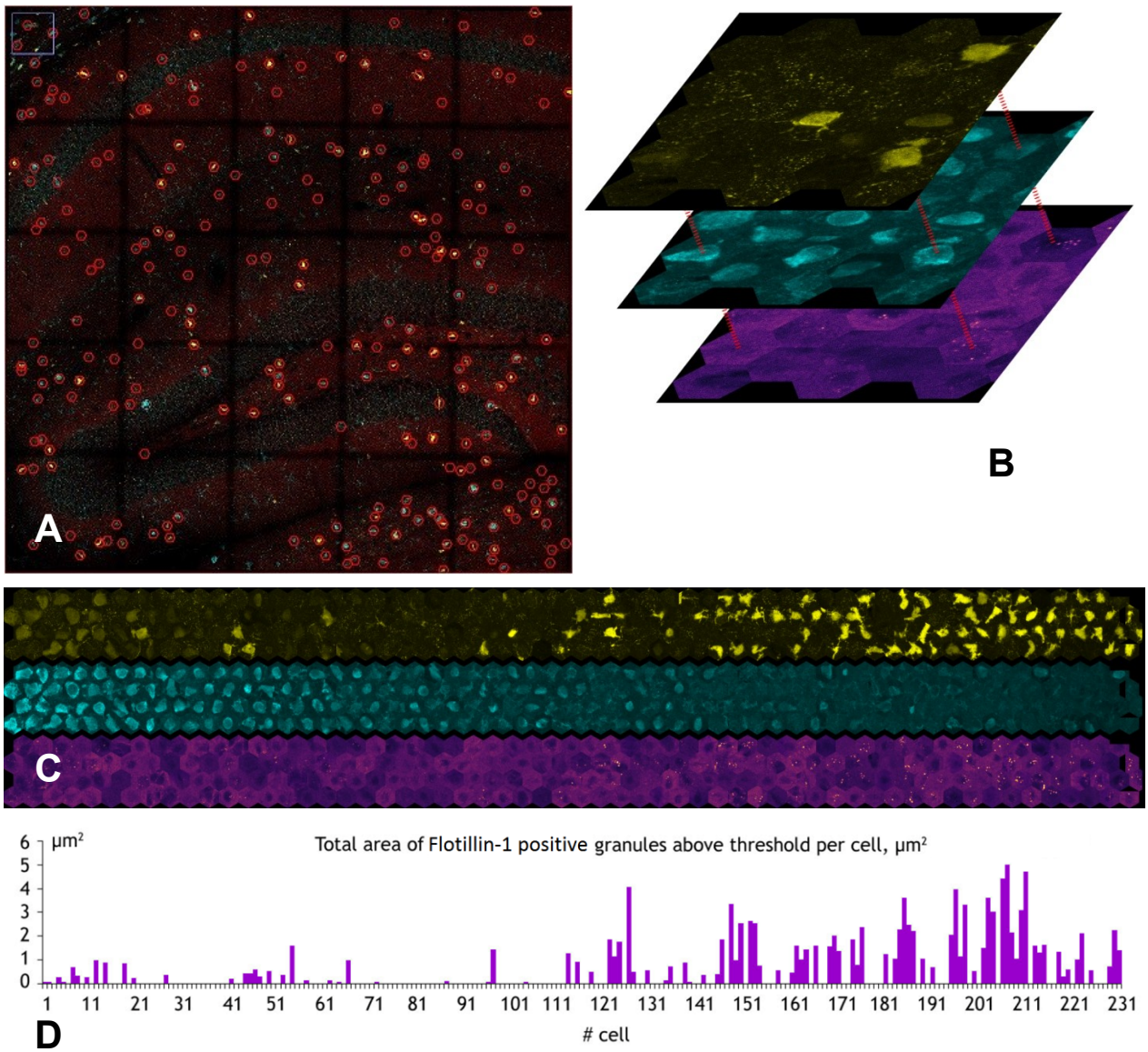

Fig. 52 Flotillin-1 positive granules appear sparse between NG2-glial cells and mature oligodendrocytes. CC1 (cyan), EYFP (yellow), Flotillin-1(magenta-hot). (**A**) Selection of cells that bind CC1 or express EYFP, using hexagonal ROI. (**B**) Cell identity is retained across channels in a ROI gallery. (**C**) One-dimensional sorting of cells by descending intensity of CC1 labeling, from left to right. (**D**) Total area of Flotillin-1 positive granules, within sorted data. Cell #1 in sorting has the most intense integrated anti-CC1 labeling.

CC1 and EYFP groups showed some overlap. Few cells were found to express both CC1 and EYFP at the same time. The cells with highest integrated intensity in CC1 channel were found to have weak EYFP expression, while cells with lower integrated intensity in CC1 channel tended to have even less EYFP expression, or none at all.

We performed a K-means clustering procedure to visualize the distribution of EYFP and CC1-positive cells (Fig. 52, C) in a more quantitative way. The negative values in the Fig.

53(A, C) are the result of data standardization (Mean value is set to 0, and SD to 1):

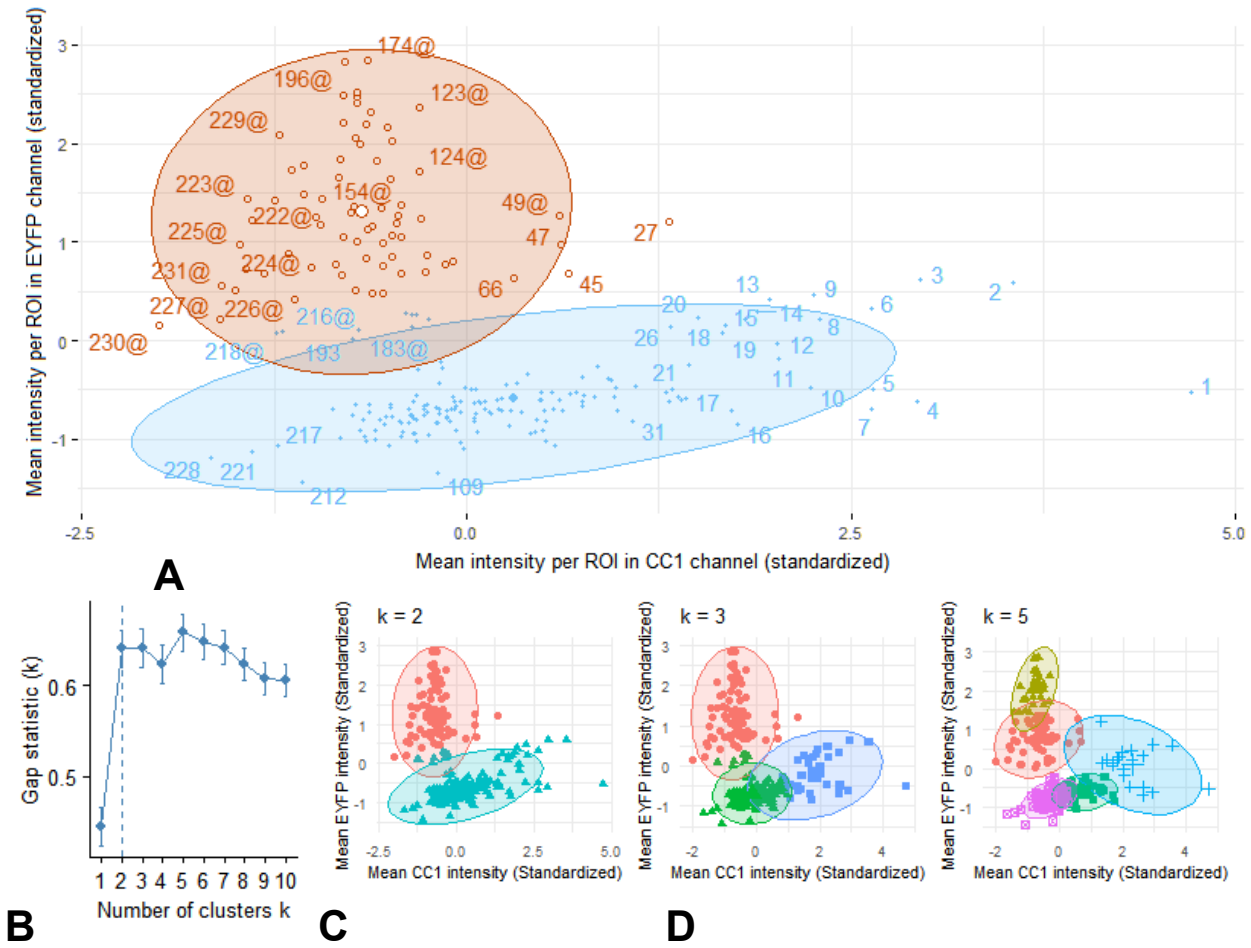

Fig. 53 (A) K-means clustering of sorted mean signal intensity of CC1 and EYFP in an NG2-EYFP mouse. Each point is equal-area ROI. Color indicates cluster. Point number indicates sorting from highest average intensity in CC1-channel (1) to lowest (231). Cells denoted with "@" were visually identified as NG2-EYFP-positive cells. (**B**) Cluster convergence. (**C,D**) Clustering with different k values

The best cluster convergence was achieved at k=2 after four to five iterations. Clustering became instable at k ≥ 5. Dunn index was highest for two clusters (k=2, index 0.0514). Gap-statistic score suggested two or three clusters as optimal as assessed by 200 bootstrapping steps. Adjusted Rand index between results of clustering and initial visual cell type identification was 0.8144. The Adjusted Rand index (ARI) provides a measure for assessing the similarity between two partitions, adjusted for chance. Its range is -1 for no agreement to 1 for perfect agreement.

High counts per cell do group around the NG2-EYFP cluster, with higher numbers closer to the center of the cluster, and lower (or zero) numbers towards the CC1 cluster (Fig. 54(B), zero is dark blue).

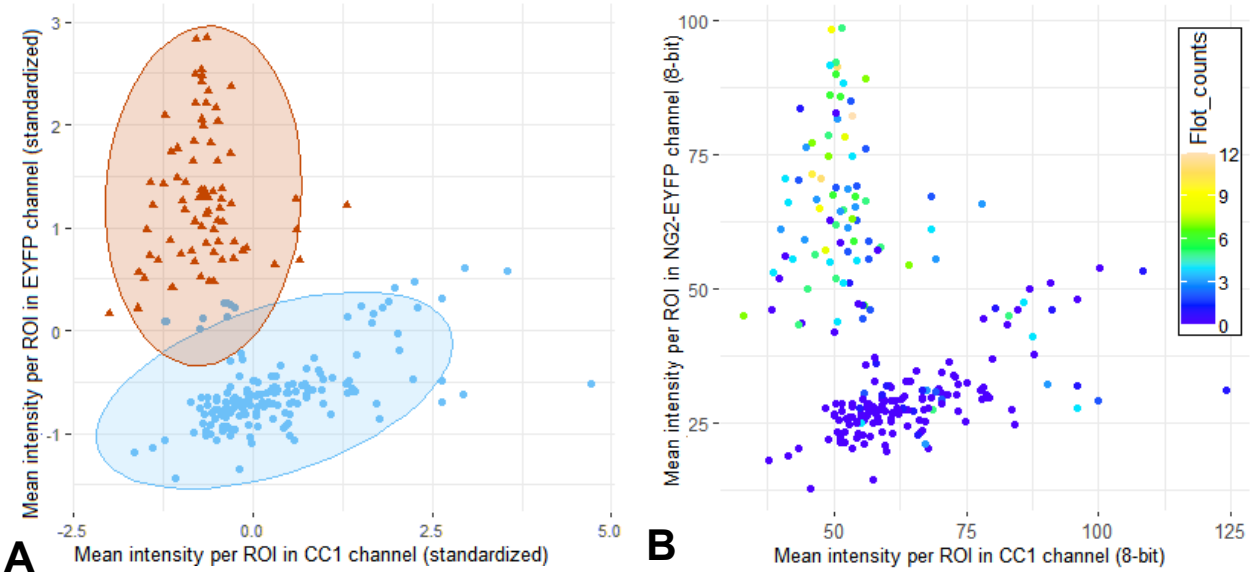

Fig. 54 Flotillin-1 positive granule counts in NG2-EYFP cells vs. maturing oligodendrocytes. (**A**) Clustering of cells, same as Fig.53 A, for reference (**B**) Flotillin-1 count per cell, coded as heatmap.

We also used the data on Flotillin-1 counts for a three-dimensional clustering (Fig. 55). The result provides marginally better separation of two clusters (Dunn index 0.054 for 3D-clustering vs. 0.0514 for two-dimensional). 7 out of 231 cells were re-assigned to CC1 cluster and one cell to NG2-EYFP cluster using 3D clustering.

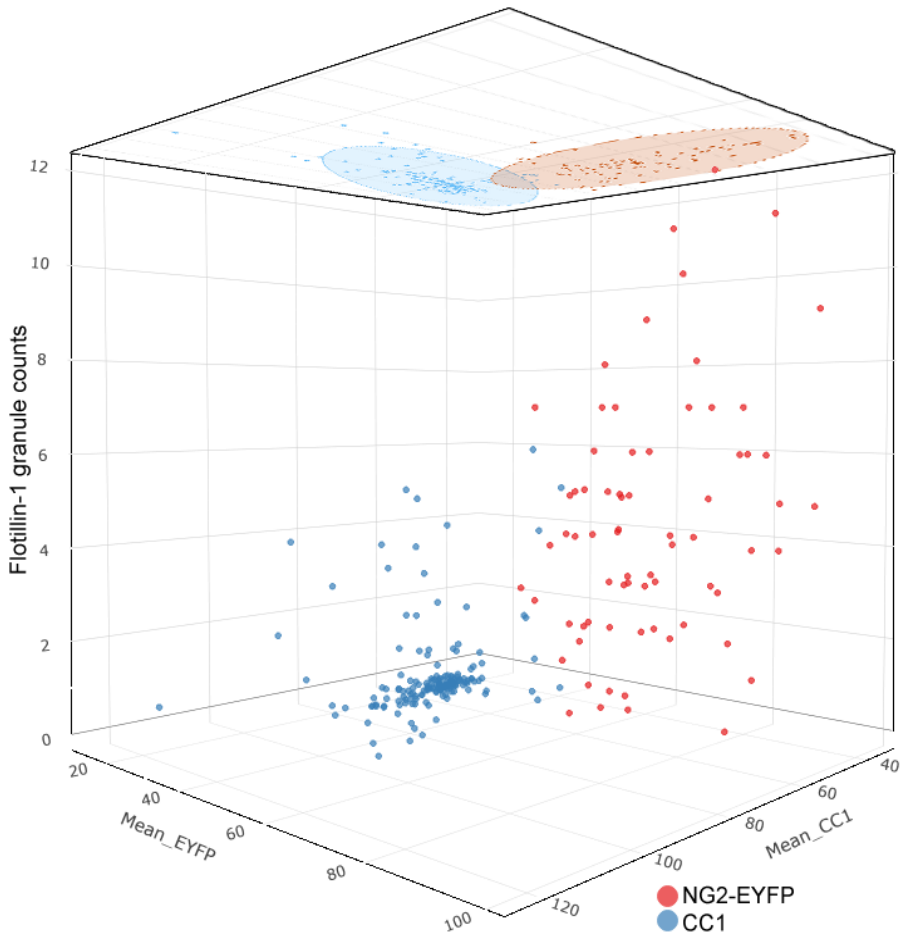

Fig. 55 Flotillin-1 positive granule counts in NG2-EYFP cells vs. CC1-positive oligodendrocytes: 3D clustering accounting for Floitillin-1 granule counts. Color indicates clustering results. Top side "lid" of the box is 2D clustering result for reference (Fig. 54).

Populations of oligodendrocytes and NG2-glial cells were identified using CC1 and EYFP respectively. Few cells expressed both EYFP and CC1, possibly indicating the ongoing differentiation of NG2-glial cells to oligodendrocytes, caught in the process. K-means clustering was carried out using two (intensity in EYFP and CC1) and three (intensity in EYFP, CC1 and Flotillin-1 positive granule count) parameters, resulting in similar attribution of cells to two clusters. Flotillin-1 positive granules were the most numerous in bona-fide NG2-glial cells. The number of Flotillin-1 positive granules decreased with the intensity of EYFP, and was zero in the majority of oligodendrocytes identified by CC1. The presence of some Flotillin-1 positive granules in cells that were intensely labeled with CC1, but only weakly expressed EYFP possibly indicated an intermediate subpopulation of cells that are in the active phase of differentiation. The

simultaneous high expression of CC1 and EYFP is perhaps due to non-linear profile of Quaking 7 expression as the cell progresses from NG2-glial towards an oligodendrocyte, resulting in higher amounts of protein after the onset of expression, and lower amounts later into maturation of oligodendrocytes.

4.2.12 Immunoelectron microscopy

In parallel to the immunohistochemical analyses, we used immunoelectron microscopy, to further evaluate the structures in question. The resin-embedding of slices, ultramicrotomy, and EM imaging was performed by Dr. Hannes Beckert of University Clinic Bonn Microscopy Core Facility.

The Flotillin-1 antibody was recognized by a secondary antibody carrying a gold nanoparticle prior to the tissue being dehydrated and embedded into resin for ultra-thin sectioning. The gold nanoparticle was then enhanced with layers of silver ions to increase the size of particle up to few nanometers, making it visible in EM picture. The pre-embedding immunogold labeling enables better signal-to-noise ratio compared to post-embedding, in which antibody is applied to a resin-fixated ultra-thin slice. Due to stochastic nature of silver-enhancement step, the final size of metal particle varies a lot, making application of more than one antibody per slice pointless. While initial application of gold particles of two different sizes is possible, the final size of both kinds of gold particles will be unpredictably altered by silver-enhancement, mixing two antibody signals together in terms of final particle size. Therefore, the first run of EM experiments with Flotillin-1 antibody was carried out for the purpose of finding out if labeling is occurring at all (Fig. 56). The second run was carried out using correlated light-electron microscopy approach (CLEM), to visualize both fluorescent EYFP of NG2-EYFP cell as well as gold nanoparticles, in same cell (Fig. 58).

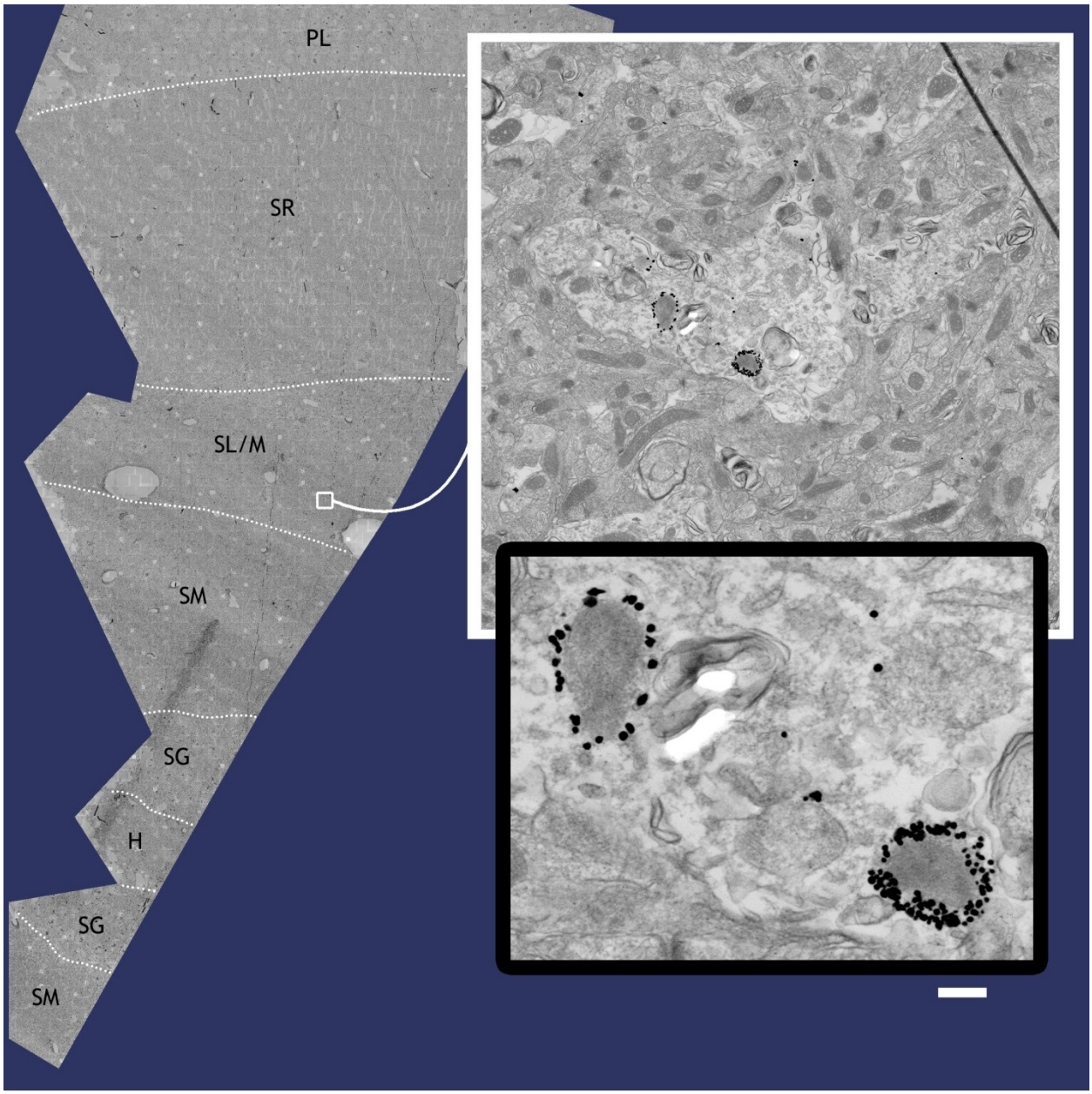

Fig. 56 Immunoelectron microscopy, non-correlated run. Flotillin-1 with surrounding tissue. Metal particles, visible as high electron dense black dots, surround lysosome-like structures in a putative NG2-cell. Scale bar is 200 nm for black box.

Curiously, the structures which were labeled with Flotillin-1 antibody did not show the appearance of MVBs. Instead, the Flotillin-1-marked structures had shape, size and electron density features of lysosomes, or similar late endosome structures. The MVBs were observed in the same sample, unlabeled, in neurons of pyramidal layer and elsewhere (Fig. 57).

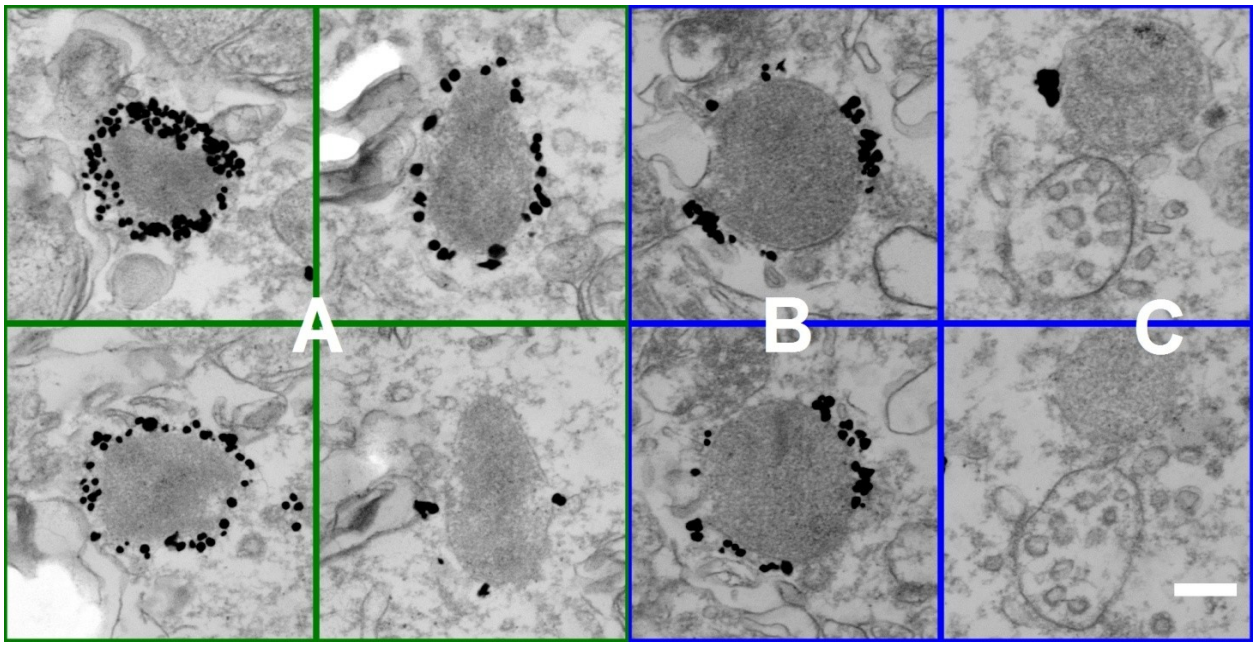

Fig. 57 Immunoelectron microscopy, non-correlated run; Flotillin-1 seen as black dots. Top and bottom row represent same structures in same cells, but in different ultra-thin slices, i.e. separated by one or few z-levels of 50 nm. **(A)**(green boxes) Putative NG2-glial cell in *str.lac./mol.*(Same cell as in Fig. 56). **(B,C)** Blue boxes – regions within *str.radiatum,* roughly 40 µm from pyramidal layer (same sample). **(B)** Putative NG2 cell. **(C)** Neighbor cell to cell B, same region; unlabeled MVB-like structures. Scale bar is 200 nm.

The spread, quantity and size of labeled structures was consistent with observations made with conventional immunofluorescence microscopy in NG2-glial cells. The counts of gold-labeled structures were appropriately sparse: 0-10 observations per slice, depending on varying area of sample block face. Considering that only a small area of hippocampus was captured in EM block, and at an extremely small thickness of few hundreds of nanometers, this was consistent with immunolabeling observations. Nevertheless, we also verified the attribution of Flotillin-1 immunogold labeling to NG2-glial cells using CLEM approach (Fig. 58):

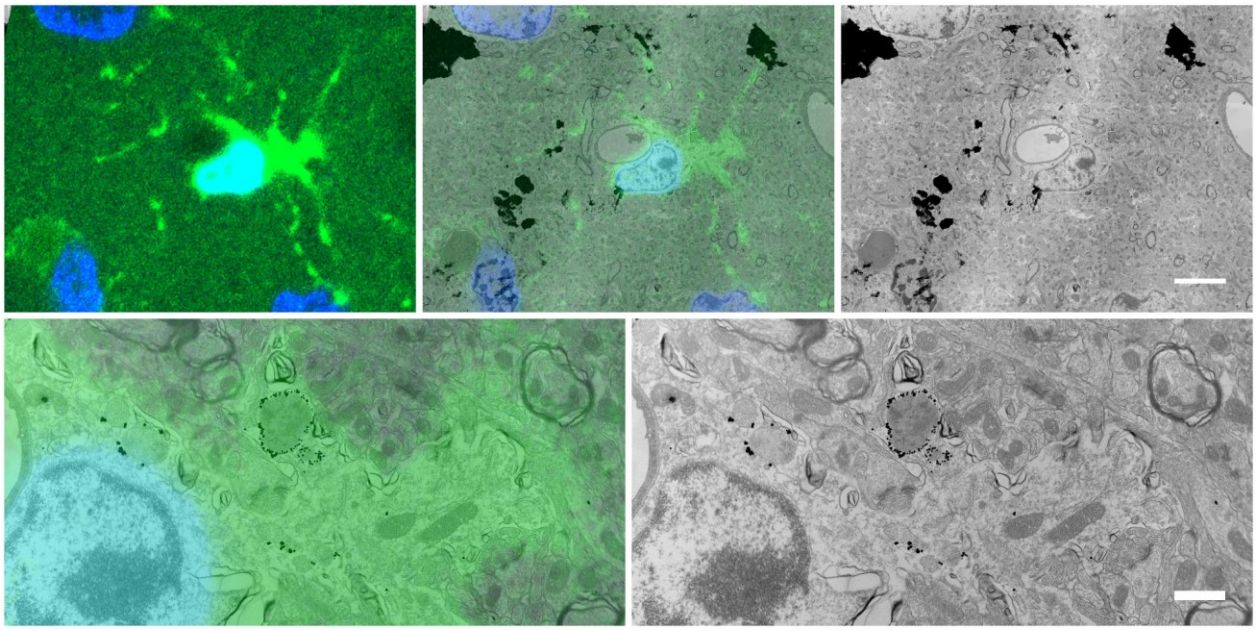

Fig. 58 Immunoelectron microscopy, fluorescence-correlated data; Flotillin-1 labeled by black dots. EYFP-expressing NG2-glial cell in *str.lac/mol*. Top row scale bar 2 µm, bottom row scale bar is 320 nm. The cell is unambiguously identified as NG2-glial by EYFP fluorescence, while subsequent immunoelectron labeling clearly shows Flotillin-1 on the cytosol side of intracellular lysosome-like structures.

An interesting observation was also made in the pyramidal layer neurons of both EM samples. Previously, to facilitate the chosen mode of analysis of the fluorescence microscopy data, the pyramidal layer and the dentate gyrus of the hippocampus were masked. In the course of some of the experiments, NG2-EYFP fluorescence and dye-coupled Flotillin-1 antibodies were observed together in green-yellow and red bands of the spectrum. With increased laser power needed for better contrast of the EYFP fluorescence, other features, such as autofluorescent lipofuscin, also became visible. Lipofuscin signal was mixed in among the signal of EYFP in the green-yellow band. Within the collected fluorescence datasets of CA1/CA2/DG regions of hippocampus, lipofuscin was observed mostly in the neurons of densely-packed molecular and pyramidal layers. Flotillin-1 antibody staining was strongly associated with granules in the NG2 glia producing large, densely-labeled fluorescent spots. Interestingly, in pyramidal layer it was found to associate with autofluorescent granules of lipofuscin, forming clumps or ring-like structures around the autofluorescent cores (Fig. 61). This observation was verified in both correlated (Fig. 60) and uncorrelated EM samples (Fig. 59).

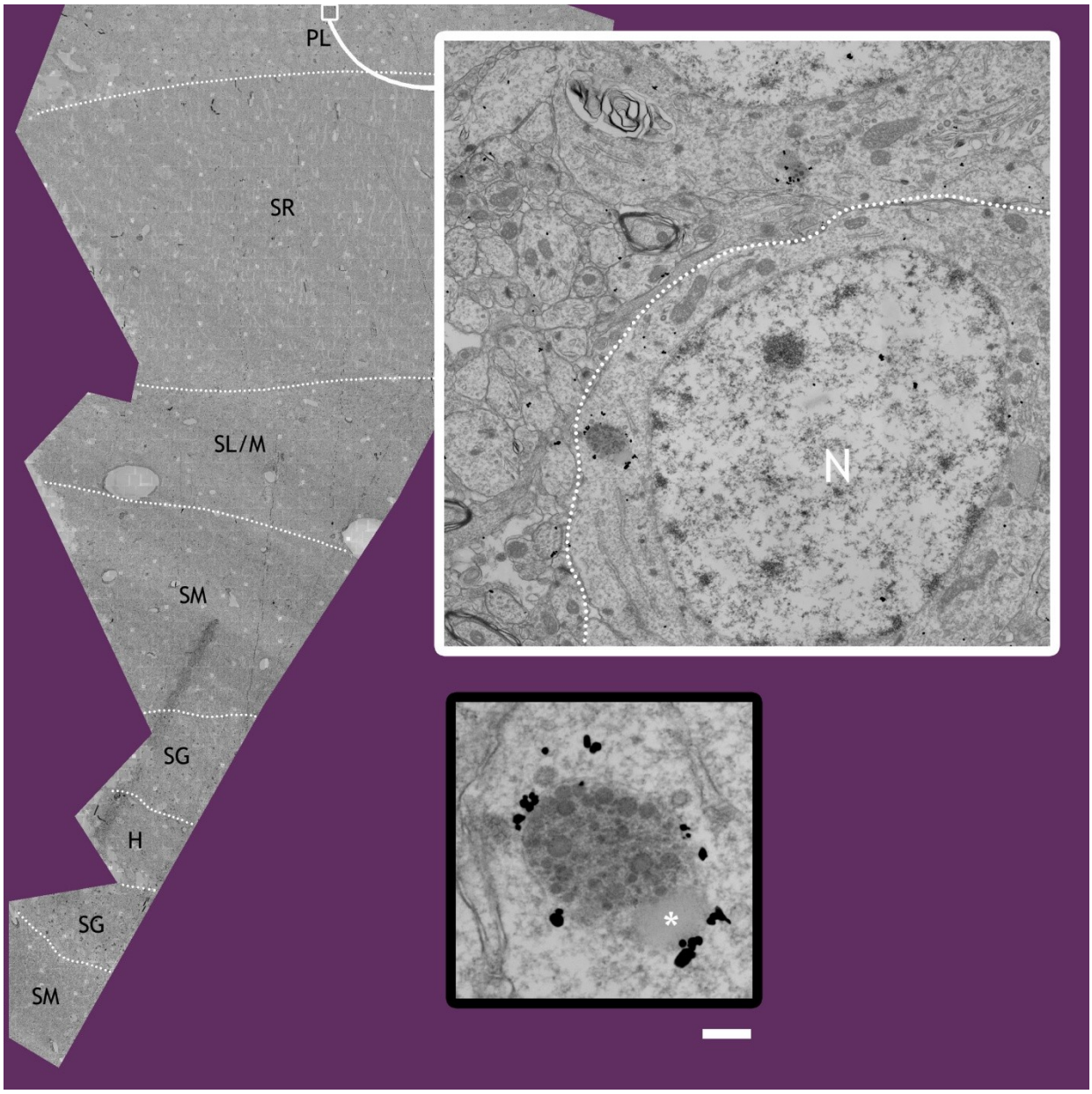

Fig. 59 Immunoelectron microscopy, non-correlated run; Flotillin-1 with surrounding tissue. Metal particles surround a telolysosome – a residual body containing lipofuscin and a fat droplet (*) inside a pyramidal layer neuron (N). Scale bar is 200 nm for black box.

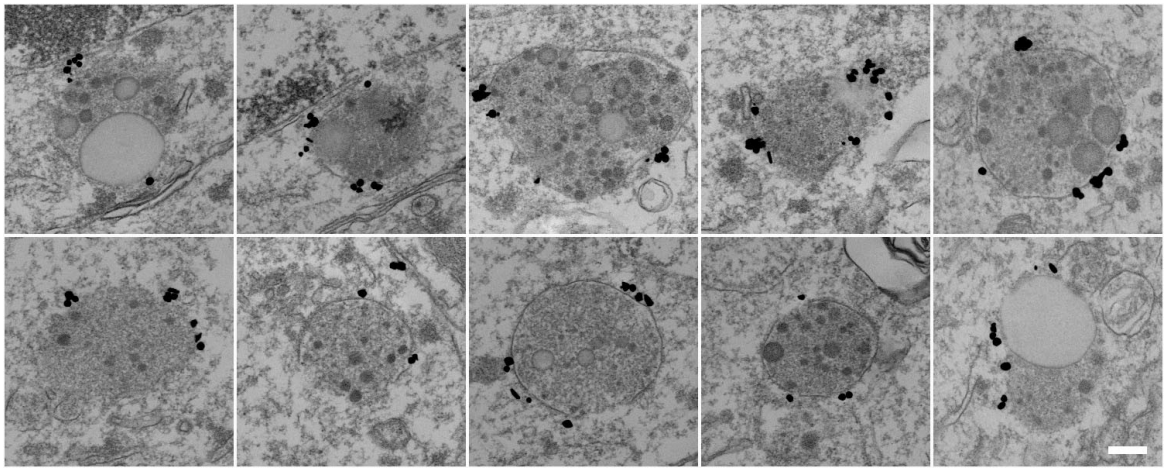

Fig. 60 Immunoelectron microscopy, fluorescence-correlated samples; Flotillin-1. Lipofuscin granules (black dots) in neurons of pyramidal layer. Scale bar 200 nm.

The different appearance of Flotillin-1 in pyramidal layer and in putative NG2 cells could also be observed in the fluorescent data:

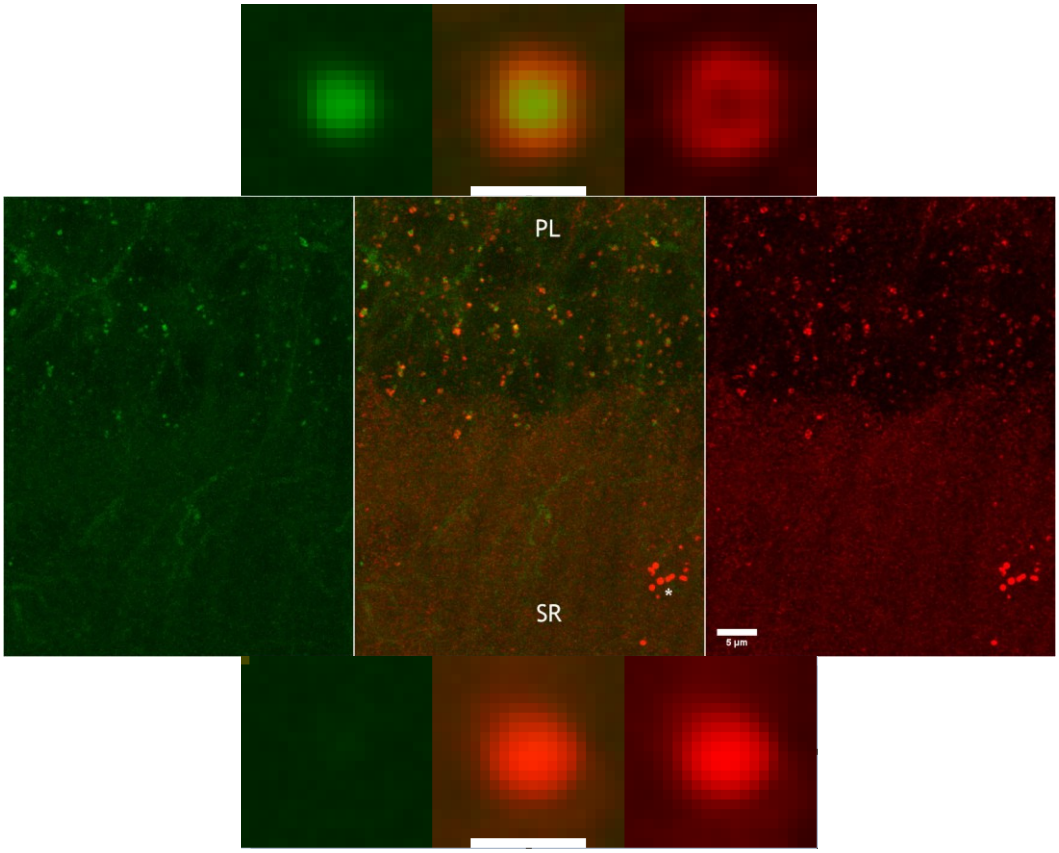

Fig. 61 Flotillin-1 (Alexa 647, red) in a P40 C57BL6J mouse. **Green** – intrinsic autofluorescense. **(A)** Average intensity projection of Flotillin-1 positive granule in the pyramidal layer. **(B)** Overview, asterisk indicates putative NG2 glial cell. **(C)** Average intensity projection of a granule derived from a putative NG2 cells in *stratum radiatum*. Scale bar **(A, C)** – 1 µm.

4.2.13 Flotillin-1 re-evaluation in pyramidal layer

Would unmasking the tilescan to reveal pyramidal neurons challenge the conclusion about a preferred affinity of Flotillin-1 positive granules towards NG2-glia (see chapter 4.2.6 for tilescan masking procedure)? Flotillin-1 binds to subcellular structures in pyramidal neurons and in NG2-glia. The previously used analysis approach where each individual cell nucleus creates a center of a circular ROI would create a lot of overlapping in a pyramidal layer (PL), and result in an inflation of granule counts. This is a consequence of the tight packaging of neurons in the PL. We changed the universal circular ROI to a net of equal-area hexagons that cover the PL. The hexagons were tiled along the PL, without positioning the center of each tile to a particular cell, but also without omitting any of the PL content. The comparison between tiles targeted to NG2-glial cells elsewhere in the slice, and tiles derived from pyramidal layer was made. This was done without a strict attribution of granules counts to particular pyramidal neurons. Rather, not the count of granules per cell was measured, but count of granules per unit area, roughly equivalent to a single cell for NG2 glial cells, or to few cells in pyramidal layer. The rare NG2 cells in pyramidal layer were excluded from pyramidal layer tiles (Fig. 62). Image processing parameters were left unchanged from chapter 4.2.6.

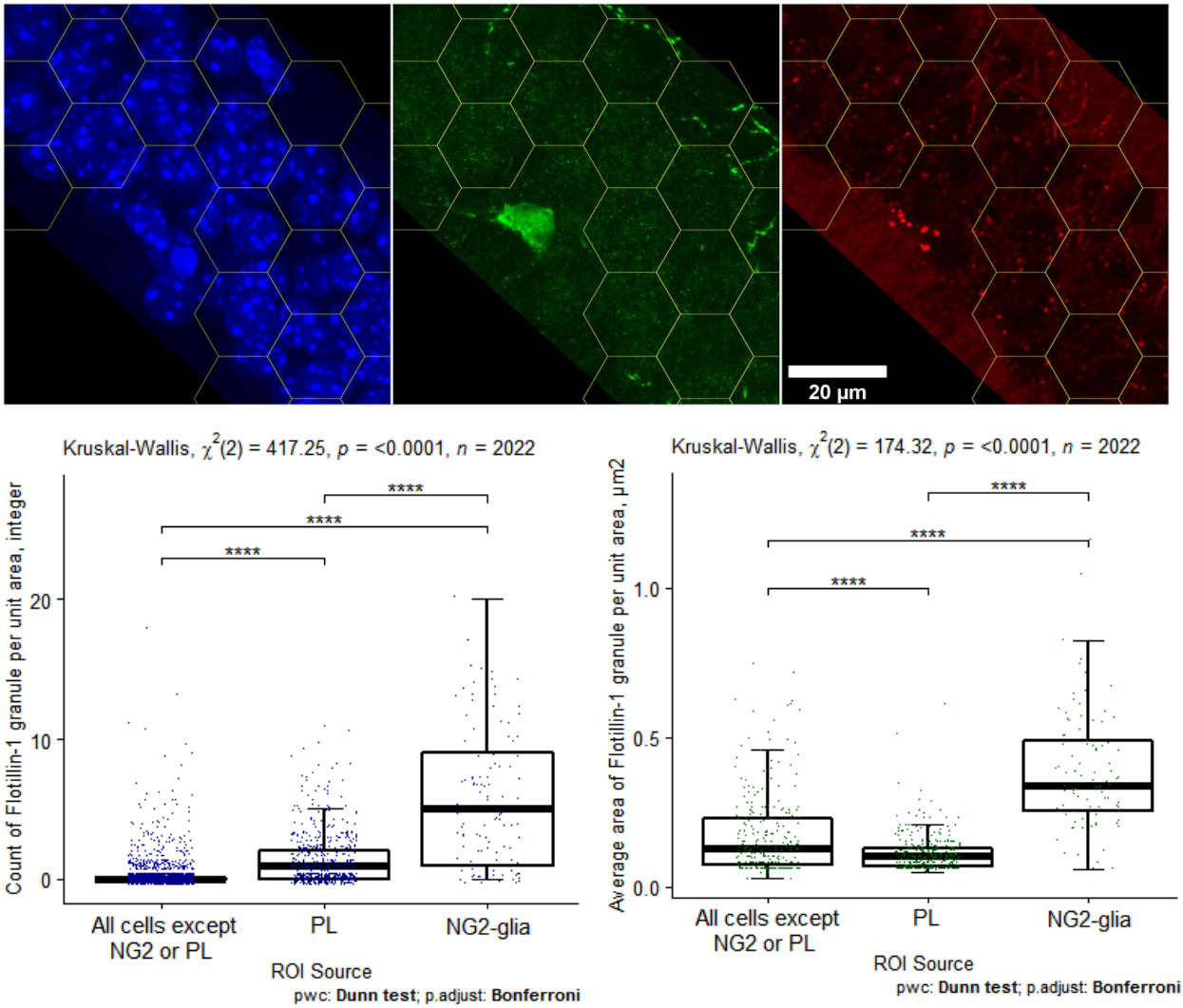

Fig. 62 Flotillin-1 positive granules in pyramidal layer (PL) are less abundant and smaller than in NG2-glial cells. Flotillin-1 positive granules were more abundant in PL neurons than in the other cells if NG2-glial cells were excluded. Section of pyramidal layer. DAPI (blue), EYFP (Alexa-488-enhanced, green), Flotillin-1 (red). Total unit area = 254.5 µm^2.

The largest and most abundant granules still located to NG2-glial cells if pyramidal neurons were accounted for. The Flotillin-1 positive granules found in the pyramidal layer also appear to be smallest in the dataset.

5. Discussion

NG2-glial cells are capable to influence the surrounding network in a controlled matter and in a number of different ways. NG2-glia is most known as the precursor cells of myelinating oligodendrocytes (Nishiyama et al., 1996; Stallcup, 1981; Stallcup and Beasley). This function is critical for development and many functions of any mammalian nervous system, under normal development and maturation, during learning, and in pathology. NG2-glia are among the first cells that respond to CNS damage. Only microglial cells migrate faster towards lesion sites and are subsequently involved in the formation of astroglial scars (Alonso, 2005; Lytle et al., 2006; Wellman and Kozai, 2018). The potency of NG2-glial cells to differentiate into oligodendrocytes or astrocytes (Zhu et al., 2008) depending on the external signals reveals the capability to discern specific external signals and to make alternative ontological “decisions” in response. The ability to migrate from one region to the next (Hughes et al., 2013), even to a point of being able to re-colonize entire regions of brain after ablation (Birey et al., 2015) may appear surprising in contrast with the fact that NG2-glial cells may also form stable postsynaptic connections with neurons in the vicinity of their processes in white or gray matter (Bergles et al., 2000, 2010). Wouldn't a cell that invests energy and resources into the ability to precisely monitor the electric activity in surrounding area be incentivized to remain where such connections remain in use? Wouldn't a, perhaps, metabolically cheaper solution such as spillover detection do instead? Is there a particular set of incoming signals, presence or absence of which determines the next action for a particular NG2-glial cell? It is almost certain that NG2-glial cells are unable to directly participate in computation together with neurons (Haberlandt et al., 2011; Jabs et al., 2005). It is widely accepted that a certain level of background network activity determines an NG2-glial cell’s actions towards becoming a myelinating oligodendrocyte (Birey et al., 2015; Wellman and Kozai, 2018; Zhu et al., 2008). Together with the ability of NG2-glial cells to detect the presence of each other (Hughes et al., 2013) and spread away into areas which do not have NG2-cells “coverage”, this may form a listening network, in which each node teeters on the brink of initiating a terminal differentiation. This popular explanation, while likely true in most part, still leaves some questions unanswered. The myelination in the brain varies considerably from one region to the next. Does it makes sense for an NG2 cell to maintain its synaptic machinery to,

presumably, the same degree in the areas where relatively little myelination is expected, like *stratum radiatum* of hippocampus? Or in the areas where myelination is relatively heavy like in *corpus callosum*? Does it make sense in terms of expected myelination for a population of NG2-glial cells to maintain vigilant presence in the grey matter, if the only thing that their postsynapses are capable of is to receive the terminal differentiation signal that is unlikely to arrive? Could it be that synapses on NG2-glia have other functions besides registering this signal?

Unpublished observations from experiments with a pseudotyped rabies virus cued us on to idea that material transfer may be occurring between the NG2-glial cells and surrounding tissue. Detailed information on rabies virus usage in this context is available in (Ginger et al., 2013). In these experiments, a GFP reporter was synthesized in the cells where the protein's sequence was introduced by the modified rabies virus. The virus first entered some of the NG2-glial cells in mouse hippocampus around the area of injection. In few days, the virus would replicate in NG2-glia and then use available neuron/NG2 glia synapses to retrogradely infect neurons that were connected to an infected NG2-glial cell. The reporter would also replicate in these neurons. By surveying the animals at different time points post-injection, together with immunofluorescent markers for different cell types, the sequential pattern of GFP replication between NG2-glia and neurons could be observed. After about 10 days post injection, all the cells involved - first NG2 -glia, then neurons - were overwhelmed by replicating virus and underwent apoptosis. Due to modifications, the generated rabies virus was not able to infect any more cells in the area except for the neurons immediately connected to NG2-glial cells. Interestingly, at 11 days post injection, large amount of dendrites in the area reported GFP. This was interesting, considering that no somata with GFP reporter could be observed at that time in proximity to these dendrites or anywhere else in tissue. The presence of reporter in dendrites but not in somata can be interpreted as a result of reporter transfer from infected cells to the surrounding tissue (Fig. 63).

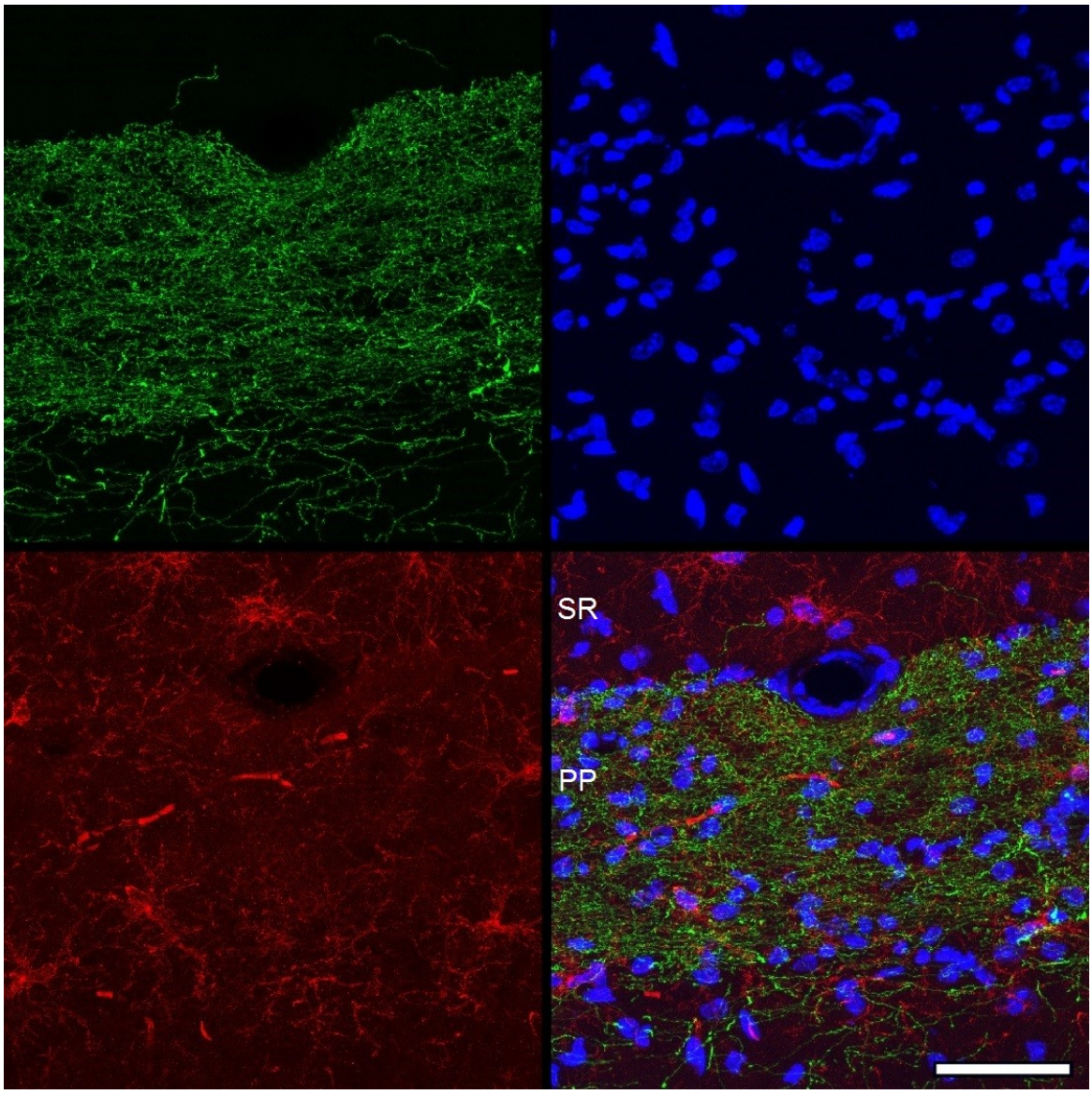

Fig. 63 Pseudotyped rabies virus experiment, 11 days post-injection: while no GFP-positive cell somata were observed at this point, indicating that all infected cells have succumbed to viral infection, strong GFP labeling of dendrites suggested that GFP was not recycled from the dead cells. Instead, the reporter became associated and persisted within or on the surface of dendrites in the area, presumably, independently from somata of neurons to which the dendrites belong. Scale bar 50 μm, SR – str.radiatum, PP – perforant pathway of DG. Red – NG2, green – GFP, blue – DAPI.

In parallel, biochemical experiments with an *in vitro* model cell for NG2-glia, the Oli-neu cell line, provided evidence for existence of exosomes in NG2-glia that carry NG2 proteoglycan as a cargo, together with some other exosome-associated proteins, such as Alix and Flotillin-1.

This, together with observations from (Frühbeis et al., 2013), where the exosomal

transfer from oligodendrocytes – immediately downstream from NG2-glial cells lineage-wise - to associated neurons was observed, led us to suggest that the protein or RNA transfer from NG2-glial cells in the form of exosomes may be occurring, and that synaptic input onto the grey matter NG2 glia may be involved in this transfer.

5.1 Electrophysiological experiments

As the first line of investigation, we decided to probe exosomal release from Oli-neu cells using electrophysiological technique of membrane capacitance tracking.

5.1.1 Capacitance tracking – a promising technique with high expertise requirements.

Among several available approaches to membrane capacitance recording, in our selection process we compromised between devices available, and availability of information on each particular implementation. In practical terms, capacitance recording is a way to analyze the data that is collected during a standard patch clamp experiment, with some modifications (Neher and Marty, 1982). While all the know-how regarding the patch-clamp experiment itself was plentiful and readily available (Gillis, 1995; Lindau, 2012), it took some time to recognize the elements which critically influence the experimental outcomes. Whole-cell sine-wave lock-in in voltage clamp mode with on-line analysis requires a full digitally controlled amplifier, such as EPC-9 or EPC-10. A legacy electronic amplifier with front-panel controls, such as EPC-800, unfortunately, did not allow full digital control of some of the functions even with proprietary software.

The particular method was chosen based on the manuals that were available for the in-house electronic amplifiers. All of them were from HEKA Company. The data collection needs high temporal resolution and must provide absolute values of membrane capacitance (Gillis, 1995). High temporal resolution allows detection of individual fusion events. Coupled to confocal video-microscopy and appropriate dye loading, it might track individual fusion events visually.

In retrospect, even in successful experiments, high temporal resolution data never provided indication of identifiable separate fusion events, at least in the whole-cell configuration. It is certain that both vesicle fusion and plasma membrane reuptake occurred in our recordings. However the ensemble signal that was created as the result presented itself as a smooth wave. The signal had parameters such as slope and noise

level, but no individual discernible objects that could be attributed to biological events, and not electrical artifacts. This knowledge, however, could not be obtained without practical collection of a considerable amount of data in the experimental mode of choice. Still, high-resolution whole-cell capacitance data, given some additional computational effort, may provide more information, for example, if an non-stationary noise analysis approach described by Neef et al.(2007) (Neef et al., 2007b) is implemented.

Reliable data verification is another important aspect in the search for best recording technique. Capacitance measurement, being a fairly advanced method, has additional caveats. While definitely observed and described in the literature, these caveats manifest themselves in a non-straightforward way that is specific to a particular electrophysiological setup. The output of recordings is influenced by electric spikes, electric noise, liquid level fluctuation in chamber and so on. Detection of biological events such as membrane fusions needs a robust verification method. Amperometry is the method that is often suggested as a back-up for a membrane capacitance recording (Haller et al., 1998; Moser and Neher, 1997; Von Gersdorff and Matthews, 1999; Westerink and Ewing, 2008). Unfortunately, the implementation requires an additional dedicated electronic amplifier, which was not available. Currently, new methods are becoming available to double-check the capacitance recording results, such as pH-sensitive dyes (Rituper et al., 2013). These dyes spread through cellular structures after loading. Since the pH is different in different compartments, as well as between inside and outside of the cell, the pH-sensitive wavelength shift may provide information about fusion events as the typically more acidic inside of an MVB encounters a typically more alkaline extracellular space (Von Bartheld and Altick, 2011).

5.1.2 BV-2 cell line – highly mobile cells

We established the capacitance measurements first in a cell culture line, before we studied Oli-neu or NG2-glial cells. Successful capacitance recordings were described for BV-2 cells (Glebov et al., 2015)]. For this reason, we started our capacitance recordings with these cells. As it quickly became evident, this cell line is poorly suited for recordings where duration and stability have high priority. BV-2 cells demonstrated impressive motility on the surface of glass coverslips, even after being patched. Most cells reacted with retraction of processes or blebbing to glass pipettes and leaking potassium-rich

intracellular solution. Even after the whole-cell configuration was established, in just a few minutes the BV-2 cells attempted to move away from the stationary tip of the pipette, often leaving behind a thin branch of cytosol sealed to the tip of the pipette (Fig. 64). Such "dynamic" connection to a cell, while seemingly stable would likely not provide a truthful readout from cell membrane due to ambiguity of space clamping as well as due to rapid changes in total available membrane. Such intense motility on scale of few minutes is also not typical for NG2-glial or Oli-neu cells. We soon moved on from BV-2 cells to PC12 cells, a popular and well-described system for studying neurochemical secretion (Westerink and Ewing, 2008).

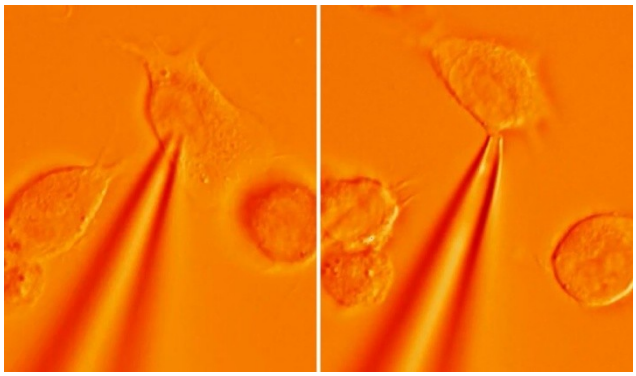

Fig. 64 BV-2 cells motility while being patched, about three and a half minutes apart.

5.1.3 PC12 cell line – whole-cell mode with perforated patch

Our experiments with BV-2 cells demonstrated the importance of stability of cell-pipette interface in the course of capacitance recordings. The capacitance recording in whole cell configuration provides three parameters as the output. These parameters are membrane capacitance (C_m), membrane resistance (R_m), and access resistance (R_a). As we were mainly interested in C_m, we found out that this parameter is very sensitive to changes in R_a. The access conductance (G_S) is inversely proportional to R_a. As the G_S would increase, the whole-cell C_m readout would normally increase as well. The change in C_m in response to change in R_a is due to "perfect" value of sine wave phase changing in dependence on R_a (see formula in Fig. 6 in (Gillis, 1995)). While it is possible to get a capacitance readout at any point in the experiment, the lower noise levels are achievable only if R_a is relatively low (i.e. G_S is high), and leak resistance (i.e. seal quality) is few orders of magnitude higher. The range of R_a values changes depending on the chosen sine wave frequency. This can be any frequency between 1 and 10 kHz

for whole cell recordings. It is hard to determine a strict numerical criterion to judge whether the recording is “true enough” (Gillis, 1995). As a general rule, one should aim to get as good of an R_a as is *usual* with the particular combination of pipette diameters and cell being patched, and to keep this value consistent across the whole project and within each experiment. We accepted values below 40 MOhm of R_a. The ultimate test for whether the observed changes in membrane capacitance is related to change in the amount of membrane and is not caused by change in R_a is the non-coincidence of these changes in time – that is, assuming that the calibration is complete and settings for sine wave interpretation are set accordingly (Gillis, 1995). It is important to keep R_a low and to avoid significant changes in R_a within experiment. Ideally, R_a is unchanged during the whole C_m recording. Time correlated changes in R_a and C_m indicate an artifact, if the calibration was performed correctly.

We chose to use perforated patch mainly to prevent wash-out of cell content. The increased stability of recordings was a welcome addition to this method. While perforated patch approach significantly increased the duration of any one recording it kept R_a stable for tens of minutes, often up to one hour. This is often difficult to achieve in patch-ruptured whole cell mode, since cells often heal up during recording, increasing R_a. These benefits of perforated patch are similarly described in the literature (Kyrozis and Reichling, 1995). The perforated patch was preferable to large fluctuations of R_a that could be seen in mechanically ruptured cells in the process of healing up, even despite the membrane of the patched cell sometimes rupturing during perforated patch access waiting time, in which case the recordings were discontinued.

We directly depolarized cell membranes to +20 mV, to evoke a response from PC12 cells. This approach was described by Harkins and Fox (Harkins and Fox, 1998). We first observed deflection of C_m trace baseline which did not coincide with changes in corresponding G_S and G_M traces. This might be due activation of voltage-gated Ca^{2+} channels that raise $[Ca^{2+}]_i$ and finally trigger membrane fusion events. The process is reversed and recorded capacitance decreases when depolarizing injections are stopped. The decrease is the result of the process of cell membrane reuptake outpacing the fusion events. The process is reversed and recorded capacitance decreases when depolarizations are stopped. The decrease is the result of the process of cell membrane reuptake outpacing the fusion events.

At this point we also realized the importance of stability of bath chamber level for the recordings. Even small fluctuations caused a significant alteration of R_a together with C_m. Interestingly, we could observe such shifts with or without Sylgard-184 coating the immersed portion of the pipette. Sylgard coating is often recommended as a countermeasure to noise sources in the literature (Neef et al., 2007a; Rituper et al., 2013). The error gets introduced if the amount of length of pipette immersed in the recording solution changes after compensation of pipette capacitance by C-fast. C-fast is an automatic amplifier procedure which compensates for pipette capacitance after the seal is established. The elastomer coating of the pipette tip insulates the outer plane of the glass pipette that acts as capacitor. This makes it indifferent to changes of bath chamber level. We found that Sylgard application to pipettes did not positively affect the recording quality. It also not reduced sensitivity of C_m and R_a recordings to bath level fluctuations. Guidelines recommend application of elastomer “50-75 μm from the tip” (Neef et al., 2007a). It is possible that due to short taper of our pipettes the coated portion was already thick enough to prevent any significant capacitance input from the pipette glass, making the coating inconsequential. Other explanations are also possible. Some kind of microfluidic effect between outer pipette surface and inner portion of Sylgard coating or imperfect hardening of Sylgard could cause the lack of good performance. We did not use Sylgard coating for further experiments. Instead, we reliably maintained a constant chamber level. Stability was achieved using a glass vertical slit suction nozzle for recording solution evacuation, a tip kindly provided by Dr. Andreas Neef.

Trains of depolarizing pulses were used to elicit capacitance increase in PC12 cells. Some PC12 cells were found to respond to depolarization to +20 mV with injections of current as short as 1 ms. A minority of PC12 cells were not found to respond to depolarization of any duration. The initial capacitance surge would usually change to a shallower slope as the train of depolarization continued, with some of the cells reaching steady state towards the end of depolarization train. Each train, on average, measured 125 s (Fig. 23). Second and third depolarization trains caused a C_m increase that reached progressively smaller amplitudes. We hypothesized that a steady state at the end of depolarization train represents the balance between fusion events and membrane reuptake. In this case, the C_m increase represents the number and/or the size of vesicles

found in PC12 cells that are poised to fusion, a kind of readily-releasable pool (RRP), as well as the capacity of the cell to maintain vesicular fusion under prolonged stimulation. The prolonged stimulation with 50-100 ms pulses was described as able to more deeply probe RRP of the PC12 cell, as opposed to a shorter, more physiological stimulation with duration of 5-30 ms (Horrigan and Bookman, 1994). More prolonged stimulation increased the amount of fusion events by a factor of 10.
We used data collected from PC12 cells as reference for evoked C_m responses.

5.1.4 Oli-neu cells – sensitive cell line, a model for NG2-glia.

Oli-neu cell line is a popular model to study NG2-glial cells (Jung et al., 1995). This cell line was previously described as a source of exosomes (Fröhlich et al., 2014; Hsu et al., 2010; Strauss et al., 2010; Trajkovic et al., 2008)The Oli-neu cell line requires more effort and optimization to maintain the cell line. PC12 cells in comparison are more robust. Oli-neu cells need a higher CO_2 concentration and a stricter protocol of medium change. Poly-L-lysine coating was critical for cell adhesion rather than optional. The main concern about Oli-neu cell culture is its lineage progression. Some cells undergo terminal differentiation to oligodendrocytes or astrocyte-like cells (Fig. 5 in (Jung et al., 1995)). These cells, while still surviving in culture from passage to passage, would no longer contribute to proliferation of the culture. Their passive electrical parameters also would not correspond to that of NG2-glia, more resembling differentiated oligodendrocytes or astrocytes. This process appears to progress as the culture ages. After few months of continuous passages the proportion of cells exhibiting atypical electrophysiological parameters would increase. Both in cell culture and in acute slices, we established the cell identity criterion of NG2-glial cells and Oli-neu cells. The criterion was defined by calculating the ratio between the maximum capacitance-compensated amplitude of transmembrane current at +20 mV, divided by 10, to maximum capacitance-compensated amplitude of transmembrane current at -70 mV. This number expresses the factor by which the outward current at +20 mV is amplified above leak conductivity, since the latter is nearly linear. In bona fide astrocytes the ratio criterion is almost 1 that indicates 100 % leak currents at +20 mV. The algorithm as well as many other scripts was kindly provided by Dr. Ronald Jabs. In NG2-glia the ratio reveals the contribution of A-type potassium currents that become downregulated as the NG2-glial

cell progresses towards an oligodendrocyte (Gallo et al., 1996), and which Oli-neu cells express as well (Jung et al., 1995). If the value was above 1.2, the cell was considered an NG2-glial cell, or an Oli-neu cell. Typical ratios for NG2-glial cells were age dependent and ranged from 3-50 for young and 1.3-2 for adult NG2-glial cells. Oligodendrocytes ranged between 0.4-1.1 and astrocytes between 0.97 and 1.05. We excluded cells with a ratio below 1.2 from analysis. We did not aim to address the problem of differentiation in Oli-neu cells, instead opting to complete electrophysiological experimentation within the reasonable time frame of several months.

Application of direct depolarization protocols did not elicit the capacitance response similar to that of PC12 cells in Oli-neu or *in situ* in NG2-glial cells. Because the function of chromaffin cells is to rapidly release large quantities of stress hormones using very large vesicles, it is expected that the C_m change in PC12 would be higher. The amount and/or size of vesicles available in Oli-neu and NG2-glial cells were likely too small to show up against background noise. The whole-cell capacitance recording in its conventional configuration did not provide a signal-to-noise ratio sufficient to resolve the fusion events of individual vesicles. While highly specialized statistics-driven approaches to whole-cell mode C_m recordings were published (Neef et al., 2007b), even the extremely well-described whole-cell capacitance measurement systems have a predicted noise level in the order of 9-10 fF (r.m.s) (Chen and Gillis, 2000; Gillis, 1995) under best conditions. A singular 300 µm MVB fusion would increase the C_m by around 2.75 fF. We were able to achieve a noise level in the order of 10 fF(r.m.s.) for best recordings, but in practice the typical noise level for cell culture in the perforated patch mode was around 20-40 fF. A more complicated morphological and electrical environment of acute brain slice drove the noise levels even higher for in-situ NG2-glia.

In PC12 cells the characteristic upward deflection of capacitance trace upon stimulation indicated ongoing fusion events. The Oli-neu C_m trace baseline tended to below zero line within the recording period. One explanation may be a change in membrane reuptake rate. Another explanation might be due to the analysis. Each recording's pre-pulse segment is normalized using a linear function to enable comparison, but the capacitance data is "convex" due to ongoing changes in the R_a on a span of 11 minutes of the recording. The R_a parameter was still changing under the influence of Gramicidin since the recording was obtained in the perforated patch mode. This change may cause

an accumulation of error in C_m estimate, because R_a differed between start and end of the recording while the calibration was performed only at the start, and not continuously. All included cells fulfilled our Oli-neu ratio criterion. However we noticed an increasing number of cells with differentiated phenotype. We discontinued the Oli-neu cell culture and approached *in situ* NG2-glial cells with the same C_m recording method. In conclusion, we found no C_m-based evidence for vesicular release from Oli-neu cells.

5.1.5 In situ NG2-glial cells – depolarization, application of substances.

The response of NG2-glial cells *in situ* is more complex as those of the Oli-neu cells. The noise levels and variability in the C_m baseline had a more complex shape. There was also a U-shaped downward deflection in averaged C_m baselines in response to depolarization trains. This deflection indicated the decrease of total plasma membrane as the effect of depolarization. This effect recovered with an overshoot after depolarization train ended. The deflection also could be the result of activation of voltage-gated channels (Gillis, 1995), which are present in the NG2-glial cells. A transient changes in the conductance component (G_M) upon depolarization was more pronounced in NG2-glial cells, compared to Oli-neu and PC12 cells. Not all cells demonstrated downward deflection of C_m, even if compared cells had similar passive membrane parameters. Some cells were indifferent to depolarization in terms of capacitance or conductance altogether, despite not showing any unusual passive membrane properties. Other explanations for G_M shifts within depolarization train may be the depolarization-induced reuptake of cellular membrane, or a calibration artifact. Reuptake mechanism and depolarization induced reuptake are not well studied yet. The calibration procedures were not altered between PC12, Oli-neu and NG2-glial cells. The averaged baseline recorded after the depolarizing phase of the protocol showed an increase of resting C_M. This may indicate an overall increase in the total cell membrane as the result of running a depolarization train.

One of the explanations for the results with NG2-glial cell direct depolarization may be that the increase in C_m was masked by effect of voltage gating, while the post-excitation C_m increase was the actual visible outcome. To address this without disturbing the physiological Ca^{2+} conductance, an extracellular mGluR agonist, DHPG, was used.

Haberlandt *et al.* (Haberlandt et al., 2011) showed that its application caused an increase in intracellular Ca^{2+} without a corresponding increase in trans-membrane current. The DHPG was delivered using a timed bath application at concentration of 0.1 µM.

The DHPG was applied to the bath solution. This did not influence the C_m trace. NG2-glial cells responded to DHPG wash-in with a gradual decrease of C_m of about 1 pF over the recording period. There were no notable deflections.

High noise levels and combined complexity of perforated-patch, bath wash-in drug application together with prolonged patching in the brain slice minimized the expected success rate. We doubted that data with acceptable quality could be collected under these conditions. For this reason we discontinued whole-cell membrane capacitance experiments in acute slices.

The method of the whole cell capacitance recording was successfully implemented at it is state of the art. The configuration was tested with PC12 cell line. In conclusion, we obtained very little information about vesicular release in Oli-neu and *in situ* NG2-glial cells. These cells do not exhibit controlled membrane fusion events as chromaffin cells, at least not to the same extend. The expertise requirements for interpretation of results and freehand troubleshooting of issues in the method with as many parameters as the whole cell capacitance recording turned out to be very high. At the same time, the complexity of the method was not compensated by unambiguity of the results. In case of an exploratory search on a sub-cellular scale, the double or, perhaps, even triple co-verification of the membrane capacitance recording is advised. Putative efflux of compounds may be verified using amperometry and/or optical methods. While unfortunate, the result highlights the very high difficulty of attempting to directly observe sub-cellular processes in real time, especially if the extent of the process is not yet well-characterized..

5.1.6 Cell-attached capacitance measurement

Recording in cell-attached mode required a change to the pulse sequences, because of the higher frequency requirements compared to the whole-cell mode. The calibration protocol had to be adjusted too. The readout of the cell-attached mode was limited with

regard to spatial information. As a trade-off, recordings at much higher resolution were possible. The best possible resolution attainable was in the order of attofarad (aF), which should have enabled registration of singular vesicles fusing with plasma membrane, if such a fusion occurred. To elicit vesicular fusion, a timed bath application of DHPG at 1 μM was used.

To verify calibration in this mode of recording, an amplifier-controlled pneumatic system was used. The calibration was corrected when the 10-30 ms suction pulse produced a change in C_m trace without the change in the G_M trace. The responsiveness of the membrane to the suction pulse was found to be indicative of the seal quality. Consistent upward deflection in response to suction indicated improved seal quality.

To maximize the chance of observing a fusion event inside a pipette lumen, DHPG wash-in was used to trigger a fusion. Indeed, soon after beginning of experiment, we were able to observe what we perceived as a collection of fusion events. The C_m trace was a staggered collection of persisting rectangular up-step. The trace also showed expected scale of capacitance change, if adjusted for non-chromaffin cells with smaller vesicles. The time scale appeared different by a factor 5, with glial cell recording being much quicker than those of chromaffin cells (Fig. 65).

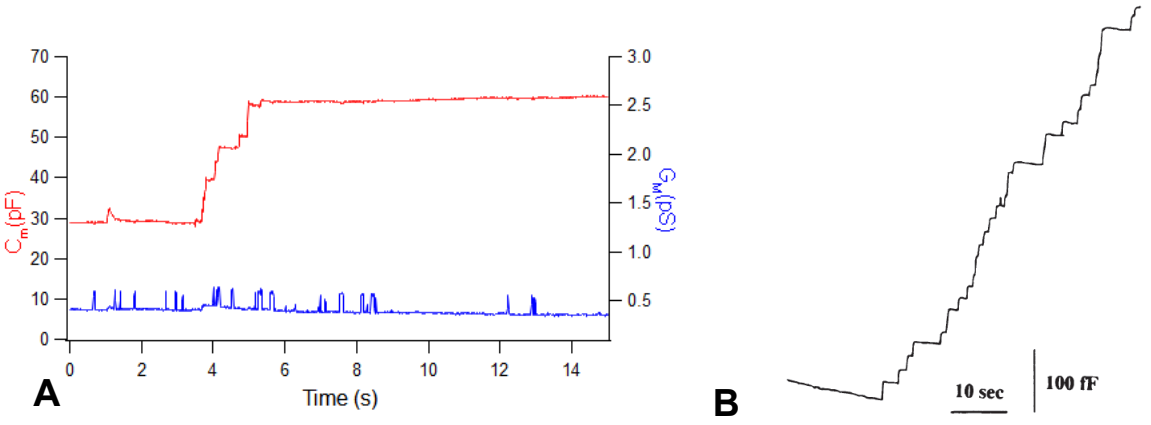

Fig. 65. An exemplary cell-attached capacitance trace (red) (A), compared to published observations (Gillis, 1995) (B).

The size of individual stepwise C_m increases should correspond to membrane area increases due to individual vesicles fusing. We were able to estimate the putative vesicle diameter using value of specific capacitance of biological membranes. The mean diameter was estimated to 351 nm. The size estimate corresponded to our expectation

of the size of MVBs (Murk et al., 2003).

We found the event of this type to be quite rare. This agreed with our expectation of how often a fusion event can be observed inside an area of a patch pipette tip. Five events were observed in the DHPG wash-in phase, recorded from a total of 62 recordings obtained from 11 mice. A successful recording also usually came within the first hour of patching in a workday. We assumed initially this bias to the beginning of the workday is result of vesicular run-off in the RRP. This expense on RRP could not be replenished by cells due to decreasing metabolic activity in the brain slice.

Later on, in the phase of control experiments, when a substance-free ACSF was washed-in, we also observed several events of the same kind. These events did not appear time correlated to the ACSF application as nicely seen as with the DHPG. Other parameters, including the time since slice preparation, were maintained. This briefly led us to believe that we might be observing vesicular release due to intrinsic activity in the slice.

The most likely source of the fusion-like events was discovered during inspection of the application tube system. The experiments were carried out under temperature-controlled conditions. ACSF was maintained at 35°C using a sensor-controlled flow-through heater. The ACSF was quickly heated just before it entered the recording chamber. In the beginning of the workday, the ACSF bottle arrived from a 4°C fridge and below room temperature. Due to lower temperature, the solubility of gasses in this solution was higher than that at room temperature. ACSF was saturated with gases during carbonization. As the solution was quickly heated in the flow-through heater, the gas left the liquid phase and formed a string of tiny bubbles that remained attached along the length of the tubing inside the heater. Eventually, the string of bubbles grew large enough and detaches, almost instantly reaching the recording area and creating a microscopic disturbance on the surface of the liquid in the chamber. The observation was quickly verified by purposefully injecting bubbles into the ACSF delivery system while patching living cells as well as non-biological objects. Non-biological seal was achieved on the surface of gel-like elastomer beads submerged in ACSF.

Contrary to the expectations however, this transient disturbance resulted in a non-transient change in baseline C_m. The persistent C_m change after a gas vesicle bursting might have been caused by the microscopic wave being sent across the recording

chamber pool and its interaction with the immersed patch pipette or the objective. It is possible that this wave, having a high and a low point, may stain the dry, i.e. above ACSF bath level, portion of the immersed patch pipette shaft. This could persist due to surface tension. As the result, this may cause a constant increase in baseline C_m. This might increase uncompensated pipette capacitance. Thus, it is possible that the added capacitance was that of the pipette itself, and not of the recorded cell.
In conclusion, the reliability of recordings made in cell-attached mode was strongly doubtful. In the context of gas bubble elicited non-transient capacitance changes it is very likely that the observed fusion-like events were artifacts.

5.2 Imaging experiments

As the second major approach to identify extracellular vesicles (EVs) in NG2-glia, we used immunofluorescent microscopy.

5.2.1 Identification of NG2-glial cells

To identify NG2-glia within the brain slice four options were available. First option was labeling against an anti-PDGFRα antibody which specifically labels NG2-glia. Another option was using an anti-NG2 antibody which would label NG2 protein on the surface of NG2-glia, but also in other locations, such as pericytes of the blood vessels in the brain. Third option was the use of heterozygous (NG2+/-) NG2-EYFP knock-in mice, where NG2-glia is brightly fluorescent, while pericytes can easily be distinguished because of their morphology. The NG2-EYFP heterozygous mice still retain one copy of NG2 proteoglycan to stand in for its' potential functional importance. Homozygous EYFP(+/+) mice with NG2 knocked out are available as well. As a fourth option, it is possible to use hGFAP-EGFP transgenic mice (Nolte et al., 2001). In these mice, NG2-glia is faintly fluorescent compared to brightly fluorescent astrocytes, since NG2-glial cells show some GFAP reporter activity (Jabs et al., 2005). In practice, the NG2-EYFP mice provided the best option for identifying NG2-glial cells in tissue, because of very high signal-to-noise ratio of EYFP fluorescence and its high load in NG2-glia. The PDGFRα antibody labels specifically NG2-glia without binding to other cell types. The subcellular pattern of PDGFRα binding however provided little information about the shape or size of the cell. Labeling with the NG2 antibody in wild type or NG2-EYFP mice provided an acceptable signal-to-noise ratio. It was sufficient to identify most of the NG2-glial cells. NG2

antibodies do not label the cytosol. Care has to be taken to distinguish pericytes from NG2-glial cells, especially those straddling blood vessels. NG2-antibody affinity also varied depending on manufacturer and batch, which had to be taken into account.

5.2.2 Selection of antibody markers.

The antibodies for the imaging experiments were selected according to preliminary data (unpublished) and published data on exosomal release from microglial cells (Glebov et al., 2015). The unpublished experiments involved ultracentrifugation of an Oli-neu cell culture supernatant. The ultracentrifugation allowed to collect the fraction of floating particles from supernatant which corresponds to objects in the size range of exosomes (around 100 nm). The pellet after the last centrifugation step was collected in a small amount of buffer and investigated with antibodies against chosen proteins using Western blotting (Fig. 66).

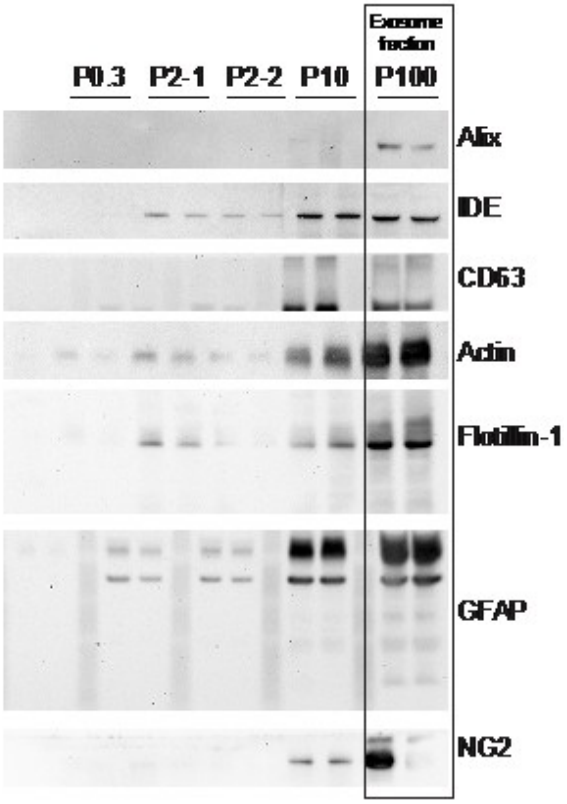

Fig. 66 A Western blot of the exosomal fraction derived from Oli-neu cell culture, two trials in each column. GFAP and IDE were proposed as hypothetical cargo for exosomes, while Flotillin-1, CD63 and Alix were previously implicated as markers for exosomes and/or multivesicular bodies (Glebov et al., 2015). P is centrifugation fraction, with P100 corresponding to a fraction collected after 100 *g*.

Three antibodies were selected to visualize subcellular components, which may indicate the presence of MVBs in NG2-glial cells. If two or more of the structures colocalize in the NG2-glial cells, this might indicate the presence of late endosomes or MVBs (Théry et al., 2018). These cellular vesicles may be tracked or otherwise manipulated. The expected features should correspond to MVBs in size, i.e. diameter around 300-500 nm (Murk et al., 2003), and location in

proximity of plasma membrane or in the cell processes. Commercially available antibodies for Alix and Flotillin-1 were created using rabbit as a host animal. While sequential co-labeling of two primary antibodies raised in the same host species is possible, it may result in ambiguous readout from secondary antibodies. It is best to avoid this strategy. The dissimilarity in labeling of Flotillin-1 and Alix, which we observed and discuss below, suggested that additional experimentation would not provide useful information. We did not attempt to observe these markers together in a single sample.

5.2.3 CD63 co-labeling with Alix and Flotillin-1

Tetraspanin protein CD63 is often quoted and marketed (!) as synonymous to LAMP3 (Kobayashi et al., 2000), a protein of lysosome-associated glycoproteins family, however, those are two distinct proteins. CD63 was first identified as a platelet activation factor and in relation to melanoma, and later associated with lysosomes as part of immune cell marker identification efforts in the late 1980 s (Metzelaar et al., 1991). It was also more broadly associated with intracellular vesicles, and was previously localized to multivesicular structures containing herpesvirus and HIV virus components in T-cells and macrophages, presumably, in the course of viral assembly and budding ((Mori et al., 2008; Raposo et al., 2002)). Along with two other tetraspanins CD9 and CD81, CD63 is considered a popular target for extracellular vesicle quantification and vesicular fraction purity assessment (Théry et al., 2018). These three proteins are accepted as standard go-to targets for identification of extracellular vesicles when unspecific transmembrane proteins of plasma membrane and/or endosomes are involved. It concerns the broadest selection of EV situations. Other proteins, such as Alix, Flotillin-1/2, VPS4A/B; ARRDC1, caveolins, and other ESCRT-associated proteins, may be found, if cytosole-originating proteins are expected in EVs. Even more detailed identification of EVs is possible by finding atypical components. This could be parts of the nucleus, mitochondria, Golgi apparatus if apoptotic process is expected. Involvement of mitochondria was previously considered unusual for the EVs, especially the small, <200 nm fraction (Théry et al., 2018), however, in recent years mitochondria were also proposed as normal cargo for “extracellular particles” or “vesicles” that are shuttled between neurons and astrocytes (Davis et al., 2014; Hayakawa et al., 2016), as well as a source of EVs (D’Acunzo et al., 2021) themselves. No single marker can strictly delimit elements of endocytic pathway.

Diverging pathway branches may feature CD63 as a marker on both sides.
The current knowledge on extracellular vesicles and their markers is based largely on cell culture models. Information about the subcellular features and organization of EV *in situ* only appeared recently. A study by Men at al. (Men et al., 2019) provided one of the first glances to visually cuing EVs in the brain. It specifically emphasized CD63 and its role in neuron-astrocyte EV-mediated communication. The publication also briefly mentions Alix as one of the other EV markers, however the report from it was deemed “ambiguous” by the authors.
The CD63 labeling, which we carried out together with Alix and Flotillin-1, was highly granular and ubiquitous in the hippocampus. This was expected, considering the broad association of CD63 with endocytic pathway. Such a pathway is a matter of housekeeping for almost all eukaryotic cells, with the exception of some specialized cells, e.g. mature erythrocytes (Johnstone et al., 1987).

The NG2-glia was not specifically enriched in CD63 compared to other cell types. A certain population of other, non-NG2-glial cells appeared enriched in CD63, when viewed in the low-magnification context of tissue. One of the main candidates for this CD63-enriched population is microglia, considering the recently published data ((Men et al., 2019), supplementary, Fig. 1, e) on the GFP-tagged CD63 expression. Microglia, being primary phagocytic entity in the brain, should maintain the most developed macromolecule digestion capability, which would engage the endocytic pathway.

5.2.4 Alix and CD63

Alix was described as involved in vesicular traffic and protein sorting in an early-late endosome pathway. It was enriched in vesicles derived from D1 cell culture under apoptotic and non-apoptotic conditions. This placed it under attention as relevant for exosome biogenesis (Théry et al., 2001). Alix controls endosome invagination, which is a necessary part of vesicles forming inside a MVB, in the presence of LBPA (Matsuo et al., 2004). Its interactions during sorting of endosomes towards exocytic pathway were described in more detail by Baietti et al. (Baietti et al., 2012), placing it as an auxiliary component to Endosomal Sorting Complexes Required for Transport (ESCRT) proteins. ESCRT proteins are a large group of interacting proteins that control the processes of

membrane remodeling needed for formation and separation of vesicles from the plasma membrane. This includes the formation of MVBs. Alix is one of the more reliable markers that implicate exosomal function, while not solely responsible.

We could not find references to previous observations of Alix antibody in hippocampal tissue. This antibody is often used in conjunction with Western Blot analysis to confirm the presence of exosomes, together with other exosome markers, such as CD63. The granular labeling pattern is described for cell cultures. Sometimes Alix is presented as cytosolic and sometimes as a mix of granular and homogenous cytosolic label (see HEK293 IF stainings in reference to Abcam ab88388 page in the store).

The complexity of anti-Alix labeling did not yield information about NG2-glia involvement. The antibody labeling for Alix was ubiquitous, highly granular in appearance. The NG2-glial cells were not enriched in Alix. In few individual cells, the NG2-glial cells had lower than ambient Alix content, specifically in the nucleus (Fig. 40B). There was no significant difference between Alix granule count in NG2-glial cell nuclei and nuclei of other cells. Alix was upregulated in some pyramidal neurons, evident by brightly-labeled apical dendrites. On at least one occasion, such neuron was adjacent to an NG2-glial cell. The direction of interaction or relevance of NG2-glial cell for Alix upregulation in neuron could not be established. The colocalization scores for CD63 and Alix were low, with no other visible interaction between the markers.

Further investigation into vesicular function of NG2-glia may include labeling against Alix, since Alix is mentioned as a reliable marker for extracellular vesicles and exosomes. Such investigations might include an immunoelectron microscopy approach or a NG2-glia specific tagging of Alix with a fluorescent protein using a virus, similarly to this described for CD63 (Men et al., 2019).

5.2.5 Flotillin-1 and CD63

Flotillin-1, also known as reggie-2, is encoded by FLOT1 gene. It‘s a highly evolutionary-conserved protein (Borner et al., 2005) that was discovered along with its homologue Flotillin-2, also termed reggie-1, with two proteins often observed together. The protein was independently discovered on few occasions (Langhorst et al., 2005). The two most widely known names for the protein, “flotillin” and “reggie”, are results of protein being purified from lipid rafts that float on the surface of solution without being digested by

detergent (Bickel et al., 1997) and from the regenerating axon in goldfish optic nerve - (Schulte et al., 1997). More recently Flotillin-1 received attention as relevant for clathrin-independent endocytosis and its anti-necroptotic function (Fan et al., 2019), and in Alzheimer's disease. It remains a popular exosomal target protein along with tetraspanins, Alix and few others (Théry et al., 2018).

The anti-Flotillin-1 antibody used in our work targets a proprietary sequence of nucleotides from a human Flotillin-1 protein C-terminal in the “400-500 range” of amino acids. It places the sequence at the C-terminal of the longest known isoform of the protein which measures 427 amino acids. The antibody was monoclonal and recombinant. It was knockout-tested using HEK293T cell line. The product analysis included western blot, to a mass of 47kDa, aligning with calculated mass predicted from protein sequence.

The successful observation of Flotillin-1 in the samples required the step of epitope unmasking. This crucial tip was kindly provided by Dr. Konstantin Glebov. The difference between inclusion and omission of antigen retrieval for the final result can only be described as “all or nothing”. With even the lightest treatment, the antigen signal becomes extremely strong and reliable. It is able to withstand even the harsher treatment of glutaraldehyde-enhanced fixative necessary for electron microscopy, which is known to quench antigenicity. The omission of this short step leads to almost complete absence of antibody labeling. This critically important step, together with an improved specificity and more rigorous antibody manufacture may be relevant for the previously published observations of Flotillin-1 *in situ,* which will be discussed further.
The molecule of Flotillin-1 is membrane-integrated, but not membrane-spanning (Bauer and Pelkmans, 2006). The N-terminus is anchored in the membrane, and features two hairpin-loop segments, while the C-terminal is presumably exposed to cell interior. This should indicate that the epitope unmasking mentioned earlier is realized not due to methanol or thiol alcohol attacking the lipid bilayer and exposing the anchored part of the protein, but perhaps by releasing the C-terminal from some kind of typical and stable interaction with cell interior, or of the protein with itself.

The observed colocalization between Flotillin-1 and CD63 in NG2-glial cells was partial. The somata of the cell usually featured a subdomain, often a section of cytosole near the opening to a large process extending away from cell body, where both CD63 and Flotillin-1 positive granules were located. These could be seen in close proximity, sometimes overlapping in part or almost completely. This partial colocalization still was scored at a higher degree for Flotillin-1 and CD63, compared to Alix and CD63. Flotillin-1 was not associated with the plasma membrane of the cells, as may have been expected from publications linking it with scaffolding of the outer cell membrane, caveolae and lipid rafts (Bickel et al., 1997; Langhorst et al., 2005). This might be due to imaging parameters, differences in the antibodies used, or due to the specific parameters of cell cultures, in which a lot of previous research was conducted.

5.2.6 Flotillin-1 marks NG2-glial cells *in situ*

We noticed that the bright Flotillin-1 positive granules are found almost exclusively in NG2-glial cells. To exclude the involvement of EYFP we analyzed wild-type C57BL6J as well as NG2-EYFP mice. We found that Flotillin-1 positive granules indeed pertain to NG2-glial cells. When viewed in Flotillin-1 fluorescence wavelength alone, clusters of brightly-labeled granules were predictive of location of NG2-glial cells, in hippocampus, in cortex and in all other areas of the brain. When ordered by intensity, the largest and brightest granules in the tissue always belonged to the interior of NG2-glial cells. There is some published data on observation of Flotillin-1 *in situ*. In none of the sources (see chapter 5.2.8) we found a description of this strong association. This observation raises a number of questions, some of which could be answered in the current work.

5.2.7 Do Flotillin-1 positive granules mark multi-vesicular bodies in NG2-glia?

The approach to establish the nature of Flotillin-1 positive granules was parallel and bi-directional. First, we attempted to perturb the immunofluorescent picture using substances (DHPG and ATP) together with acute brain slices, or by employing animals with altered membrane parameters of NG2-glial cells, namely the genetically modified NG2-glia specific Kir4.1 KO mouse line. In this mouse model, the NG2-glia-specific knock out of voltage gated Kir4.1 potassium channels was induced. This leads to a permanent depolarization of NG2-glia and chronic hyperexcitability. Second, we used

immunoelectron microscopy to view the subcellular anatomy and parameters of the granules. The wash-in of substances that might trigger membrane fusion events could potentially alter the immunofluorescent appearance of the MVBs, if it was indeed Flotillin-1 that was marking them. If a membrane fusion of an MVB occurs under the influence of the substance, the sphericity of the MVB would be lost and the numbers of granules after application of substance and control groups would be altered. The change of immunofluorescent picture may have occurred in control and Kir4.1ko groups of mice of NGCE and Kir4.1ko lines as well, due to increased excitability.

In all approaches, no significant effect of substances or genetic conditions was found for Flotillin-1 positive granule counts. This indicates no interactions of the observed structures with the substances or with time parameters of substance application.

The observation of subcellular anatomy using immunoelectron microscopy, and, subsequently CLEM, revealed that the observed granules were not MVBs. The morphological and densitometric parameters of the Flotillin-1 positive granules corresponded to that of late endosomes and/or lysosomes. The CLEM approach, implemented together with Dr. Hannes Beckert, allowed unambiguous identification of NG2-glial cells in the brain samples. No MVBs were found in the available sections of the somata of NG2-glial cells. Classical MVBs were located in neurons of the pyramidal layer within the same electron-microscopy samples. The anti-Flotillin-1 gold particles also marked the residual bodies in neurons of pyramidal layer, also known as telolysosomes. Those structures are associated with ageing and contain indigestible autofluorescent lipoprotein detritus, known as lipofuscin.

5.2.8 What is the state of the art regarding observation of Flotillin-1 *in situ*?

Many publications on Flotillin-1 concern its role in surfactant production in human lung, and the related medical importance in newborns. We attempted to locate information regarding Flotillin-1 observation in the brain tissue. Few publications explored the potential role of Flotillin-1 in Alzheimer's disease. In publications by Kokubo et al. (Kokubo et al., 2000) some features of Flotillin-1 *in situ* were recognized, for example, different background intensity from layer to layer of tissue. The observations were made using immunohistochemical staining in human brain. The Flotillin-1 staining was described as "punctate" and it was associated with pyramidal neurons and with

astrocytes in the white matter, but not in granular cells. In the study (Kokubo et al., 2000), the astrocytes were seemingly not identified in any way except morphologically. This potentially might explain the conclusion. The concept of NG2-glia/OPC was also not firmly established around the time of publication. The used antibody was monoclonal. It targeted the amino-acid sequence of Flotillin-1 in the 331-344 range (Volonte et al., 1999), and not at the 400+ range. This leaves a possibility for observations being associated with a shorter isoform of Flotillin-1 (e.g. A0A140T9R1). In a subsequent publication by Kokubo (Kokubo et al., 2003), immunoelectron staining was performed with focus on the neurons, in which the Flotillin-1 was shown to label cytosolic sides of lysosomes and lipofuscin bodies – an observation which we confirm with similar immunoelectron approach.

In publication by Stuermer et al. (Stuermer et al., 2001) the Flotillin-1 was similarly attributed to endolysosomes of the astrocytes. However, this was also done in culture.

Girardot (Girardot et al., 2003) studied neurofibrillary tangles and Flotillin-1 in human Alzheimer's disease brain. Flotillin-1 positively correlated with tangle protein accumulation in neurons. It was located to lysosomes, but did not colocalize with APP. The Flotillin-1 was upregulated in neurons of Alzheimer's disease patients, but without spatial association with AD proteins. A distinction between granular labeling and diffuse labeling of individual cells was made. We were not able to observe diffuse labeling on a subcellular scale. Labeling in glial cells was acknowledged, but not evaluated. Flotillin-1 colocalized with Cathepsin-D, a lysosomal marker. The problematic accessibility of Flotillin-1 epitopes was also acknowledged and resolved by use of wet autoclaving with acidic buffers.

In a more recent publication by Nakadate (Nakadate, 2015) Flotillin-1 was explored in rat visual cortex from a developmental point of view, in range between few weeks to few months. The used polyclonal antibody targeted the very end of C-terminal of the longest Flotillin-1 isoform. Between cell types, Flotillin-1 was ascribed to some cells of all cell types in the study, including neurons, astrocytes and microglia; but in the "diffuse" sense. No granularity was reported. The labeling patterns of Flotillin-1 presented in the images were reminiscent of the results that we obtained without inclusion of epitope unmasking step. Such a step was not mentioned in the methods section of this publication. It is possible that high laser intensity was used during imaging. This brings out very low level

of antibody binding and unspecific background signals.
In the paper by Trajkovic (Trajkovic et al., 2008), the intracellular sorting of PLP to EVs on the model of Oli-neu cells was studied, with involvement of Flotillin-1 in the context of lipid rafts, however, without any links to NG2-glia suggested.
Santiago et al. (Santiago et al., 2013) studied the close homologue of Flotillin-1, Flotillin-2, in the context of spinal cord trauma. Flotillin-2 was immunohistochemically ascribed to peripheral neurons, reactive astrocytes, myelinating oligodendrocytes, but not with OPC/NG2-glial cells, as potentially a signal molecule.

5.2.9 Is the antibody really binding what we think it is binding?

We believe that the antibody specificity is at least not worse than the state of the art, and does not require additional verification. This is considering the observed parallels between earlier publications and our work in terms of labeling patterns. Labeling of tissue layers (Kokubo et al., 2000), granularity (Girardot et al., 2003), and results of immunoelectron microscopy (Kokubo et al., 2003) seem to be in agreement with our results. The extensive testing of the antibody performed by the manufacturer also appears sufficient.

5.2.10 Was Flotillin-1 labeling found with astrocytes *in situ*?

The granular (or other) type of Flotillin-1 labeling was not found with the astrocytes of hGFAP-EGFP mice. It is possible that the prior publications describing Flotillin-1 *in situ* were not yet aware of the class of the glial cells that are known as NG2-glia today. The emphasis of the prior work (Girardot et al., 2003; Kokubo et al., 2000, 2003) was also on neurons and Alzheimer's disease, and not on glial cells.

5.2.11 Can Flotillin-1 be considered a novel marker for NG2-glia?

Flotillin-1 can be considered a novel marker for NG2-glia, with some limitations. While the strongest labeling is indeed found with lysosomes of NG2-glial cells, and the granular pattern is highly characteristic, the much weaker labeling in neurons nevertheless suggests that the FLOT1 gene is active in NG2-glial cells and in some neurons. If fluorescent protein is expressed under FLOT1 promoter without cell-specific targeting, it may manifest in neurons and NG2-glia, possibly with noticeably different

intensity. If, however, the chosen fluorescent protein emission spectrum is in red, parallel imaging of lipofuscin granules in green channel may help distinguish NG2-glial cells from pyramidal and cortical neurons by criterion of autofluorescent protein deposits.

Additionally, the existing data on mRNA expression of Flotillin-1 (Fig. 67) suggests that the expression levels are high in neurons of pyramidal layer and dentate gyrus, and, possibly, also in the cortical neurons. The expression in cells of *stratum radiatum* and other non-neuronal layers of the hippocampus is lower in comparison. The spread of these low-intensity cells in Fig. 67 across the layers is reminiscent of that of NG2-glial cells (see Fig. 37 for comparison). It is possible that these low-intensity cells in the image (Fig. 67) are, in fact, NG2-glial cells. The other possibility is that these cells might be interneurons.

This differentiated expression may interfere with identification of NG2-glial cells, if, for example, a fluorescent protein is expressed under the FLOT1 promoter, since the high signal intensity may turn out to be from neurons, and dimmer signal to be from NG2-glia. Yet, it is not uncommon for an accepted cell type marker to be expressed in more than one cell type – for example, the NG2 proteoglycan is expressed in pericytes as well as NG2-glia, and GFAP, typically associated with astrocytes, is also found in NG2-glial cells. However, we believe that the importance of the Flotillin-1 association with NG2-glia is more in its potential functionality, which requires additional investigation.

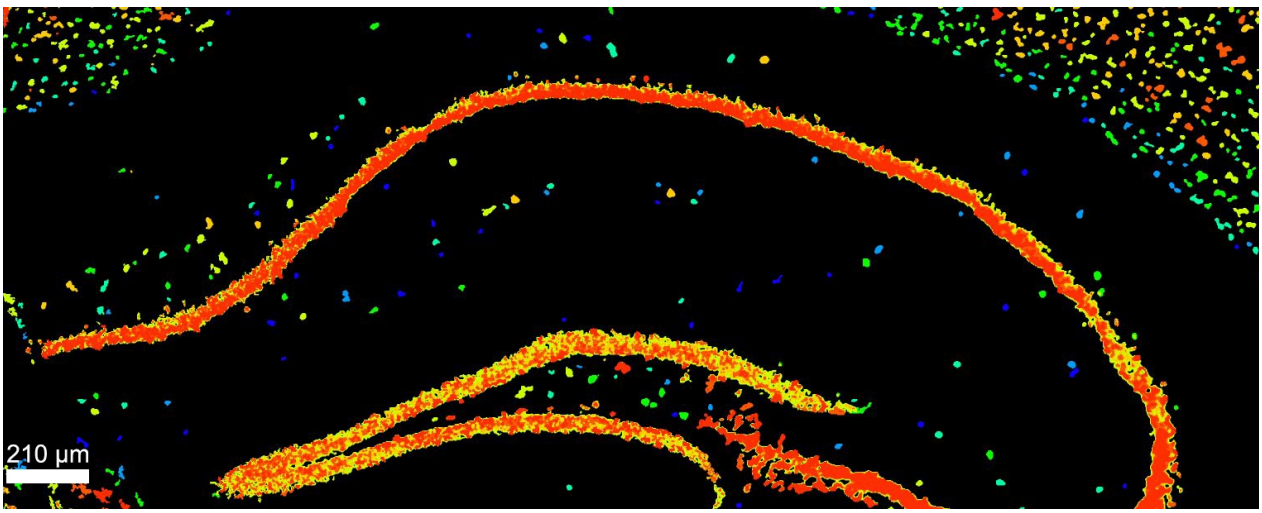

Fig. 67 In-situ hybridization expression data of FLOT1, in mouse hippocampus, retrieved from Allen Mouse Brain Atlas, experiment ID 67752111. High expression denoted in red, low – in blue. The distribution of cells visible in *str.radiatum*, *str.oriens* and DG *hilus* is reminiscent of that for NG2-glial cells.

5.2.12 Does the granular pattern of Flotillin-1 in NG2-glial cells change with age?

The effects of age on the pattern of Flotillin-1 labeling may be expected, since Flotillin-1 was described as involved in mitosis (Santamaría et al., 2005). We were not able to detect significant differences in Flotillin-1 labeling between a young and an adult animal. A larger experimental group may uncover some dynamic there. This might be interesting in the context of lipofuscin buildup and ageing, since there appears to be a Flotillin-1-mediated connection between lipofuscin management in neurons and NG2-glial cells. One of the possibilities is that there are degrees of faultiness of lipofuscin management, since lipofuscin is deposited in neurons but is not found in NG2-glia. The Flotillin-1-marked lysosomes in pyramidal neurons, even in the very young animals, have an autofluorescent lipofuscin core in the middle, marking them as possible early residual bodies. These granules are dense and heterogeneous in electron micrographs, often containing lipid droplets. The intensity of Flotillin-1 labeling of these neuronal (telo)lysosomes, however, is weak and/or fragmented in comparison with intense labeling of lysosomes in NG2-glial cells. The lysosomes of NG2-glial cells are free of any signs of deposition. They appear homogeneous and with density normal for that of a typical lysosome. Whether this difference has to do with cell-type intrinsic properties or metabolic levels between pyramidal neurons and NG2-glia is unclear. Has this anything to do with lifelong capability for cell division in NG2-glia versus the lifelong persistence of non-dividing neurons? Why do neurons get unmanageable deposits in Flotillin-1-marked lysosomes, while NG2-glial cells seem to not get any deposits in similarly, but more strongly labeled lysosomes? Why don’t any other cell types appear to have their lysosomes marked with Flotillin-1? Why do granular layer neurons of the dentate gyrus not have Flotillin-1 labeling around their lipofuscin granules, while the pyramidal layer neurons do? Could it be that Flotillin-1 is involved in conditions such as neuronal ceroid lipofuscinosis (Mukherjee et al., 2019)? These questions would be interesting to answer with future studies, starting, perhaps, with conditional over- or under- expression of Flotillin-1 in the NG2-glial cells, and its effects on the hippocampus at different ages, including more aged adults.

5.2.13 Does the granular pattern of Flotillin-1 in NG2-glial cells change as they mature into oligodendrocytes?

It is believed that all oligodendrocytes originate from oligodendrocyte precursors. The term oligodendrocyte precursor (OLP) refers to cells known to originate from different sources during embryogenesis (Richardson et al., 2006). Most often the OLPs are defined through expression of Olig2, PDGFRα or NG2 (Dimou et al., 2008). NG2 proteoglycan was described as interchangeable with PDGFRα for OLP identification (Rivers et al., 2008) in tissue. NG2 glia, therefore, is commonly considered to have the functionality of OLP, along with other possible functions – that is, disregarding the possibility that NG2 glia as a cell type may have an unknown degree of heterogeneity. The NG2 glia is known to behave differently in grey and white matter in terms of their potential for differentiation into oligodendrocytes. In the grey matter the NG2 glia demonstrates a much lower readiness to differentiate into myelinating oligodendrocytes, than in the white matter (Dimou et al., 2008; Huang et al., 2014). Whether this is a result of intrinsic/lineage differences or influence of immediate cellular surroundings is a matter of research, with some evidence to the latter (Viganò et al., 2013). In grey matter only about 18 % of resident OLP cells (as defined by Olig2 origin) were shown to differentiate into oligodendrocytes in mice over the course of 6 months when observed starting from age of 2.5 months or older (Dimou et al., 2008). This number likely represents the “adult” rate of differentiation of NG2 glia to oligodendrocytes in grey matter, which is maintained through the lifetime. Therefore, with age not all NG2 glial cells are likely to become oligodendrocytes in the grey matter, yet all oligodendrocytes did originate from NG2 glia. Closer to birth however the rate of differentiation of embryonic and early post-embryonic NG2 glia to oligodendrocytes is different. Between P10 and P21 the percent of NG2 glia differentiating to oligodendrocytes increases from 17.5 % to 51 % in dorsal cortex, when observed starting from P3 (Huang et al., 2014), Fig.4E]. It is likely that in younger mice a higher proportion of oligodendrocytes in grey matter have recently differentiated from NG2 glia, compared to adults. We examined one NG2-EYFP mouse of P28 in our study. We defined oligodendrocytes using CC1, a popular marker that identifies mature oligodendrocytes without highlighting the myelin. The CC1 antibody is raised against adenomatous polyposis coli, a protein that is mainly expressed in neurons. The CC1 antibody however does not bind APC in mouse tissue, it binds protein Quaking 7 instead

(Bin et al., 2016). The resulting labeling nevertheless highlights mature and maturing oligodendrocytes. NG2 expression is downregulated as the NG2-glial cell differentiates towards oligodendrocyte. A descending gradient of EYFP expression was observed between *bona fide* NG2-EYFP-glial cells and cells identified as oligodendrocytes using CC1. The intensity of CC1 was found to be highest in the cells that still have some weak expression of EYFP. It is possible that the intensity of CC1 is increasing quicker than the intensity of EYFP decreases with tapering of EYFP production and recycling of remaining protein as the cell differentiates. It is also possible that CC1 peaks in content soon after its production begins, and later decreases to a more stable baseline as the oligodendrocyte differentiation is complete. The cells clustered into two distinct groups following the EYFP and CC1 expression. Clustering in three groups is also possible with slightly lower scores. The third group in this case would appear by separating oligodendrocyte group into, presumably, a more numerous “stable” cluster with almost no EYFP expression and into a smaller “differentiating” cluster with some EYFP still present in the cells and higher than “stable” CC1 expression (Fig. 53 D). If Flotillin-1 count is included as the third dimension, the direction along which the count of Flotillin-1 decreases aligns to that of decreasing integrated intensity of EYFP. This might be interpreted as downregulation of Flotillin-1 in the NG2-glial lysosomes as the cells mature towards oligodendrocytes. This may indicate that whatever is the function of Flotillin-1 in the NG2-glia, it is not conducive to long-term maintenance of associated neurons and/or long-distance connectivity. A more comprehensive study with a larger number of animals and timepoints is needed to verify this probability.

5.2.14 What is the potential function for Flotillin-1 in NG2-glia?

Flotillin-1 is a highly-conserved molecule (Borner et al., 2005), and the list of functionality that is ascribed to it is quite long (for review, see (Langhorst et al., 2005)). It is most known for its association with lipid rafts. Lipid rafts are sections of plasma membrane on the outside of cells that are rich in ceramide and other components that make them impregnable to detergents such as Triton (Bickel et al., 1997). This outward placement is linking Flotillin-1 to protein-protein interactions at synapses (Swanwick et al., 2010), cell adhesion and cholesterol metabolism (Trajkovic et al., 2008). Flotillin-1 was also associated with caveolae – the structured invaginations of outer plasma membrane that

are associated with clathrin-independent endocytosis. It was also mentioned as important for cell cycle together with its close homologue Flotillin-2, and involved in mitosis (Santamaría et al., 2005). Cell to cell signaling is another function ascribed to Flotillin-1 and 2 (Langhorst et al., 2005). It is currently unclear which one (or which of the several) functions of the mentioned (or yet unknown) may be relevant to Flotillin-1 in NG2-glia. The relative abundance of Flotillin-1 molecules in this particular cell type that is apparent from the antibody binding pattern may suggest that it's a function that is quite specific for NG2-glia. As of now, it appears to us that among the conditions that should be tested first to begin revealing this functionality of Flotillin-1 may be the inhibition of cell cycle, and, as the result, the change to NG2-glial cell proliferation. Secondly, the conditional downregulation or overexpression of Flotillin-1 and its effects on oligodendrocyte differentiation on one side, and on peptide deposits in neurons on the other, can be evaluated. The animal models for Alzheimer's disease and/or other protein deposition diseases may be an interesting target as well. The release of extracellular vesicles is probably not one of the functions to which Flotillin-1 is directly related at the point of MVBs fusing to outer cell membrane, but it should be kept in mind for any further investigation into EVs as molecule important for endocytic pathway in NG2-glial cells.

6. Conclusion

NG2-glia is a type of cell that remains somewhat obscure despite its remarkable features, such as bipotency, proliferation in adult brain and receiving synaptic input from neurons, in white and grey matter. In this project, we approached the question of extracellular vesicle release from NG2-glia that might be the way of material transfer from NG2-glial cells to surrounding network. Recently published (Timmermann et al., 2021) data from our Institute suggests that the myelin content of oligodendrocytes in hippocampus increases with changes in excitability of NG2-glia, but without changes in absolute numbers or proportion of NG2-glial cells and oligodendrocytes. The mRNA for MBP was increased in the oligodendrocytes, and while there is currently no proof of material transfer between NG2-glial cells and mature oligodendrocytes, the EV-based transfer of mRNA and/or MBP subassemblies might be one of the mechanism by which NG2-glia can influence oligodendrocytes, or other cells in the surrounding network.

We approached the question of extracellular vesicle release from two directions. First, by attempting to observe changes in plasma membrane capacitance, and later by using a combined immunofluorescence-immunoelectron microscopy. Initially, we implemented a technique of single cell membrane capacitance recording that was never previously used to study NG2-glia, and successfully verified it to be in agreement with state of the art using PC12 cell line. We later examined the Oli-neu cell line. Oli-neu is best existing cell culture model for NG2-glia cell, and a known source of exosomes. Functional data collected using fast membrane capacitance recording, however, did not reveal the vesicular fusion. This method seems not sufficient to register the expected fusion events using the current implementation. We later targeted *in situ* NG2-glial cells in acute brain slices using the same technique as with the PC12 and Oli-neu cells cultures, and a modification of the technique to achieve higher resolution. This, however, resulted in higher than expected complexity. The results of the electrophysiological experiments could not confirm or deny the release of EV from NG2-glial cells, but provided some information regarding the method itself.

In the second approach, we attempted to visualize the exosomes at the very end of endocytic pathway, poised for release from multi-vesicular bodies of NG2-glial cells. For this we used the NG2-EYFP knock-in mice as well as wild-type mice. For immunofluorescence microscopy, we selected the subcellular markers that were

described in the literature as most relevant for detection of exosomes. The colocalization of two of the markers, CD63 and Flotillin-1, cued us to evaluate the immunofluorescence picture in more detail, as it was a good candidate to mark an MVB. Curiously, we found that Flotillin-1 showed a very strong connection to NG2-glial cells that was previously undescribed. In the literature, Flotillin-1 positive granules were ascribed, instead, to astrocytes – an observation which we do not confirm.

In further examination, using correlated light-electron microscopy, we established that the Floitllin-1-marked granules in the NG2-glial cells did not correspond to multivesicular bodies, as we previously thought. The structures marked have turned out to have features of lysosomes, or late endosomes. The MVBs were not found in projections of cell somata of NG2-glial cells in electron micrographs, however they were found in the other cell types, namely neurons, where they were not marked with Flotillin-1. This leaves the possibility that multivesicular bodies, if present, are located in the processes of NG2-glial cells, not unlikely in proximity of NG2-glia postsynapses.

The labeling of Flotillin-1 in electron micrographs has supported another previous observation – that Flotillin-1 marks the cytosolic side of neuronal telolysosomes – residual bodies containing undigested or indigestible lipoproteins, also known as lipofuscin. This material is known to accumulate with age due to lifelong persistence of neurons, and in human neurons it was found to occupy a significant volume of the cell in aged individuals. The Flotillin-1-marked, lipofuscin-containing bodies were, nevertheless, found in pyramidal neurons of mice as young as two weeks. The Flotillin-1 labeling of these structures, however, was weak or partial in comparison to intense labeling found in NG2-glial cells in the same samples. The content of the lysosomes of NG2-glial cells at the same time was not different from that expected of a normal lysosome. In contrast to telolysosomes, which are believed to be incapable of digesting their content, normal appearance of NG2-glia lysosomes suggests their nominal proteolytic operation. This establishes a previously unknown connection between groups of neurons, particularly pyramidal and cortical neurons, and most, if not all, NG2-glial cells.

The available data on Flotillin-1 mRNA expression suggests that the mRNA content may be higher in neurons than in NG2-glial cells. Our observation of intense Flotillin-1 labeling in NG2-glia suggest that, if mRNA content is indeed higher in the neurons, the conversion rate between mRNA and the actual Flotillin-1 protein may be different

between these cell types. This may impose a limitation on use of Flotillin-1 as an NG2-glia marker, but this hypothesis requires additional verification. It should be noted that synthesizing fluorescent proteins under control of some other known cell type markers, for example NG2 or GFAP, also results in a fluorescent image that includes more than one cell type (i.e. NG2-glia and pericytes, astrocytes and NG2-glia). Therefore the value of Flotillin-1 as a potential marker for NG2-glia might be highly depend on the context of the experiment, even if the resulting immunofluorescent picture might include NG2-glial cells and neurons, possibly with different intensity.

The Flotillin-1 labeling of lysosomes that was present in almost all NG2-glial cells was mostly absent in oligodendrocytes in a four-week old mouse. This was interesting considering that up to 51 % of NG2 glia in the cortex of mice undergoes differentiation into oligodendrocytes between birth and third week of age (Huang et al., 2014). While almost all mammalian cells do have lysosomes at the end of their endosome pathways, Flotillin-1 labeling appears to change between NG2-glial and oligodendrocyte lysosomes, suggesting that the associated function is likely downregulated in oligodendrocytes. A more detailed investigation into this observation is needed for a definite answer.

Despite their prominent role in proteolytic digestion of material in the brain, the Flotillin-1 marking of lysosomes was not found in microglia.

Overall, the Flotillin-1 may appear as a new important “handle” to study the role of NG2-glia in grey matter, potentially, with yet unknown connections to neurons, ageing, and proteolipid deposition diseases.

We could not locate more evidence to support a transfer of compounds from NG2-glial cells to the surrounding network. We gained the invaluable information on the viable approaches to studying this function in the future. The exosomes, thanks to their small size, are elusive and difficult to locate in the overwhelming complexity of the actual brain tissue, where most cell types are expected to perform vesicular release. There is not a single marker that would allow a firm grasp on the exosomes as a class of vesicles, reliably delimiting them from other kinds of extracellular vesicles, debris, viruses and micelles. It is important to bridge the biochemical approach with other techniques chosen to study the exosomes, be it the super-resolution microscopy, viral vectors or other. The recently observed connection between increased excitability of Kir4.1ko NG2-

glia and increase in oligodendrocyte MBP expression may be a target for a subsequent study. The NG2-glia cell-specific RAB5 dominant negative mice should be limited in the NG2-glia ability to release exosomes, which might also influence the surrounding network in an identifiable manner.

7. Abstract

NG2-glial cells is an abundant and widely distributed subtype of glia, featuring properties not typically associated with mature glial cells, such as the ability to receive synaptic input from neurons, or an often discussed degree of multipotency. Fast information flow from neurons to NG2-glia through synaptic structures was confirmed in several studies. The purpose of such a fast communication, where, apparently no computation is occurring, remains unclear. It was suggested that neuronal activity through innervation of NG2-glia controls its differentiation into myelinating oligodendrocytes according to the requirements of the neural circuit. However in grey matter – which features persisting populations of NG2-glial cells together with sparse myelination – function of NG2-glia is still largely unknown. Our preliminary results suggest exosome release from NG2-glia model cells *in vitro*.

In our project, we searched for exosome release from NG2-glia in different *in situ* and *in vitro* preparations using both a functional approach and morphological evaluation of candidate structures on subcellular scale. In functional approach we established the high resolution membrane capacitance recording technique using patch clamp method. The technique however proved insufficient to confirm or deny exosomal release from Oli-neu cell line or NG2-glial cells *in situ*.

In the imaging approach, we used laser confocal microscopy to identify candidate structures for exosomes. In the process, we identified that one of the candidate marker proteins, Flotillin-1, features a previously undescribed association with NG2-glial cells in hippocampus. Having quantified this association using large-scale semi-automated detection of fluorescent markers, we attempted to alter the parameters of Flotillin-1 labeling in a way that would support its role as mediator of exosomal release, but to no visible effect.

Using correlated light-electron immune microscopy we were able to establish the morphology of Flotillin-1-labeled structures in NG2-glial cells, identifying them as lysosomes or late endosomes. We also supported the previous observations which describe Flotillin-1 in association with age pigment, also known as lipofuscin, in hippocampal neurons, specifically in neuronal telolysosomes.

Despite not providing new evidence for exosomal release from NG2-glial cells, our research identified new putative marker for NG2-glial cells, Flotillin-1. Flotillin-1 was

previously described in astrocytes, however, our data does not support this observation. Strong subcellular association of Flotillin-1 with cytosolic side of NG2-glial cell lysosomes also reveals an obscure parallel of NG2-glial cells with hippocampal neurons, in which Flotillin-1 is known to sparsely label the cytosolic side of telolysosomes, the residual bodies containing the ageing pigment, lipofuscin. Our work may provide new tools to interact with NG2-glial cells, as well as potential for yet unknown functionality of these glial cells. The Flotillin-1-mediated connection between neurons and NG2-glial cells may prove valuable for future studying of neuronal ageing and deposition disease.

8. List of figures

9. List of tables

10. References

Akers, J.C., Gonda, D., Kim, R., Carter, B.S., and Chen, C.C. Biogenesis of extracellular vesicles (EV): exosomes, microvesicles, retrovirus-like vesicles, and apoptotic bodies. J Neurooncol 2013; *113*, 1–11.

Alonso, G. NG2 proteoglycan-expressing cells of the adult rat brain: Possible involvement in the formation of glial scar astrocytes following stab wound. Glia 2005; *49*, 318–338.

Amaral, D.G., and Witter, M.P. The three-dimensional organization of the hippocampal formation: A review of anatomical data. Neuroscience 1989; *31*, 571–591.

Araque, A., Parpura, V., Sanzgiri, R.P., and Haydon, P.G. Tripartite synapses: glia, the unacknowledged partner. Trends in Neurosciences 1999; *22(5)*, 208–215.

Bachiller, S., Jiménez-Ferrer, I., Paulus, A., Yang, Y., Swanberg, M., Deierborg, T., and Boza-Serrano, A. Microglia in Neurological Diseases: A Road Map to Brain-Disease Dependent-Inflammatory Response. Front. Cell. Neurosci. 2018; *12*, 1–17.

Baietti, M.F., Zhang, Z., Mortier, E., Melchior, A., Degeest, G., Geeraerts, A., Ivarsson, Y., Depoortere, F., Coomans, C., Vermeiren, E., et al. Syndecan–syntenin–ALIX regulates the biogenesis of exosomes. Nat Cell Biol 2012; *14*, 677–685.

Barbour, B. Electronics for electrophysiologists. 2014. Institut de Biologie de l'École Normale Supérieure (IBENS) https://www.ibens.ens.fr/spip.php?article296&lang=en (accessed 16.11.2021)

Barres, B.A., and Raff, M.C. Proliferation of oligodendrocyte precursor cells depends on electrical activity in axons. Nature 1993; *361*, 258–260.

Bauer, M., and Pelkmans, L. A new paradigm for membrane-organizing and -shaping scaffolds. FEBS Letters 2006; *580*, 5559–5564.

Bergles, D.E., Roberts, J.D.B., Somogyi, P., and Jahr, C.E. Glutamatergic synapses on oligodendrocyte precursor cells in the hippocampus. Nature 2000; *405*, 187–191.

Bergles, D.E., Jabs, R., and Steinhäuser, C. Neuron-glia synapses in the brain. Brain Res Rev 2010; *63*, 130–137.

Berridge, M.J., and Irvine, R.F. Inositol trisphosphate, a novel second messenger in cellular signal transduction. Nature 1984; *312*, 315–320.

Bickel, P.E., Scherer, P.E., Schnitzer, J.E., Oh, P., Lisanti, M.P., and Lodish, H.F. Flotillin and Epidermal Surface Antigen Define a New Family of Caveolae-associated Integral Membrane Proteins. J. Biol. Chem. 1997; *272*, 13793–13802.

Bin, J.M., Harris, S.N., and Kennedy, T.E. The oligodendrocyte-specific antibody “CC1”

binds Quaking 7. Journal of Neurochemistry 2016; *139*, 181–186.

Birey, F., Kloc, M., Chavali, M., Hussein, I., Wilson, M., Christoffel, D.J., Chen, T., Frohman, M.A., Robinson, J.K., Russo, S.J., et al. Genetic and Stress-Induced Loss of NG2 Glia Triggers Emergence of Depressive-like Behaviors through Reduced Secretion of FGF2. Neuron 2015; *88*, 941–956.

Blasi, E., Barluzzi, R., Bocchini, V., Mazzolla, R., and Bistoni, F. Immortalization of murine microglial cells by a v-raf/v-myc carrying retrovirus. J. Neuroimmunol. 1990; *27*, 229–237.

Boda, E., and Buffo, A. Beyond cell replacement: unresolved roles of NG2-expressing progenitors. Front Neurosci 2014; *8*.

Bolte, S., and Cordelières, F.P. A guided tour into subcellular colocalization analysis in light microscopy. Journal of Microscopy 2006; *224*, 213–232.

Borner, G.H.H., Sherrier, D.J., Weimar, T., Michaelson, L.V., Hawkins, N.D., MacAskill, A., Napier, J.A., Beale, M.H., Lilley, K.S., and Dupree, P. Analysis of Detergent-Resistant Membranes in Arabidopsis. Evidence for Plasma Membrane Lipid Rafts. Plant Physiol 2005; *137*, 104–116.

Chen, P., and Gillis, K.D. The noise of membrane capacitance measurements in the whole-cell recording configuration. Biophys J 2000; *79*, 2162–2170.

Colombo, M., Raposo, G., and Théry, C. Biogenesis, Secretion, and Intercellular Interactions of Exosomes and Other Extracellular Vesicles. Annual Review of Cell and Developmental Biology 2014; *30*, 255–289.

Costes, S.V., Daelemans, D., Cho, E.H., Dobbin, Z., Pavlakis, G., and Lockett, S. Automatic and Quantitative Measurement of Protein-Protein Colocalization in Live Cells. Biophys J 2004; *86*, 3993–4003.

D'Acunzo, P., Pérez-González, R., Kim, Y., Hargash, T., Miller, C., Alldred, M.J., Erdjument-Bromage, H., Penikalapati, S.C., Pawlik, M., Saito, M., et al. Mitovesicles are a novel population of extracellular vesicles of mitochondrial origin altered in Down syndrome. Science Advances 2021; *7*, 1–18.

Davis, C.O., Kim, K.-Y., Bushong, E.A., Mills, E.A., Boassa, D., Shih, T., Kinebuchi, M., Phan, S., Zhou, Y., Bihlmeyer, N.A., et al. Transcellular degradation of axonal mitochondria. PNAS 2014; *111*, 9633–9638.

Dimou, L., and Gallo, V. NG2-glia and their functions in the central nervous system. Glia 2015; *63*, 1429–1451.

Dimou, L., Simon, C., Kirchhoff, F., Takebayashi, H., and Götz, M. Progeny of Olig2-Expressing Progenitors in the Gray and White Matter of the Adult Mouse Cerebral Cortex. J. Neurosci. 2008; *28*, 10434–10442.

Dunn, K.W., Kamocka, M.M., and McDonald, J.H. A practical guide to evaluating colocalization in biological microscopy. American Journal of Physiology-Cell Physiology 2011; *300*, C723–C742.

Egawa, N., Suzuki, H., Takahashi, R., Hayakawa, K., Li, W., Lo, E.H., Arai, K., and Inoue, H. From in vitro to in vivo reprogramming for neural transdifferentiation: An approach for CNS tissue remodeling using stem cell technology. J Cereb Blood Flow Metab 2020; *40*, 1739–1751.

Fan, W., Guo, J., Gao, B., Zhang, W., Ling, L., Xu, T., Pan, C., Li, L., Chen, S., Wang, H., et al. Flotillin-mediated endocytosis and ALIX–syntenin-1–mediated exocytosis protect the cell membrane from damage caused by necroptosis. Sci. Signal. 2019; *12*, 1–10.

Fok-Seang, J., Matthews, G., Jacqueline, T., and Fawcett, J. Migration of Oligodendrocyte Precursors on Astrocytes and Meningeal Cells. Developmental Biology 1995; *171*, 1–15.

Fröhlich, D., Kuo, W.P., Frühbeis, C., Sun, J.-J., Zehendner, C.M., Luhmann, H.J., Pinto, S., Toedling, J., Trotter, J., and Krämer-Albers, E.-M. Multifaceted effects of oligodendroglial exosomes on neurons: impact on neuronal firing rate, signal transduction and gene regulation. Philos Trans R Soc Lond B Biol Sci 2014; *369*, 1–13.

Frühbeis, C., Fröhlich, D., Kuo, W.P., Amphornrat, J., Thilemann, S., Saab, A.S., Kirchhoff, F., Möbius, W., Goebbels, S., Nave, K.-A., et al. Neurotransmitter-Triggered Transfer of Exosomes Mediates Oligodendrocyte–Neuron Communication. PLOS Biol 2013; *11*, e1001604.

Gallo, V., Zhou, J.M., and Armstrong, R. Oligodendrocyte Progenitor Cell Proliferation and Lineage Progression Are Regulated by Glutamate Receptor-Mediated K channel Block. The Journal of Neuroscience 1996; *16*, 2659–2670.

Gillis, K. 1995. Techniques for Membrane Capacitance Measurements. In Single-Channel Recording, (Springer Science+Business Media LLC 2009), pp. 155–197.

Ginger, M., Haberl, M., Conzelmann, K.-K., Schwarz, M.K., and Frick, A. Revealing the secrets of neuronal circuits with recombinant rabies virus technology. Front. Neural Circuits 2013; *7*, 1–15.

Girardot, N., Allinquant, B., Langui, D., Laquerrière, A., Dubois, B., Hauw, J.-J., and Duyckaerts, C. Accumulation of flotillin-1 in tangle-bearing neurones of Alzheimer's disease. Neuropathology and Applied Neurobiology 2003; *29*, 451–461.

Glebov, K., Löchner, M., Jabs, R., Lau, T., Merkel, O., Schloss, P., Steinhäuser, C., and Walter, J. Serotonin stimulates secretion of exosomes from microglia cells. Glia 2015; *63*, 626–634.

Gómez, V., Sesé, M., Santamaría, A., Martínez, J.D., Castellanos, E., Soler, M., Thomson, T.M., and Paciucci, R. Regulation of Aurora B Kinase by the Lipid Raft Protein Flotillin-1. J Biol Chem 2010; *285*, 20683–20690.

Greene, L.A., and Tischler, A.S. Establishment of a noradrenergic clonal line of rat adrenal pheochromocytoma cells which respond to nerve growth factor. Proc Natl Acad Sci U S A 1976; *73*, 2424–2428.

Haberlandt, C., Derouiche, A., Wyczynski, A., Haseleu, J., Pohle, J., Karram, K., Trotter, J., Seifert, G., Frotscher, M., Steinhäuser, C., et al. Gray Matter NG2 Cells Display Multiple Ca2+-Signaling Pathways and Highly Motile Processes. PLoS One 2011; *6*, 1–17.

Haller, M., Heinemann, C., Chow, R.H., Heidelberger, R., and Neher, E. Comparison of secretory responses as measured by membrane capacitance and by amperometry. Biophys J 1998; *74*, 2100–2113.

Harkins, A.B., and Fox, A.P. Activation of Nicotinic Acetylcholine Receptors Augments Calcium Channel-mediated Exocytosis in Rat Pheochromocytoma (PC12) Cells. J Gen Physiol 1998; *111*, 257–269.

Hayakawa, K., Esposito, E., Wang, X., Terasaki, Y., Liu, Y., Xing, C., Ji, X., and Lo, E.H. Transfer of mitochondria from astrocytes to neurons after stroke. Nature 2016; *535*, 551–555.

Hill, R.A., and Nishiyama, A. NG2 Cells (Polydendrocytes): Listeners to the Neural Network with Diverse Properties. Glia 2014; *62*, 1195–1210.

Horrigan, F.T., and Bookman, R.J. Releasable pools and the kinetics of exocytosis in adrenal chromaffin cells. Neuron 1994; *13*, 1119–1129.

Hsu, C., Morohashi, Y., Yoshimura, S., Manrique-Hoyos, N., Jung, S., Lauterbach, M.A., Bakhti, M., Grønborg, M., Möbius, W., Rhee, J., et al. Regulation of exosome secretion by Rab35 and its GTPase-activating proteins TBC1D10A–C. J Cell Biol 2010; *189*, 223–232.

Huang, W., Zhao, N., Bai, X., Karram, K., Trotter, J., Goebbels, S., Scheller, A., and Kirchhoff, F. Novel NG2-CreERT2 knock-in mice demonstrate heterogeneous differentiation potential of NG2 glia during development. Glia 2014; *62*, 896–913.

Hughes, E.G., Kang, S.H., Fukaya, M., and Bergles, D.E. Oligodendrocyte progenitors balance growth with self-repulsion to achieve homeostasis in the adult brain. Nat Neurosci 2013; *16*, 668–676.

Jabs, R., Pivneva, T., Hüttmann, K., Wyczynski, A., Nolte, C., Kettenmann, H., and Steinhäuser, C. Synaptic transmission onto hippocampal glial cells with hGFAP promoter activity. J Cell Sci 2005; *118*, 3791–3803.

Johnstone, R.M., Adam, M., Hammond, J.R., Orr, L., and Turbide, C. Vesicle formation during reticulocyte maturation. Association of plasma membrane activities with released vesicles (exosomes). Journal of Biological Chemistry 1987; *262*, 9412–9420.

Jung, M., Krämer, E., Grzenkowski, M., Tang, K., Blakemore, W., Aguzzi, A., Khazaie, K.,

Chlichlia, K., von Blankenfeld, G., Kettenmann, H., et al. Lines of Murine Oligodendroglial Precursor Cells Immortalized by an Activated neu Tyrosine Kinase Show Distinct Degrees of Interaction with Axons In Vitro and In Vivo. European Journal of Neuroscience 1995; *7*, 1245–1265.

Karperien, A., Ahammer, H., and Jelinek, H. Quantitating the subtleties of microglial morphology with fractal analysis. Front. Cell. Neurosci. 2013; *7*, 1–18.

Karram, K., Goebbels, S., Schwab, M., Jennissen, K., Seifert, G., Steinhäuser, C., Nave, K.-A., and Trotter, J. NG2-expressing cells in the nervous system revealed by the NG2-EYFP-knockin mouse. Genesis 2008; *46*, 743–757.

Kessaris, N., Fogarty, M., Iannarelli, P., Grist, M., Wegner, M., and Richardson, W.D. Competing waves of oligodendrocytes in the forebrain and postnatal elimination of an embryonic lineage. Nat Neurosci 2006; *9*, 173–179.

Kobayashi, T., Vischer, U.M., Rosnoblet, C., Lebrand, C., Lindsay, M., Parton, R.G., Kruithof, E.K.O., and Gruenberg, J. The Tetraspanin CD63/lamp3 Cycles between Endocytic and Secretory Compartments in Human Endothelial Cells. Mol Biol Cell 2000; *11*, 1829–1843.

Kokubo, H., Lemere, C.A., and Yamaguchi, H. Localization of flotillins in human brain and their accumulation with the progression of Alzheimer's disease pathology. Neuroscience Letters 2000; *290*, 93–96.

Kokubo, H., Helms, J.B., Ohno-Iwashita, Y., Shimada, Y., Horikoshi, Y., and Yamaguchi, H. Ultrastructural localization of flotillin-1 to cholesterol-rich membrane microdomains, rafts, in rat brain tissue. Brain Research 2003; *965*, 83–90.

Kondo, T., and Raff, M. Oligodendrocyte Precursor Cells Reprogrammed to Become Multipotential CNS Stem Cells. Science 2000; *289*, 1754–1757.

Kukley, M., Capetillo-Zarate, E., and Dietrich, D. Vesicular glutamate release from axons in white matter. Nat Neurosci 2007; *10*, 311–320.

Kukley, M., Nishiyama, A., and Dietrich, D. The Fate of Synaptic Input to NG2 Glial Cells: Neurons Specifically Downregulate Transmitter Release onto Differentiating Oligodendroglial Cells. J. Neurosci. 2010; *30*, 8320–8331.

Kyrozis, A., and Reichling, D.B. Perforated-patch recording with gramicidin avoids artifactual changes in intracellular chloride concentration. J. Neurosci. 1995; Methods *57*, 27–35.

Langhorst, M.F., Reuter, A., and Stuermer, C. a. O. Scaffolding microdomains and beyond: the function of reggie/flotillin proteins. Cell. Mol. Life Sci. 2005; *62*, 2228–2240.

Lin, S., and Bergles, D.E. Synaptic signaling between GABAergic interneurons and oligodendrocyte precursor cells in the hippocampus. Nat Neurosci 2004; *7*, 24–32.

Lindau, M. High resolution electrophysiological techniques for the study of calcium-activated exocytosis. Biochim Biophys Acta 2012; *1820*, 1234–1242.

Lytle, J.M., Vicini, S., and Wrathall, J.R. Phenotypic Changes in NG2+ Cells after Spinal Cord Injury. Journal of Neurotrauma 2006; *23*, 1726–1738.

Matsuo, H., Chevallier, J., Mayran, N., Blanc, I.L., Ferguson, C., Fauré, J., Blanc, N.S., Matile, S., Dubochet, J., Sadoul, R., et al. Role of LBPA and Alix in Multivesicular Liposome Formation and Endosome Organization. Science 2004; *303*, 531–534.

Men, Y., Yelick, J., Jin, S., Tian, Y., Chiang, M.S.R., Higashimori, H., Brown, E., Jarvis, R., and Yang, Y. Exosome reporter mice reveal the involvement of exosomes in mediating neuron to astroglia communication in the CNS. Nat Commun 2019; *10*, 1–18.

Metzelaar, M.J., Wijngaard, P., Peters, P.J., Sixma, J.J., Nieuwenhuis, H.K., and Clevers, H.C. CD63 antigen. A novel lysosomal membrane glycoprotein, cloned by a screening procedure for intracellular antigens in eukaryotic cells. The Journal of Biological Chemistry 1991; *266*, 3239–3245.

Mori, Y., Koike, M., Moriishi, E., Kawabata, A., Tang, H., Oyaizu, H., Uchiyama, Y., and Yamanishi, K. Human Herpesvirus-6 Induces MVB Formation, and Virus Egress Occurs by an Exosomal Release Pathway. Traffic 2008; *9*, 1728–1742.

Moser, T., and Neher, E. Estimation of mean exocytic vesicle capacitance in mouse adrenal chromaffin cells. Proc Natl Acad Sci U S A 1997; *94*, 6735–6740.

Mukherjee, A.B., Appu, A.P., Sadhukhan, T., Casey, S., Mondal, A., Zhang, Z., and Bagh, M.B. Emerging new roles of the lysosome and neuronal ceroid lipofuscinoses. Mol Neurodegener 2019; *14*, 1–23.

Murk, J.L. a. N., Humbel, B.M., Ziese, U., Griffith, J.M., Posthuma, G., Slot, J.W., Koster, A.J., Verkleij, A.J., Geuze, H.J., and Kleijmeer, M.J. Endosomal compartmentalization in three dimensions: Implications for membrane fusion. PNAS 2003; *100*, 13332–13337.

Nakadate, K. Developmental changes in the flotillin-1 expression pattern of the rat visual cortex. Neuroscience 2015; *292*, 101–111.

Neef, A., Heinemann, C., and Moser, T. Measurements of membrane patch capacitance using a software-based lock-in system. Pflugers Arch. 2007a; *454*, 335–344.

Neef, A., Khimich, D., Pirih, P., Riedel, D., Wolf, F., and Moser, T. Probing the Mechanism of Exocytosis at the Hair Cell Ribbon Synapse. J. Neurosci. 2007b; *27*, 12933–12944.

Neher, E., and Marty, A. Discrete changes of cell membrane capacitance observed under conditions of enhanced secretion in bovine adrenal chromaffin cells. Proc Natl Acad Sci U S A 1982; *79*, 6712–6716.

Nishiyama, A., Lin, X.H., and Stallcup, W.B. Generation of truncated forms of the NG2

proteoglycan by cell surface proteolysis. Mol Biol Cell 1995; *6*, 1819–1832.

Nishiyama, A., Lin, X.H., Giese, N., Heldin, C.H., and Stallcup, W.B. Co-localization of NG2 proteoglycan and PDGF alpha-receptor on O2A progenitor cells in the developing rat brain. J. Neurosci. Res. 1996; *43*, 299–314.

Nishiyama, A., Yang, Z., and Butt, A. Astrocytes and NG2-glia: what's in a name? Journal of Anatomy 2005; *207*, 687–693.

Nishiyama, A., Komitova, M., Suzuki, R., and Zhu, X. Polydendrocytes (NG2 cells): multifunctional cells with lineage plasticity. Nat. Rev. Neurosci. 2009; *10*, 9–22.

Nolte, C., Matyash, M., Pivneva, T., Schipke, C.G., Ohlemeyer, C., Hanisch, U.K., Kirchhoff, F., and Kettenmann, H. GFAP promoter-controlled EGFP-expressing transgenic mice: a tool to visualize astrocytes and astrogliosis in living brain tissue. Glia 2001; *33*, 72–86.

O'Keefe, J., and Nadel, L. The Hippocampus as a Cognitive Map (Oxford, UK: Oxford University Press) 1978.

Paddock, S.W., and Eliceiri, K.W. Laser Scanning Confocal Microscopy: History, Applications, and Related Optical Sectioning Techniques In Confocal Microscopy, (Humana Press, New York, NY), 2014; pp. 9–47.

Paolicelli, R.C., Bolasco, G., Pagani, F., Maggi, L., Scianni, M., Panzanelli, P., Giustetto, M., Ferreira, T.A., Guiducci, E., Dumas, L., et al. Synaptic Pruning by Microglia Is Necessary for Normal Brain Development. Science 2011; *333*, 1456–1458.

Papez, J.W. A proposed mechanism of emotion. Arch NeurPsych 1937; *38*, 725–743.

Passlick, S., Trotter, J., Seifert, G., Steinhäuser, C., and Jabs, R. The NG2 Protein Is Not Required for Glutamatergic Neuron–NG2 Cell Synaptic Signaling. Cereb. Cortex 2016; *26*, 51–57.

Raff, M.C., Miller, R.H., and Noble, M. A glial progenitor cell that develops in vitro into an astrocyte or an oligodendrocyte depending on culture medium. Nature 1983; *303*, 390–396.

Raposo, G., Nijman, H.M., Stoorvogel, W., Liejendekker, R., Harding, C.V., Melief, C.J., and Geuze, H.J. B lymphocytes secrete antigen-presenting vesicles. J Exp Med 1996; *183*, 1161–1172.

Raposo, G., Moore, M., Innes, D., Leijendekker, R., Leigh-Brown, A., Benaroch, P., and Geuze, H. Human Macrophages Accumulate HIV-1 Particles in MHC II Compartments. Traffic 2002; *3*, 718–729.

Richardson, W.D., Kessaris, N., and Pringle, N. Oligodendrocyte Wars. Nat Rev Neurosci 2006; *7*, 11–18.

Rituper, B., Guček, A., Jorgačevski, J., Flašker, A., Kreft, M., and Zorec, R. High-

resolution membrane capacitance measurements for the study of exocytosis and endocytosis. Nat. Protocols 2013; *8*, 1169–1183.

Rivers, L.E., Young, K.M., Rizzi, M., Jamen, F., Psachoulia, K., Wade, A., Kessaris, N., and Richardson, W.D. PDGFRA/NG2 glia generate myelinating oligodendrocytes and piriform projection neurons in adult mice. Nat Neurosci 2008; *11*.

Sakry, D., Neitz, A., Singh, J., Frischknecht, R., Marongiu, D., Binamé, F., Perera, S.S., Endres, K., Lutz, B., Radyushkin, K., et al. Oligodendrocyte Precursor Cells Modulate the Neuronal Network by Activity-Dependent Ectodomain Cleavage of Glial NG2. PLOS Biol 2014; *12*, e1001993.

Santamaría, A., Castellanos, E., Gómez, V., Benedit, P., Renau-Piqueras, J., Morote, J., Reventós, J., Thomson, T.M., and Paciucci, R. PTOV1 Enables the Nuclear Translocation and Mitogenic Activity of Flotillin-1, a Major Protein of Lipid Rafts. Mol Cell Biol 2005; *25*, 1900–1911.

Santiago, J.M., Torrado, A.I., Arocho, L.C., Rosas, O.R., Rodríguez, A.E., Toro, F.K., Salgado, I.K., Torres, Y.A., Silva, W.I., and Miranda, J.D. Expression Profile of Flotillin-2 and its Pathophysiological Role after Spinal Cord Injury. J Mol Neurosci 2013; *49*, 347–359.

Schubert, D. The modulation of neurotransmitter synthesis by steroid hormones and insulin. Brain Research 1980; *190*, 67–79.

Schulte, T., Paschke, K.A., Laessing, U., Lottspeich, F., and Stuermer, C.A. Reggie-1 and reggie-2, two cell surface proteins expressed by retinal ganglion cells during axon regeneration. Development 1997; *124*, 577–587.

Scoville, W.B., and Milner, B. LOSS OF RECENT MEMORY AFTER BILATERAL HIPPOCAMPAL LESIONS. J Neurol Neurosurg Psychiatry 1957 *20*, 11–21.

Simons, M., and Nave, K.-A. Oligodendrocytes: Myelination and Axonal Support. Cold Spring Harb Perspect Biol 2016; *8*.

Srinivas, S., Watanabe, T., Lin, C.-S., William, C.M., Tanabe, Y., Jessell, T.M., and Costantini, F. Cre reporter strains produced by targeted insertion of EYFP and ECFP into the ROSA26 locus. BMC Developmental Biology 2001; *1*, 4.

Stallcup, W.B. Sodium and calcium fluxes in a clonal nerve cell line. J Physiol 1979; *286*, 525–540.

Stallcup, W.B. The NG2 antigen, a putative lineage marker: immunofluorescent localization in primary cultures of rat brain. Developmental Biology 1981; *83*, 154–165.

Stallcup, W.B. The NG2 proteoglycan: Past insights and future prospects. J Neurocytol 2002; *31*, 423-435.

Stallcup, W.B., and Beasley, L. Bipotential glial precursor cells of the optic nerve express

the NG2 proteoglycan. J. Neurosci. 1987; *7*, 2737–2744.

Steinhaüser, C., Berger, T., Frotscher, M., and Kettenmann, H. Heterogeneity in the Membrane Current Pattern of Identified Glial Cells in the Hippocampal Slice. European Journal of Neuroscience 1992; *4*, 472–484.

Steinhäuser, C., Kressin, K., Kuprijanova, E., Weber, M., and Seifert, G. Properties of voltage-activated Na+ and K+ currents in mouse hippocampal glial cells in situ and after acute isolation from tissue slices. Pflugers Archiv : European Journal of Physiology 1994; *428*, 610–620.

Strauss, K., Goebel, C., Runz, H., Möbius, W., Weiss, S., Feussner, I., Simons, M., and Schneider, A. Exosome Secretion Ameliorates Lysosomal Storage of Cholesterol in Niemann-Pick Type C Disease. J Biol Chem 2010; *285*, 26279–26288.

Stuermer, C.A.O., Lang, D.M., Kirsch, F., Wiechers, M., Deininger, S.-O., and Plattner, H. Glycosylphosphatidyl Inositol-anchored Proteins and fyn Kinase Assemble in Noncaveolar Plasma Membrane Microdomains Defined by Reggie-1 and -2. MBoC 2001; *12*, 3031–3045.

Sun, W., Matthews, E.A., Nicolas, V., Schoch, S., and Dietrich, D. NG2 glial cells integrate synaptic input in global and dendritic calcium signals. eLife Sciences 2016; *5*, e16262.

Swanwick, C.C., Shapiro, M.E., Vicini, S., and Wenthold, R.J. Flotillin-1 Promotes Formation of Glutamatergic Synapses in Hippocampal Neurons. Dev Neurobiol 2010; *70*, 875–883.

Théry, C., Boussac, M., Véron, P., Ricciardi-Castagnoli, P., Raposo, G., Garin, J., and Amigorena, S. Proteomic Analysis of Dendritic Cell-Derived Exosomes: A Secreted Subcellular Compartment Distinct from Apoptotic Vesicles. The Journal of Immunology 2001; *166*, 7309–7318.

Théry, C., Witwer, K.W., Aikawa, E., Alcaraz, M.J., Anderson, J.D., Andriantsitohaina, R., Antoniou, A., Arab, T., Archer, F., Atkin-Smith, G.K., et al. Minimal information for studies of extracellular vesicles 2018 (MISEV2018): a position statement of the International Society for Extracellular Vesicles and update of the MISEV2014 guidelines. J Extracell Vesicles 2018; *7*, 1–43.

Timmermann, A., Jabs, R., Boehlen, A., Domingos, C., Skubal, M., Huang, W., Kirchhoff, F., Henneberger, C., Bilkei-Gorzo, A., Seifert, G., et al. Dysfunction of grey matter NG2 glial cells affects neuronal plasticity and behavior. bioRxiv 2021; 2021.08.20.457086.

Trajkovic, K., Hsu, C., Chiantia, S., Rajendran, L., Wenzel, D., Wieland, F., Schwille, P., Brügger, B., and Simons, M. Ceramide Triggers Budding of Exosome Vesicles into Multivesicular Endosomes. Science 2008; *319*, 1244–1247.

Valadi, H., Ekström, K., Bossios, A., Sjöstrand, M., Lee, J.J., and Lötvall, J.O. Exosome-mediated transfer of mRNAs and microRNAs is a novel mechanism of genetic exchange

between cells. Nature Cell Biology 2007; *9*, 654–659.

Viganò, F., Möbius, W., Götz, M., and Dimou, L. Transplantation reveals regional differences in oligodendrocyte differentiation in the adult brain. Nat Neurosci 2013; *16*, 1370–1372.

Volonte, D., Galbiati, F., Li, S., Nishiyama, K., Okamoto, T., and Lisanti, M.P. Flotillins/cavatellins are differentially expressed in cells and tissues and form a hetero-oligomeric complex with caveolins in vivo. Characterization and epitope-mapping of a novel flotillin-1 monoclonal antibody probe. The Journal of Biological Chemistry 1999; *274*, 12702–12709.

Von Bartheld, C.S., and Altick, A.L. Multivesicular Bodies in Neurons: Distribution, Protein Content, and Trafficking Functions. Prog Neurobiol 2011; *93*, 313–340.

Von Gersdorff, H., and Matthews, G. Electrophysiology of synaptic vesicle cycling. Annu. Rev. Physiol. 1999; *61*, 725–752.

Wallraff, A., Odermatt, B., Willecke, K., and Steinhäuser, C. Distinct types of astroglial cells in the hippocampus differ in gap junction coupling. Glia 2004; *48*, 36–43.

Wellman, S.M., and Kozai, T.D.Y. In vivo spatiotemporal dynamics of NG2 glia activity caused by neural electrode implantation. Biomaterials 2018; *164*, 121–133.

Westerink, R.H.S. Heterogeneity of Catecholamine-Containing Vesicles in PC12 Cells. Biochemical and Biophysical Research Communications 2000; *270*, 625–630.

Westerink, R.H.S., and Ewing, A.G. The PC12 cell as model for neurosecretion. Acta Physiol (Oxf) 2008; *192*, 273–285.

Wightman, R.M., Jankowski, J.A., Kennedy, R.T., Kawagoe, K.T., Schroeder, T.J., Leszczyszyn, D.J., Near, J.A., Diliberto, E.J., and Viveros, O.H. Temporally resolved catecholamine spikes correspond to single vesicle release from individual chromaffin cells. Proc Natl Acad Sci U S A 1991; *88*, 10754–10758.

Wilson, S.-S., Baetge, E.E., and Stallcup, W. Antisera specific for cell lines with mixed neuronal and glial properties. Developmental Biology 1981; *83*, 146–153.

Zappulli, V., Friis, K.P., Fitzpatrick, Z., Maguire, C.A., and Breakefield, X.O. Extracellular vesicles and intercellular communication within the nervous system. J Clin Invest 2016; *126*, 1198–1207.

Zhu, X., Bergles, D.E., and Nishiyama, A. NG2 cells generate both oligodendrocytes and gray matter astrocytes. Development 2008; *135*, 145–157.

11. Acknowledgements

I would like to thank Prof. Dr. Christian Steinhäuser for giving me the opportunity to work under his supervision in the Institute of Cellular Neurosciences in the UKB, up on Venusberg hill in Bonn. Despite me being a foreign student and disregarding all the problems that come with the fact, in the face of little experience that I had before and all the scientific hurdles that came in the project, Prof. Steinhäuser granted me trust to carry out this work to the end. My involvement with IMPRS was also possible thanks to his advice. IZN became home away from home for me, for years.

I would like to thank my supervisors, Prof. Dr. Jochen Walter, Prof. Dr. Volkmarr Gieselmann, and Dr. Etienne Audinat for accepting my request to be part of my dissertation committee and devoting their valuable time to review my dissertation. I would like to specially thank Prof. Walter for providing materials for the project and rooms for my training in cell culture methods, and Prof. Gieselmann for providing stocks of the cell cultures.

I would like to most sincerely thank Dr. Ronald Jabs for spending countless hours planning, teaching, offering advice and reviewing the results, and often just being there to cheer me up when things did not go as planned. Before we spoke first time, I had no idea about NG2-glial cells, and only the faintest, most basic idea about the glia. Learning electrophysiology in all of its complexity, coding, and statistics to a standard necessary for scientific work would be impossible without him. Thanks to his constant involvement, this project could be brought to a conclusion. His enthusiasm and love of local Köln-Bonn culture and holidays is what made them so much more fun to attend.

I would also like to thank Dr. Konstantin Glebov for supporting the initial phase of the project, providing data on the prior experiments and for offering critical tips that led to interesting results in the final phase. Without his training and support, the cell culture aspect of the work would be much more difficult to carry out.

I would like to the warmest thanks to Dr. Gerald Seifert, who always managed to sort out the mistakes that I made interacting with HET (Fax!), and to always offer me help in

everything regarding experimental animals. His reliable support was always there when I needed it.

I would like to thank Prof. Henneberger for his advice on data analysis and thoughtful questions for the times when project was in need of a fresh look.

I thank Dr. Hannes Beckert for his enthusiastic involvement in the late phase of the project. The daring CLEM experiment that was new for both of us was the result of his dedicated effort. We were able to work together even after I left Germany. I would also like to thank his assistant, Ms. Pia Stausberg, for her careful work on the EM samples.

My warmest thanks goes to Dr. Julia Müller and Dr. Aline Timmerman for being the first to train me in the basic lab work when I was fresh out of masters, and a new arrival to Germany. Julia spent her time behind my shoulder making sure I can do things properly, and the amount of help from Aline on all the little formal and informal matters simply can't be measured. The teapot that we relentlessly used every day should get a mention here somewhere too :).

I thank Dr. Peter Bedner for walking into my room one day with Katerina in tow. I thank Dr. Ekaterina Pershina, Катя ☺, for being with me in the darkest moments and in the happiest of times. Without her, I would not succeed.
I want to thank my parents, Dr. Elena Fedorova and Andrey Fedorov, MD, for everything that I have.
I also extend the warmest wishes to Mr. and Ms. Volhardt and Mr. and Ms. Von Bülow for allowing me a safe and pleasant stay in Germany.
I want to thank also;
Leah Schüler and Charlotte von dem Knesebeck helped me greatly during the meanest time of the pandemic, in the zeitnot of the last year.
Ms. Sandra Theil of Prof. Walter's group for helping me with cell culture materials and antibodies.
Mr. Thomas Erdmann for his work on procuring a hundred useful things and always knowing where to find them ☺.

Ms. Silke Künzel for helping to fight through the bureaucracy and the occasional paperwork.
Dr. Andreas Neef for offering me advice on membrane capacitance recording technique.
Prof. Dr. Alexey Semyanov for offering me the needed workspace to complete the writing of the dissertation.

I want to thank IMPRS Professors, instructors and educators for accepting me into the International Max Planck Research School (IMPRS) for Brain and Behavior. It is thanks to them that I met the lovely people of the research school, and for the richness of the moments of science and travel that I would never in my life would see otherwise. My experience of PhD was no less than doubled thanks to the research school.

I would like to thank our coordinators, Denise Butler and Ezgi Bulca of IMPRS, for offering guidance and support in all the matters of the research school. Without their effort and enthusiasm in dealing with many PhD students (talk about herding cats!) this school would unravel in just few months after conception.

My best wishes go to all of my colleagues at IMPRS and IZN:
Dr. Camille Phillipot (A fellow electrophysiologist and SP5 user), Lukas Henning, Dr. Kirsten Bohmbach (Friday seminar pro, and hat supplies master), Nehal Gebril (who taught me how to immuno-stain, and brought delicious sweets), Dario Tascio, Dr. Daniel Minge, Dr. Alberto Pauletti, Dr. Petr Unichenko, Dr. Magdalena Skubal, Dr. Michel Herde and others at the IZN!

I thank Joanna Komorowska and Daniel Müller, (now Komorowska-Müller and Müller-Komorowska) for the warmest times at their home in Ippendorf, for the game nights, birthdays and dinner parties, and for the wedding party in Poland! My best wishes go to Pedro Royero and Katarina Ferreira, Eleonora Ambrad, André Haubrich, Özer İlkin, Arne Monsees, Max Schelski, Petra Mocellin, Chi Wai Chan and all the others at IMPRS!

Thank you all!